Effects of Moisture Aging on the Mechanical Behaviour of Bio-based Composites: Adapting Glass Fiber Numerical Models to Flax Composites

Abhinanda Napa Ravikumar

August 13, 2024

Effects of Moisture Aging on the Mechanical Behaviour of Bio-based Composites: Adapting Glass Fiber Numerical Models to Flax Composites

by

Abhinanda Napa Ravikumar

in partial fulfillment of the requirements for the degree of

Master of Science
in Civil Engineering

at the Delft University of Technology,
to be defended publicly on Monday August 19th, 2024 at 16:00

Student number:	5458455
Project duration:	September 22, 2023 – August 19th, 2024
Thesis committee:	

Dr. ir. Y. Mosleh,	TU Delft,	Chair, Supervisor
Dr. ir. F. P. Van der Meer,	TU Delft,	Supervisor
Ir. V. P. Perruchoud,	TU Delft,	Daily Supervisor
Dr. ir. I.B.C.M. Rocha,	TU Delft,	Supervisor

TU Delft

Abstract

The use of Glass Fiber Reinforced Composites is increasing across the world in its use in booming industries such as wind energy, construction and electronics due to the advantages it offers. A replacement for glass fiber composites is being researched widely in Europe because of sustainability reasons. Bio-based composites such as Flax Fiber Reinforced Composites offer higher degradability and better mechanical properties for the same specific weight ratio as glass fiber composites. Although flax composites are an attractive alternative to traditional, petroleum-based composites, they have higher susceptibility to moisture degradation due to the presence of hygroscopic natural fibers. The moisture degradation of flax composites negatively affects its durability and strength performance.

In this thesis work, existing work employing the use of state of the art numerical techniques used to model hygrothermal aging of glass fiber composites is used to model moisture aging mechanisms seen in flax composites. A literature review is performed to identify the crucial degradation mechanisms affecting flax composites due to moisture aging. Interface debonding between phases is found to be a possible crucial damage mechanism due to moisture uptake. Presently, there is a lack of experimental studies on the effect of moisture degradation effect on the interface the significance of the same in the loading configuration of transverse flax-epoxy composites in literature. There is also presently a lack of numerical modelling efforts that describe the complex multi-physics and multi-scale nature of natural fibers and bio-based composites consistently and wholistically in literature. The goal of this thesis is to carry out exploratory work in the numerical modelling of swelling and tensile behaviour of transverse flax composites, based on existing modelling techniques for GFRP and supported by parameters from literature and experiments.

The swelling and transverse tensile behaviour of the flax fiber reinforced composites is modelled at the micro-scale. The state-of-the-art numerical framework used to model moisture degradation and quasi-static and fatigue behaviour in glass fiber composites is adapted for simplified micro-scale modelling using a Representational Volume Element (RVE). The sensitivity of the modelling parameters obtained from literature is studied to understand the effects of geometry variation and material degradation on the swelling strain in a linear-elastic micro-scale RVE analysis.

An experimental campaign is carried out to obtain relevant parameters for the numerical model that is missing from literature. The aim of the experimental campaign is also to characterize the moisture aging behaviour of transverse flax composites and its constituent phases. The material stiffness degradation of transverse flax composites and epoxy is studied with tensile tests before and after moisture uptake in the climate chamber. The swelling co-efficients of both transverse flax composites and epoxy are calculated. Microscopy imaging is used to qualitatively assess damage mechanisms due to moisture uptake and the fracture surface from tensile tests.

An elasto-plastic material for epoxy is calibrated with the tensile test experiments performed on the epoxy. A final iteration of the swelling numerical model based on the experimental benchmark is presented. The transverse tensile tests for composites from experiments are numerically simulated. The capabilities and the shortcoming of the final model are discussed for improvements in future work.

Acknowledgement

First of all, I extend sincere thanks to Dr. Yasmine and Dr. Frans for offering me the opportunity to work on this thesis topic and for continuously providing their valuable guidance and expertise along the way. It is a topic in an important area of research that combines two departments conducting complex research within their respective domains of bio-based composites and physics-based numerical simulation which constantly challenged me to learn more.

I owe an immense debt of gratitude to my daily supervisor Valentin for helping and guiding me in the lab with all the experiments in such a short time. I have a learned a lot about composites and about effectively conducting experiments in a laboratory because of this. I also thank you for helping me with writing and pushing me to think critically about the research insights. The guidance I have received on analytical and scientific thinking from you will continue to be invaluable to me going forward in my career.

I sincerely thank Iuri for advising me on this thesis journey from the start and helping me navigate the practical hurdles of research, providing me with motivation and support and helping me clearly define my goals for the thesis. I thank you for inspiring me to become a better coder and for offering me critical support with the numerical issues.

I want to thank my housemates Sjoerd, Maikel, Dima, Abina, Yuting and Andrei for accepting me into their home and making me feel welcome here and supporting me during my tough times. I would like to thank my friends Nicky, James, Martin, Pascalle, Arend, Jeroen, Uri, Alef and Kyle for continuing to believe in me and pushing me to do better.

I would like to thank my family and all my friends for supporting me during my master studies. I have overcome many hurdles along this journey to hone my scientific skills, discipline and work ethic because of your support and guidance along the way.

A. N. Ravikumar
Delft, June 2024

Contents

List of Figures

List of Tables

1 Introduction

1.1 Research Context

The state of the art numerical modelling techniques used in simulating the hygrothermal aging in glass fiber composites [76] is used to simulate moisture degradation mechanisms such as swelling and transverse tensile behaviour of flax composites. The suitability of the modelling techniques used for glass fiber composites for flax fiber reinforced composites is researched in this thesis work.

1.2 Problem Statement

The increasing demand for sustainability makes bio-based composites an attractive option in the replacement of petroleum and artificial fiber based synthetic composites. The physical structure of natural fibers and its composites is complex. The increased susceptibility of natural composites to moisture degradation presents an added complexity in its usage. Therefore, a consistent characterization and modelling of the critical degradation inducing phenomena related to moisture absorption and its effects on the tensile properties of natural composites become crucial. It is important to assess the moisture durability of bio-based composites and the effects of moisture degradation on the strength/performance of the bio-based composites.

1.3 Aim & Scope

- To review experimental and numerical techniques used for synthetic and bio-based composites in literature
- To perform experiments to assess moisture absorption and tensile behaviour of flax composites and characterize the parameters for modelling absent in literature
- To adapt an existing numerical model to flax fiber reinforced composites by implementing fiber swelling, matrix plasticization and also model transverse tensile behaviour

1.4 Research Questions

- How to adapt the Glass Fiber Composite numerical model for modelling moisture uptake and degradation in flax fiber reinforced epoxy composites?
  - What are the primary degradation mechanisms in Flax Fibre Reinforced Epoxy Composites due to moisture absorption?
  - How can swelling and moisture degradation of flax composites be characterized for the purpose of numerical modelling?
  - How can the complex geometry of flax fibers be represented with sufficient accuracy in a microscale numerical model?
  - How to build a microscale numerical analysis model for simulating swelling and tensile behaviour of transverse flax composites?

1.5 Thesis Outline

This thesis work presents an initial exploratory effort focussing on some of the fundamentally important mechanisms in the moisture degradation and material behaviour of flax fiber composites and its numerical modelling. The introduction chapter of this thesis work gives an outline of the research scope and objectives of the thesis. The chapter on Flax FRP Composites presents an overview of literature on flax composites, regarding moisture degradation, mechanical behaviour and the mechanisms of importance in

modelling of hygrothermal aging. It is found from literature review that interface degradation is a possible crucial damage mechanism due to moisture uptake. The chapter on the Numerical Modelling of (Bio)based composites presents the numerical modelling techniques and concepts used in this thesis work, as adapted from [76] and relevant literature review on existing numerical modelling efforts in synthetic and bio-based composites. The chapter on Model Parameters presents the experiments performed to characterize swelling and material degradation. The chapter also presents all the parameters that is obtained from literature and back-calculation of values to be used in the numerical models along with the results of microscopy image analysis of different types of flax reinforced composites. The hypothesis that the tensile tests in transverse direction is governed by interface loading in that configuration is tested through transverse tensile tests Figure 80 on parallel-sided flax fiber reinforced composites in the Numerical Results, Experimental Benchmark & Discussion chapter. This chapter further outlines the data and results from the swelling sensitivity analysis performed with values obtained from different literature sources in order to get an understanding of the influence of geometry, material models and the parameters used for modelling. This chapter also presents the benchmark numerical model for swelling and transverse tensile tests of composites based on experimentally obtained parameters missing from literature. Finally, in the Conclusions & Recommendations chapter is suggested crucial improvements in numerical modelling and experimental efforts based on the literature overview and results observed from modelling. An example input properties file used to build the models and modules for an analysis is given in the Appendix.

2 Flax FRP Composites

Composites are structural materials with two or more phases. Generally, composites consist of a weaker continuous phase of matrix within which is embedded stronger, continuous or discontinuous and stiffer fibers (reinforcement phase). These individual constituents are in the macroscopic scale and there is an interphase present between fiber and matrix which deals with the bonding between phases [35] [49].

The flexibility in design, absence of corrosion and high specific strength of composite materials has seen the massive replacement of traditional materials employed in a wide range of industries. From automobiles to aircraft manufacturing and marine to fashion, the continuous requirement for lighter, stronger materials with greater durability is responsible for the increase in usage of composite materials [51]. Composites are widely used for their enhanced mechanical properties in the manufacturing industry, for use in products that are prevalent in the daily life of most citizens. Traditional composites employ the use of petroleum based matrix material and synthetic fibers due to their resistance to degradation [65]. The increasing demand for sustainability within the European Union [32] makes bio-based composites an attractive replacement for traditional composites.

Bio-based composites are manufactured by replacing the synthetic fibers with natural fibers such as flax or jute and reinforced with thermoset plastics [9], or replacing both fiber and matrix with natural alternatives. The hygroscopic nature of the natural constituents [74] [54] used in bio-based composites is responsible for the absorption of moisture within their structure. The overall absorption of moisture and the consequent damage to the composite consituents is studied through hygrothermal aging experiments where temperature and moisture conditions are controlled [56] [83] [10] to simulate and observe the moisture absorption physics and degradation in composites.

Flax fibers are a potential alternative to synthetic fibers in composite materials due to their potential production capacity, cheap cost and high specific modulus and higher strain plateau [55], which means that for the same density of glass fibers, the tensile strength characteristics of flax fiber composites are comparable, and in some cases exceed that of glass fiber composites. The disadvantages of flax fibers is that they are hydrophilic in nature, which results in interface debonding due to moisture absorption against relatively hydrophobic polymer matrices due to differential swelling [42] [36]. Flax fibers have highly anisotropic swelling characteristics [57]. The mechanical and morphological properties of flax fiber are also largely varied along different directions. The swelling and moisture absorption characteristics of natural fibers depend heavily on its highly complex and multi-scale physical structure, geometry and chemical composition.

2.1 Flax Fiber Microstructure and Mechanical Properties

The most commonly used vegetable fibers are of the bast and leaf qualities that are hard fibers, where cellulose is the main component [18]. The cellulose macromolecule has the elementary unit of anhydro-d-glucose with three hydroxyl groups, enabling it to form intramolecular and intermolecular hydrogen bonds with water molecules, making it hydrophilic in nature [18]. Table I and Table II from [18] gives the chemical composition and mechanical properties respectively, of widely used vegetable fibers. The fibrils of cellulose macromolecules form spirals along the fiber axis. They are the building blocks of the fibers that provide strength in tensile loading. Lignin/hemicellulose acts as a cementing material between fibrils. Fibres with higher cellulose content, higher degree of polymerization and a lower microfibrillar angle exhibit higher tensile strength and modulus [86]. Moudood et. al provides an extensive overview about flax fiber composites from its structure, to

manufacturing, to moisture absorption and the influence of these processes on the strength of the flax fibers and its composites [64].

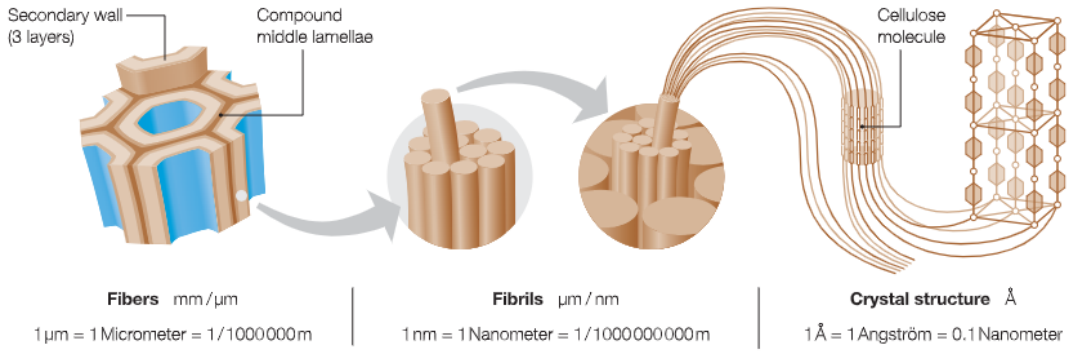

Figure 1: Multi-scale Structure of the wood cell wall [96]

Flax fibers have a highly complex structure with variable hierarchy depending on the scale of observation. There is a lumen present in the middle of the fiber responsible for water absorption. The lumen along with the primary cell wall, can both be identified at the meso-scopic scale of observation. The S2 layer of the secondary cell wall present between the lumen and the primary cell wall represents the bulk of the fiber. In the S2 layer are present highly crystalline cellulose micro-fibrils oriented at a tilt angle of $10° - 11°$ [20] wound in a matrix of amorphous lignin and hemi-cellulose. The S2 Wall is reinforced at decreasing scale of observation with macro-fibrils which consists of micro-fibrils, which further consists of elementary fibrils that are composed of cellulose molecules [11]. Each constituent within the fiber has distinct mechanical, geometrical and chemical properties which determines its effect on the tensile deformation behaviour of the fiber.

A bundle of around 10-40 elementary fibers are naturally bonded with pectin that are termed technical fibers [11]. Flax fibers, after the retting process are found as a combination of both elementary and technical fibers, as used in composites. Elementary and Technical Fibers can also be twisted into yarns to increase increase tensile resistance due to surface friction from the twist. These yarns are woven into fabrics spanning the warp and weave directions [94]. Fabrics and yarns offer streamlining of the large dispersion in mechanical properties to an extent. Due to anisotropy at different scales of the fiber and the large spread in mechanical and geometry parameters, it becomes increasingly complicated to enable a consistent definition of the fiber at different scales of observation.

The centre of the fibre structure consists of a hollow lumen which is covered by the secondary cell wall. The secondary wall can be further sub-divided into the S3, S2 and S1 parts. The secondary cell wall houses the cellulose micro-fibrils which are oriented at a variable tilt angle [20]. The micro-fibrils are in the amorphous region dispersed between hemi-cellulose and lignin. The outer primary cell wall layer is 0.2 µm thick [11] and consists of disorderdly arranged crystalline cellulose micro-fibrils [86].

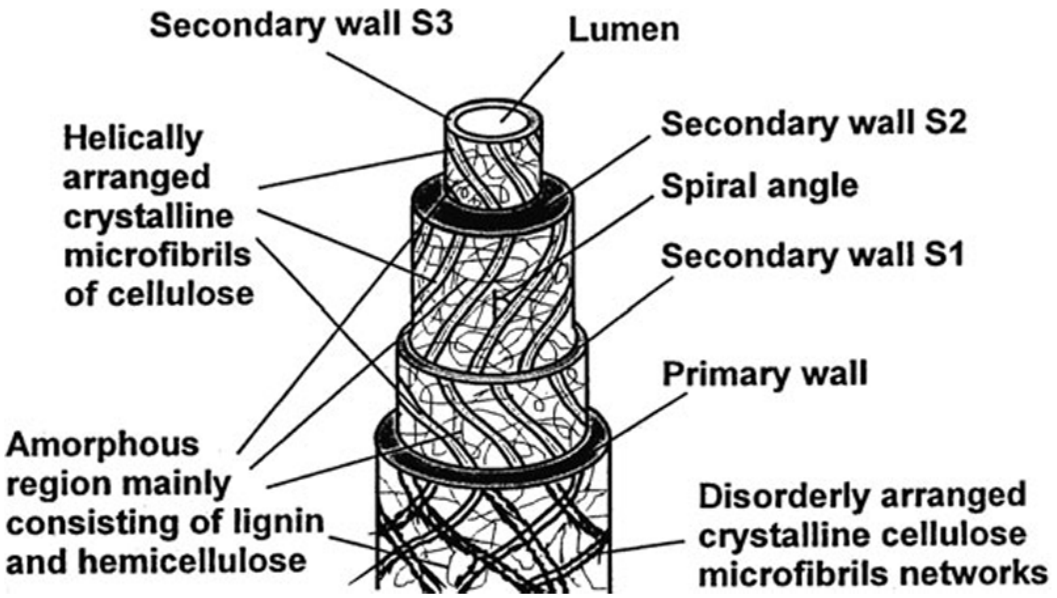

Figure 2: Structure of a natural fiber [77]

The elementary flax fiber is a natural fiber with predominantly similar structure to most natural fibers as depicted below in Figure 2. Figure 4 shows the section of a technical fiber which is a bundle of 10-40 elementary fibers that are bonded together by naturally occurring pectin [11]. The fibers retted from the flax stem are a combination of both elementary and technical flax fibers. The diameter of the elementary fibers varies from 5 µm and 76 µm as seen in literature with the significance in variation. Charlet et. al studied the diameter dispersion in flax fibers owing to its natural occurrence and derived relationships between the diameter and mechanical properties of the fibers [29]. Baley et. al and Charlet et. al enlist the morphological and mechanical parameters of the fibre and the constituents of its micro-structure as part of their studies [29] [12] [11].

Figure 3: Side View of Technical Flax Fibre [11]

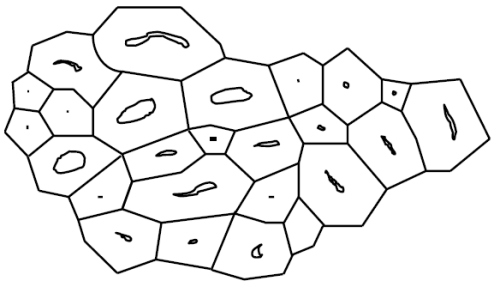

Figure 4: Section of Technical Flax Fibre [11]

The flax fiber has significant scatter in mechanical properties due its natural occurrence and the presence of defects (kink bands). Andersons et. al studied the effects of these kink bands as a function of fiber length, on fiber tensile properties and concluded that it has an influence in the strength parameters of the flax fiber. Optical microscopy was performed with polarized and non-polarized light to characterize the kink bands experimentally with analytical formulations based on the defect occurrence along the length [7]. Baley et. al performed tensile tests on 3000 single flax fibers of several cultivation varieties from different regions of France grown from 1993 to 2011 to obtain tensile properties. The tensile strength at break of fiber is found to decrease with increase in diameter of fiber. The tensile strength at break of fiber is found to decrease with an increase in the Young's Modulus of the fiber. The strain at break stays relatively constant with an

increase in the Young's Modulus of fiber. The average values of strain and strength at break and the tensile modulus are reported and were found to be independent of cultivation period and variety [12]. Coroller et. al studied the tensile properties dependence on the individualisation of fibers from fiber bundles based on flax cultivation variety by fitting to a Weibull statistic. The individualization of some variants of flax fibres are related to the hackling step after cultivation. The individualization of elementary fibres from bundles is compared for variants of flax based on origin. Rule of mixtures is used to predict composite properties at the macro-scale [34].

The typical tensile behaviour of a flax fiber in longitudinal direction can be seen in Figure 5. The decrease in modulus in the stress-strain curve between 0.05 and 0.1 strain in Figure 5 is estimated to be due to micro-fibril angle re-orientation. This phenomenon is validated by performing tensile fatigue tests at small cycles, through the resultant observed increase in Young's Modulus of the fibers without any other significant observable change in structural composition of the fiber [11]. Baley and Charlet et. al performed studies and derived analytical methods to calculate fiber Young's modulus which take into account the phenomenon of micro-fibril angle re-orientation as a function of the observed tilt angle of the micro-fibrils [11] [27].

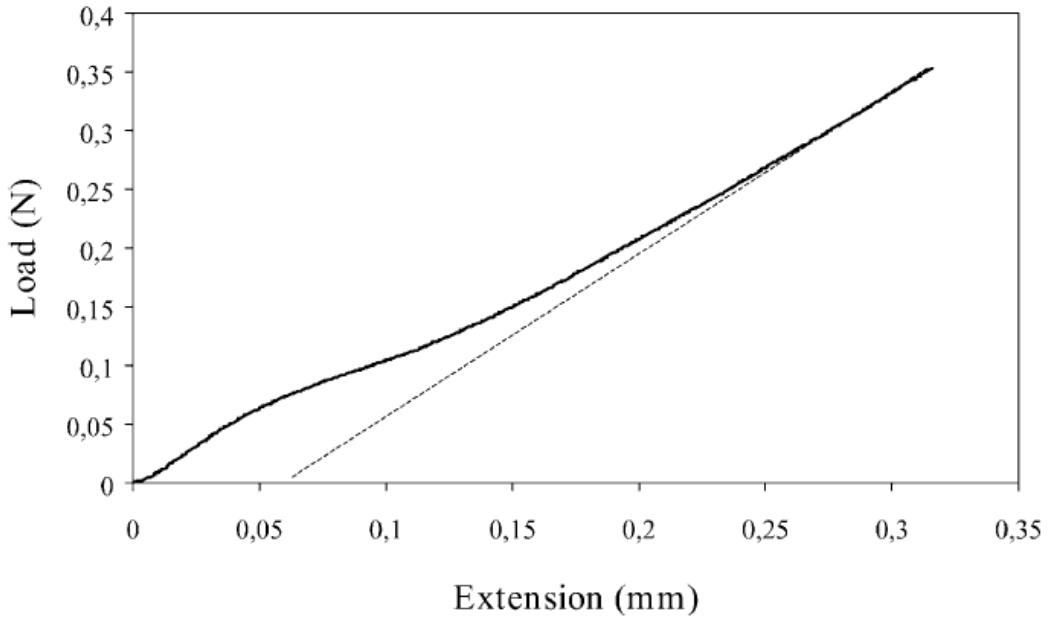

Figure 5: Typical Longitudinal Tensile Behaviour of a Flax Fiber [11]

Bourmaud et. al studied the relationship between mechanical properties, micro-fibrillar angle and bio-chemical composition of the flax fiber with extensive chemical tests and X-ray diffraction methods [23].

Baley et. al studied the tensile properties such as stiffness and stress and strain at break in a large sample of flax elementary fibres of well-documented origin and of various varieties to obtain a design value for flax fibre and study the scatter in the same. Finally, average values of the longitudinal tensile modulus were estimated. The diameter of the fibers were found to have significant correlation with some mechanical properties. The Young's modulus randomness of flax fibers in represented in distributions [12].

Baley et. al studied the tensile behaviour of flax fiber extensively by examining the tensile stiffness increase due to micro-fibrillar angle re-orientation is studied through novel fatigue tests. A micro-mechanical equation is derived from existing Halpin-Tsai equations to calculate the fibre stiffness while accounting for the re-orientation behaviour. The

stiffness properties of each micro-scale constituent of the fiber is given as procured from literature [11]. Bourmaud et. al performed an extensive study on the micro-fibrillar angle and micro-structure of variants of flax and its mechanical properties by the use of X-ray diffraction and studying the role of pectin acids on the Young's modulus and micro-fibrillar angle orientation. It was demonstrated that the lower the Micro-fibrillar angle, the greater the Young's Modulus of fiber and that the ratio between hemicelluloses and pectins has a high correlation with the tensile properties [23].

Bos et. al investigates loop tests in characterizing the compressive strength of the fibers and microscopy imaging was performed to study the failure behaviour [19]. Bourmaud et. al studied the crystallinity properties of randomly dispersed flax fiber composites with calorimetric tests and used SEM micro-graphs to characterize micro-structure damage initiation in flax composites from tensile tests [22].

2.2 Laminate Microstructure

The homogeneity of the composite depends on the fiber volume fraction and the uniformity and orientation of the dispersion of the reinforcement phase within the matrix. The homogenized material properties of composites can be optimized by privileging orientation of the reinforcement phase at different angles by forming laminated composites.

The structure of the flax yarn composite can be described in the micro and nano scales at the fiber level, at the meso-scale at the yarn level and at the macro-scale at composite level. Yarns can be represented in an RVE at the meso-scale of observation. Yarns can be inter-woven in different configuration into fabrics with their own RVE representation at the meso/macro-scale. There are several complexities presented in the structure of the yarn like twist and linear density, which further influence the composite tensile properties. Hearle et. al provides a clear description of the structural mechanics of fibers [41]

Hearle et. al studied the effects of the twist angle on the tensile modulus of yarn composites by accomodating changes to the idealized helical model by including the effect of forces transverse to the fiber axes [46]. The work of Hearle et. al lays the foundation for the structure mechanics of twist in yarn composites.

[60] Madsen et. al studied the yarn structure characteristics such as fibre density and the chemical composition of 2 hemp yarn types in relation to the efficiency of its use as composite reinforcement. The microscopy images of the yarn were analysed to create an analytical model considering the mean twist angle of the yarn. The areas of the fibers were found to depend linearly with respect to the number of fibers. The low hemi-cellulose content in the hemp meant lower water absorption rates than other plant fibers. The study Madsen et. al was expanded upon in a further study with the use of aligned hemp fiber composites, aligned at increasing angles to the longitudinal axis. The fiber weight fractions were estimated considering the linear densities of the yarns. The tensile properties of fibers were back-calculated from composite properties and used to predict the off-axis tensile properties theoretically for comparison with experiments on hemp yarns aligned at an angle in the composites. The effects of moisture absorption and temperature due to processing of the composite was also studied in [59].

Teng et. al presents an improvement for the assumed circular cross-section of the yarn in the tensile effective properties estimation model by [46] and [60]. The yarn tensile properties were predicted using the updated theoretical model as well as with a 3D RVE finite element model of 4 types of yarns with different twist properties. An analytical model to quantify the friction force between the fibers in the yarn was presented to explain increase in tensile strength observed in experiments due to yarn twist [85].

Virk et. al a micro-mechanical model of the yarn structure, with a modified rule of mixtures formulation, incorporating a Fiber Area Correction Factor (FACF) to predict the tensile properties of jute-epoxy composites, along with factors considering orientation and diamater spacing of the fibers. The model was compared with experiments. The study presents an improvement from the conservative estimation of modulus values [2].

Omrani et. al studied the tensile properties of flax fabric composites at the yarn, fabric and composite scales [67]. A similar study by Aldroubi et. al [5] presented the viability of failure strain as a design criterion due to its consistency at different scales. Another similar study was conducted by Blanchard et. al [17] to extensively study the variability in tensile properties at the different scales of observation of the yarn structure.

2.3 Hygroscopicity

The hydrophilic nature of flax fibers causes it to swell in the presence of moisture. The swelling co-efficients and sorption curves of both elementary and technical flax fibers and their epoxy and polymer based composites are studied through hygrothermal aging experiments [57]. In the study by Lu et. al, the sorption curves were fit to Park's prediction model. The degradation of the tensile strength properties in flax composites due to moisture uptake was also studied [57]. Damage mechanisms like fibre splitting and interface debonding typical to moisture degraded flax composites are observed. The damage mechanisms are predicted to be possibly due to the differential swelling stresses generated from the difference in swelling rates of fiber and matrix. Abida et. al also studies the sorption and swelling characteristics of flax composites by demonstrating the use of such parameters [3].

Moisture uptake is measured as the percentage weight gain of the composite. The rate of moisture absorption increases rapidly with respect to time till an equillibrium moisture content percentage is reached, at saturation of the composite material, for the given climate conditions. Moudood et. al presents an overview of the trends seen in sorption curves and equillibrium moisture content at different relative humidity levels of flax composites [64] with relevant citations, along with a literature overview of moisture absorption related effects on the different components of the flax composite structure. Micro-cracks in matrix due to differential swelling of the phases is seen to cause a decrease in flexural strength of composite. The tensile strength at break is seen to increase for some composites and decrease for others depending on the type of matrix used [64].

Scida et. al presents the climate chamber ageing of flax composites to observe a decrease in the Young's Modulus with increase in moisture absorption, increase in strain at failure and slight decrease in tensile strength. This is estimated to be due to the plasticization of the matrix and re-orientation of micro-fibrils due to moisture [83]. The re-orientation of micro-fibrils is concluded to occur at lower strain levels with increase in aging time through acoustic emission tests [10]. The micro-fibril re-orientation is proposed to be activated and accentuated due to moisture absorption. Reversible aging mechanisms like fiber swelling are found to occur at lower temperatures, and irreversible mechanisms such as hydrolysis of matrix, development of micro-cracks in matrix, chemical degradation of fiber surface and interface debonding are observed at higher temperatures by studying aging, damping and dynamic modulus tests [74]. The reversible and irreversible degradation mechanisms in flax composites are further elaborated through immersion tests, and the process of degradation is characterized through ageing experiments and novel experimental methods such as FTIR spectroscopy and microscopy images of damage [56]. Water is sorbed at the capillarities such as the lumen and progressively over the interface open-

ings and consequently causing cracks and permanent changes to the chemical constitution of fiber and matrix as seen in Figure 6 [56].

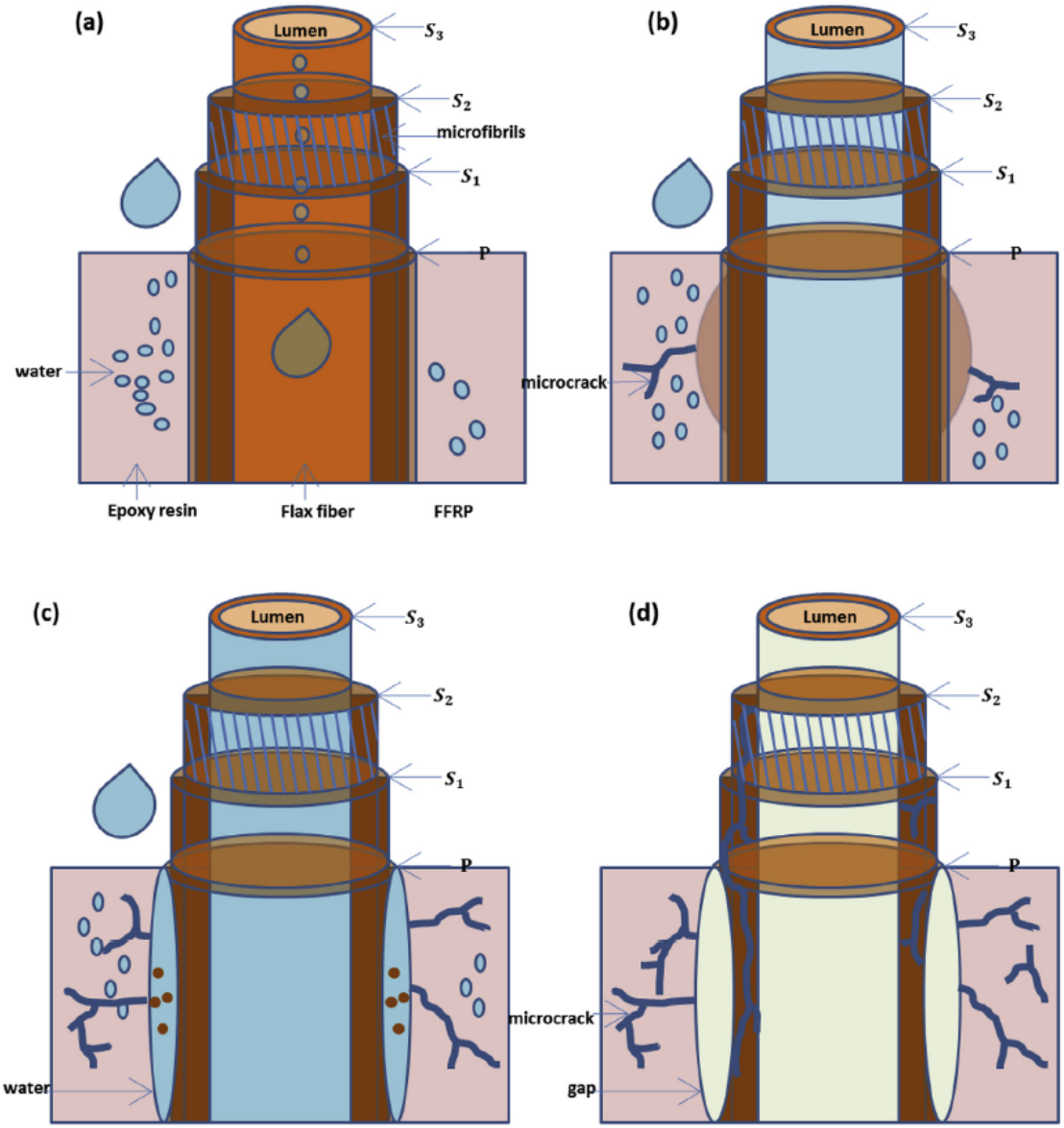

Figure 6: Degradation mechanism progression due to hygrothermal aging of flax composites [56]

Hygroscopic expansion co-efficients are used as a material parameter to define swelling as the increase in strain with respect to the moisture concentration increase of fibre and/or composite. While studying the hygroscopic expansion of flax fibers in composites, Le Duigou et. al estimated the hygroscopic expansion co-efficients of single flax fibres using Environmental Scanning Electron Microscopy [36]. The water content in the fibres is also estimated through weight variation measurements during the composite manufacturing process and the sorption isotherms are plotted for the composites.

Lu et. al studied the hygroscopic swelling co-efficients and behaviour of the matrix, single fibers and composites. Sorption isotherms were plotted for the constituents at different Relative Humidity Levels [57].

Abida et. al derived the hygroscopic swelling co-efficients for flax yarns and its reinforced resin composites [3]. The tensile properties were also determined. The hygroscopic swelling co-efficients of yarns were found to be comparable to that of flax fibers.

The effects of moisture degradation in composites can be studied by simulating in different environments corresponding to the application. Chow et. al studies the degradation of mechanical properties of some bio-based composites due to moisture and temperature induced effects [31], Arbelai et. al studies the same of sisal fiber reinforced polypropylene composites [8]. George et. al studies the same but for short flax fibers by modifying the fiber and matrix and in chemically treated pineapple leaf fibre reinforced low density polyethylene composites [38]. Thwe et. al studied the long term moisture absorption effects on the combined tensile and fatigue properties of bamboo-glass hybrid fibre reinforced composites [87]. baley et. al studied the sea-water ageing of flax-PLA resin composites where several specialized experimental techniques are used to identify and study the various degradation mechanisms [1]. Scida et. al and Li et. al use immersion tests at different temperatures to extensively study and delineate the process of degradation in flax-fibre composites in through various specialized experiments to isolate and characterize the respective degradation behaviour intrinsic to the phases of the composite [83] [56].

Generally, the experiments involve water immersion or humidity controlled tests at varying temperatures for composites. Uptake is intrinsic to hygrothermal aging. It explains the trends in the water absorption through the composite when undergoing hygrothermal aging and its relation to chemical and physical changes within the composite (micro)structure due to degradation mechanisms. The water absorption (weight gain) of the composite over time is fitted with a suitable moisture uptake model as a standard to describe and derive the moisture absorption parameters of the composites studied. Fick's model [37] generally corresponds to when a composite absorbs moisture rapidly for a certain period of time, eventually reaching a saturation plateau in equillibrium with exposed environment. It does not account for irreversible damage mechanisms which result in anamolous uptake, where the water absorption trend varies from the conventional Fick models. Carter performs an extensive study about a Langmuir-type anomalous model in epoxy resin composites [25]. Saidane et. al studied the 3D moisture diffusion parameters for longitudinal flax composites and fit Fick's Model [79]. The key conclusions for the hygroscopicity of flax fibers are as follows:

- Moisture degradation is accelerated and accentuated by increasing temperature and RH level (water content)
- Flax fiber is responsible for most of the moisture absorption in flax composites
- Moisture absorption causes reduction in tensile strength and modulus of the flax composite and its constituents
- Interface opening is estimated to be the crucial damage mechanism in moisture degraded flax fiber composites

The moisture from the environment is absorbed by the composite. The moisture is absorbed initially through the lumen of the fiber and by matrix. The differential swelling of fiber and matrix causes internal stresses at the fiber-matrix interface. Interface opening occurs at the fiber-matrix interface along with micro-cracks at the matrix, near the interface. The interface openings and micro-cracks drive further moisture absorption and subsequent degradation of fiber and matrix. The moisture degradation mechanisms in flax-composites are listed in Figure 7

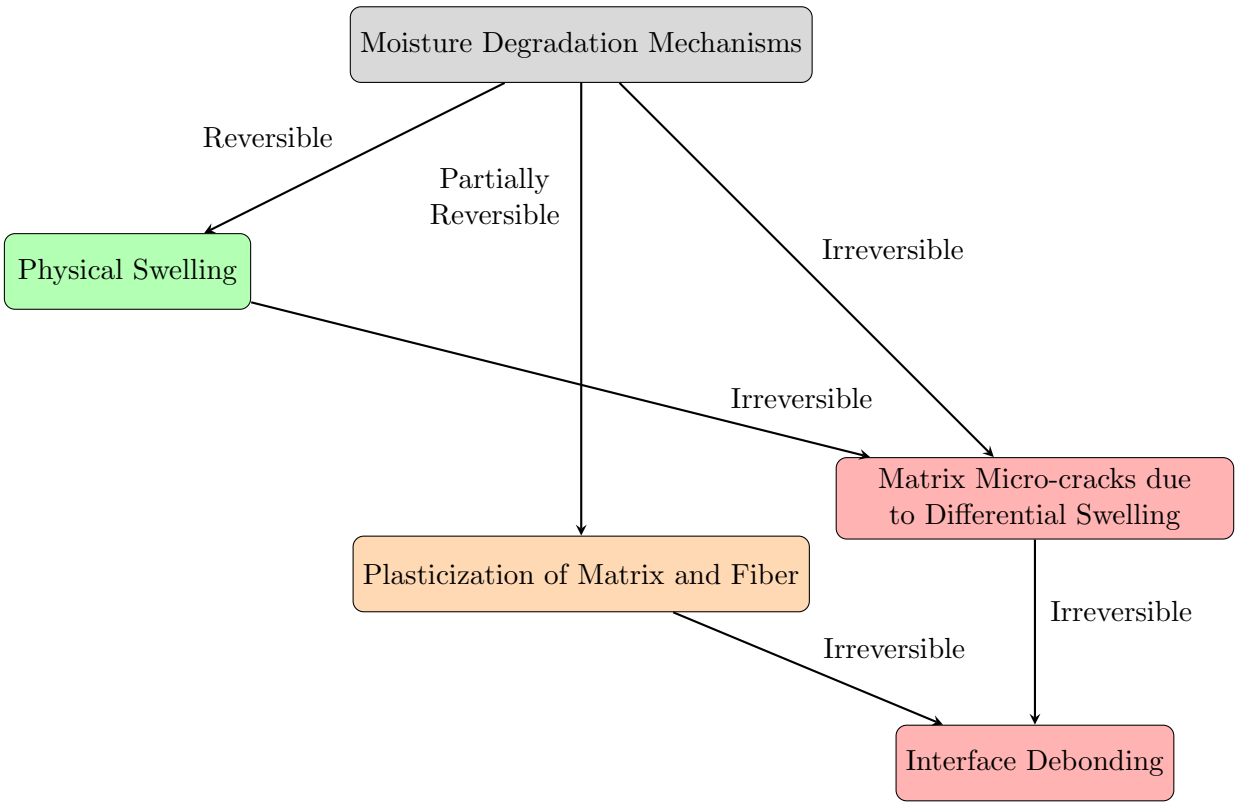

Figure 7: Flowchart of Moisture Degradation Mechanisms

Interface debonding is found to be a crucial damage mechanism due to moisture absorption. It is estimated that absorption of moisture may have a significant impact on the transverse mechanical properties of flax composites due to the interface loading in this configuration. There is presently a significant lack of articles on transverse tensile properties of flax composites [13] and on the combined moisture absorption effects in transverse flax composites [26] to the author's best knowledge. Therefore, a numerical simulation of transverse tension in flax composites is modelled to gain insights into the interface loading in the transverse configuration of flax composites. The model is supported and validated with experiments on transverse flax composite specimens. Differential swelling drives interface debonding in flax composites and therefore is given utmost importance in modelling.

3 Numerical Modelling of (Bio)Composites

Numerical modelling efforts in bio-based composites are predominantly seen to be an additional segment of experimental work in literature. There are independent staggered efforts in different areas of numerical modelling of bio-based composites. An overview of the numerical modelling efforts is presented below.

Regazzi et. al modelled the reversible degradation in short flax fiber composites [73] in addition to assessing the reversible and irreversible degradation processes as part of another study by the same author [74]. The model employs a two-stage moisture uptake model which provides a good fit to the experiments. Dynamic elastic modulus of the composite with respect to water content change was studied which enables non-destructive testing of tensile stiffness degradation. Orthotropic swelling was related to hydric strains as a part of the total strains, which was activated beyond an initial swelling concentration. Swelling was proved to be predicted with sufficient accuracy. The young's modulus of fiber was back-calculated. Joffre et. al modelled the swelling in cellulose fibers [48] and compared experimentally in a non-destructive manner with X-Ray Microtomography. A laminate analogy considering fiber angle orientation was used to calculate the composite properties from constituents.

In an attempt to numerically predict the visco-plastic behaviour in fully natural composites, Rubio Lopez et. al [78] makes use of rheological elements to capture non-linear elastic, viscous and plastic behaviour in the composite. These model parameters are experimentally fitted using relaxation tests on jute/flax/cotton-PLA composites. Three approaches are also delineated in the numerical modelling of flax-fiber composites, by citing relevant literature for the same. The strain-rate dependence on stiffness of the composite is well-captured, except for cotton-PLA composites because of the dependence of yield strength on the frictional element. In conclusion, viscous behaviour is attributed to flax fibers warrantedly. Poilane et. al [71] creates a phenomenological numerical model of polymer reinforced with flax fibers as a visco-elastoplastic material, separating elastic and inelastic strains attributed to state laws and free potential variables, with parameters (validated by identifiability analysis) derived naturally from experiments. Repetitive Loading Tests and creep tests differentiate elastic and inelastic behaviours well. The methods of preparing fibers and composites and yarns are explained clearly with citation of relevant literature.

Sliseris et. al carried out numerical modelling of both short flax fibre and flax fabric reinforced composites [84]. Prior modelling efforts cited were improved upon in the current effort. Extensive mesh generation considering the effects of bundle geometry, defects and fibre orientation was carried out. The fiber, defects and interface were defined by a brittle material model and the resin with Von-Mises plasticity with isotropic hardening. The damage evolution is shown over increase in strain to be first occurring in the fiber defects, followed by plastic deformation close to fibre damage and fibre endings. The dependency of tensile properties with respect to fiber orientation, length/diameter ratio of fibres is given. The weave geometry of the yarns are explicitly modelled in resin for the flax fabric composite. Yan et. al managed to obtain the different properties of flax yarns and fibers through experimental efforts [94] with sufficiently accurate prediction of the same, which were used in the models by Sliseris et. al. The transverse modulus of the reinforcing phase was predicted.

Keryvin et. al analysed the visco-elastic behaviour of flax fibres at the micro and nano scales [50]. Prior literature of time-dependent behaviour of plant fibers is cited in the work. A rheological Maxwell model is fit to relaxation experiments at the fiber micro-scale and to nano-indentation tests at the nano-scale. Trivaudey et. al describes the non-linear

tensile behaviour of elementary hemp fibres using an anisotropic visco-elastic constitutive law in a material rotating frame [90].The study by Trivaudey et. al is the second part to an experimetnal study by Placet et. al [70]. The causes of tensile non-linearity are cited from literature along with other constitutive models. A theoretical micro-fibrillar angle orientation dependence with increasing tensile stress is formulated. Visco-elastic parameters are identified with creep tests. A Dislocation model is employed. A strain-induced crystallisation law was used. A good fit between FEM and experiments was obtained for different analyses.

The study by Beakou et. al is an extension of a study describing the experimental methods employed to study by Charlet et. al [28] in order to characterize interface strength of fibers within a bundle where a bi-linear cohesive zone model is employed with the middle lamella characterized through optical micrographs [15]. A calibration model with a pair of fibers was created to validate the non-linear algorithm adapted from experiments and the scale-up law used, which is then used to predict the tensile strength of bundle of fibers as gauge length varies. The interface as a Cohesive Zone Model between fibers in a bundle is modelled.

3.1 Representative Volume Element (RVE)

Meshes of the 2D Representative Volume Elements at the microscale, satisfying periodicity at the boundaries were generated using the Hades module from Jive, where $(n_f)^2$ fibres with a specified diameter are positioned randomly by colliding with each other at a specified velocity and displacement. The generated meshes only contain elementary fibers. The same method of RVE mesh generation was used in [76].

Initially, looking inside the yarn, meshes are generated ranging from the smallest 1 X 1 RVE that can be seen in Figure 8 to a full yarn 18 X 18 RVE that can be seen in Figure 9. The mean diameter and volume fraction of the fibers in yarn bundles from 4.1.1 were used for mesh generation representation. The generated RVEs are capable of only elementary, circular fibers and matrix elements. The interface around the circular fibers can be defined as well. The packing of fibers is random. The fibers can never be in contact but can be closely spaced depending on the mesh generation criteria, such as length of the RVE, diameter and volume fraction of the fibers.

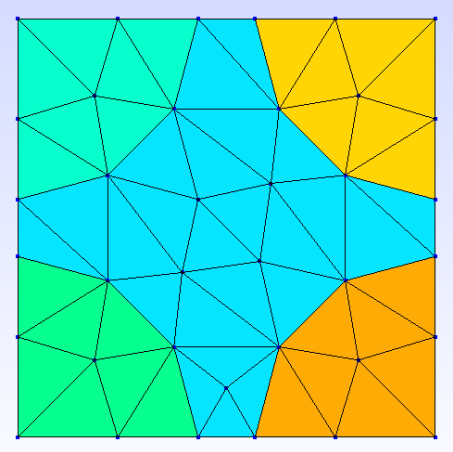

Figure 8: 1x1 RVE of an Idealised Yarn Bundle - Blue colour indicates the matrix

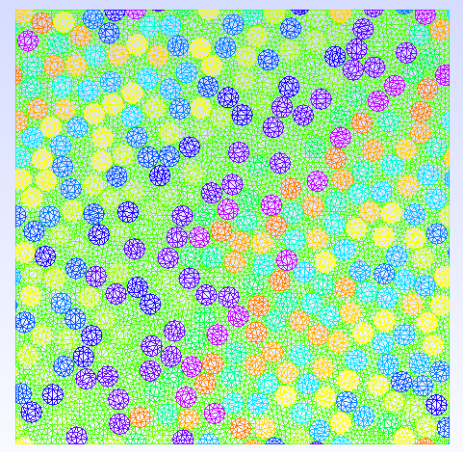

Figure 9: 18x18 RVE of an idealised Yarn Bundle - Green colour indicates the matrix

For the final analysis 2D 7x7 RVE meshes were generated and used with a fiber diameter of 19 micro meter [11] with a fiber volume fraction of 28% as determined for the manufactured transverse flax composites through analytical formulae. For the analyses us-

ing literature parameters, RVE meshes were re-generated as required based on the volume fraction and geometry parameters as used in the literature.

3.2 Continuum Mechanics Model

The material models used for simulating the matrix, fiber and interface in the numerical model are listed below. The models are taken from [76].

3.2.1 Linear Isotropic Material

The stress-strain relationship for a 2D linear isotropic material is given as follows:

$$\begin{bmatrix} \sigma_{xx} \\ \sigma_{yy} \\ \tau_{xy} \end{bmatrix} = \begin{bmatrix} E & \nu E & 0 \\ \nu E & E & 0 \\ 0 & 0 & G \end{bmatrix} \begin{bmatrix} \varepsilon_{xx} \\ \varepsilon_{yy} \\ 2\varepsilon_{xy} \end{bmatrix} \tag{1}$$

Where:

σ_{xx}, σ_{yy} - in-plane normal stresses
τ_{xy} - in-plane shear stress
$\varepsilon_{xx}, \varepsilon_{yy}$ - in-plane normal strains
ε_{xy} - in-plane shear strain
E - Young's modulus (elastic modulus)
ν - Poisson's ratio
G - Shear modulus

Flax fibers are modelled as linear isotropic assuming transverse isotropy and plane strain conditions. Constitutive models accounting for the characteristic deformation behaviour of natural fibers are studied in [90] [50], and of natural fiber based composites in [6] [71].

3.2.2 Elasto-Plastic Material

The pressure dependent elasto-plastic material formulated by [62] is used to model the epoxy to include plasticity effects due to swelling in the epoxy. The model behaves elastically until the yield stress is reached. A paraboloidal yield criterion is used in the model using the compressive and tensile yield strengths, σ_c and σ_t respectively. The volumetric deformation in plasticity is defined using a non-associative flow rule. Elaborate details about the yield criterion formulation can be found in [62]. For this thesis work, damage using fracture strength of the epoxy is not modelled.

3.2.3 Cohesive Zone Interface

The interface used [76] between phases of the composite is a cohesive zone model based on [91] and [92] based on a damage traction separation law that is activated only in tension. The development of cohesive tractions in compression is prevented in P by applying the $\langle x \rangle = (x + |x|)/2$

$$t = [I - d_i P][\![u]\!] \tag{2}$$

Damage is defined based on the intial and final equivalent displacement jumps normal to the interface surfaces, which are in turn dependent on the single mode displacement jumps at damage onset and final opening. The initial and final equivalent displacement jumps are defined based on their relationship between the shear energy dissipation and total dissipation.

The single mode displacement jumps at damage onset and final opening are based on the specified fracture toughness from experiments and initial stiffness values. Extensive details of the cohesive zone interface model can be found in [76].

3.3 Solver & Software Tools

Numerical modelling is done with the modelling software Jive and using the prediction model for glass-fiber composites as seen in [76]. The numerical analysis of swelling in composite is carried out with values from literature and experiments. One important assumption for modelling is transverse isotropy of fibers and matrix within the 2D RVE element of the composite cross-section. The framework for numerical modelling is as follows:

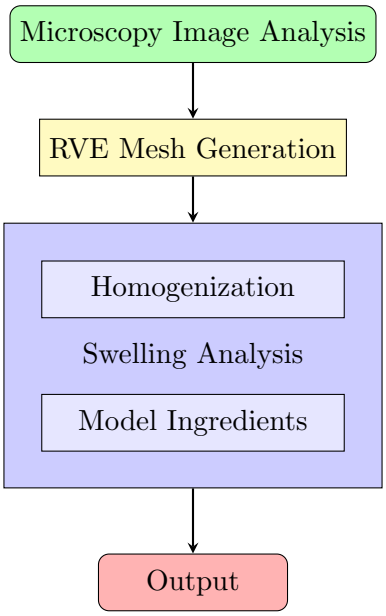

Jive is an open-source numerical analysis software based in C++ that employs models and modules to allow the user flexibility to define and solve complex partial differential equations [66]. The existing prediction model used for hygrothermal aging and tensile behaviour in laminated composites in [76] is based on Jive and contains model ingredients defining required physics, loading, analysis methods and material model contributions to behaviour of glass composites.

FE Homogenization FE^2 homogenization is used in [76] to model swelling and degradation in a coupled multi-scale analysis to model diffusion at the macro-scale. The resulting strain and concentration are passed to each embedded micro-model material point. Assuming constant water concentration for the each respective diffusion step at each embedded micro-model material point in the macro-scale, the resultant micro-scale stresses and tangent stiffness are homogenized and upscaled to the macro-scale. In the context of this thesis work, FE Homogenization coupled with Periodic Boundary Conditions (PBCs) is used to ensure consistent homogenization of mechanical properties of the phases to simulate swelling at the micro-scale. The theory behind FE homogenization is as follows:

The volume average of a function $f(\mathbf{x})$ (micro-field such as stress or strain) for each of the phases over RVE the domain ω is given by:

$$\langle f \rangle = \frac{1}{|\omega|} \int_{\omega} f(\mathbf{x})\, d\omega \tag{3}$$

Hill's law [43] states:

$$\langle \sigma : \epsilon \rangle = \langle \sigma \rangle : \langle \epsilon \rangle \tag{4}$$

Equation 4 ensures consistency of energy levels of the microscopic stress and strain fields with that of the effective energy of the homogenized composites as long as the RVE is representative of the macroscopic scale. The RVE should be representative in terms of capturing sufficiently the structural heterogeneity of phases and the number of inclusions, ensuring surface traction and displacement to be 'macroscopically uniform' [43].

The average stress $\langle \sigma_{ij} \rangle$ and strain $\langle \epsilon_{ij} \rangle$ are then given as [88]:

$$\langle \sigma_{ij} \rangle = \frac{1}{\omega} \sum_{e=1}^{n_e} \omega_e \left[\sum_{I=1}^{n_e int} \sigma_{ij}(y_I) \cdot J(y_I) \cdot W(y_I) \right] \tag{5}$$

$$\langle \epsilon_{ij} \rangle = \frac{1}{\omega} \sum_{e=1}^{n_e} \omega_e \left[\sum_{I=1}^{n_e int} \epsilon_{ij}(y_I) \cdot J(y_I) \cdot W(y_I) \right] \tag{6}$$

To ensure consistency with Hill's Law and the FE homogenization of effective properties in its requirement with respect to boundary conditions, PBCs are used to represent the infinite continuation of the RVE at the edges.

Periodic Boundary Conditions Considering two opposite boundaries $\partial\omega^+$ and $\partial\omega^-$ where each point x^+ is associated with a unique point x^- on each respective boundary, that are termed the so-called master and slave nodes where displacement continuity is ensured [88], the following Equation 7 holds true.

$$u_i(x_1, x_2, x_3) = u_i^0 + u_i^*(x_1, x_2, x_3) \tag{7}$$

where,

$$u_i^0 = \epsilon_{ij}^0 x_i j$$

As stated in Equation 7, the displacement at each node of the opposing boundaries, is a combination of the contributions due to constant linear displacement and microscopic heterogeneity of the RVE elements/phases. Therefore, given the kth pair of parallel boundaries $k+$ and $k-$ and that u_i^* is identical at the 2 parallel boundary surfaces due to periodicity [88], the following displacement constraint holds true:

$$u_i^{k+} - u_i^{k-} = \epsilon_{ij}^0 (x_j^{k+} - x_j^{k-}) \tag{8}$$

Traction continuity conditions are given as [88],

$$t_i^+ = -t_i^- \tag{9}$$

where,

$$t_i = \sigma_{ij}^0 * n_j$$

$$n^- = -n^+$$

The traction and displacement difference boundary condition are specified for PBCs. In the model used for the thesis based on [76], the corner node 0 is fixed so that rigid body motions are restrained.

3.4 Moisture Swelling Model

Linear isotropic material models are used for both fiber and matrix elements in the mesh to simulate swelling of the composite. The interface is also modelled as seen in 3.2.3. The initial analysis is performed with mechanical parameters and swelling properties obtained from literature and back-calculation as seen in Table 2. The parameters are changed to observe the effect of geometry and material degradation on the composite swelling and stresses. An iteration with an elasto-plastic material model for matrix is performed to account for plasticization of matrix.

Moisture uptake is simulated as a concentration step loading from 0 to 1, in 10 steps using the Multiphysics Module from Jive. A plane strain isotropic material model is used for all the analyses. The maximum swelling strain is defined for the final concentration step for fiber ($\varepsilon_{f,max}$) and matrix ($\varepsilon_{e,max}$) respectively. The maximum swelling strain of each phase is used to represent the swelling coefficient required for the isotropic material model definition for fiber and matrix. During the analysis, the concentration increases equally at all integration points within the micro-scale RVE. The swelling strain computed at each fiber/matrix element is the result of the multiplication function between the concentration at every step and the input final swelling strain of the respective fiber/matrix element. Therefore, at the final concentration step, all fiber/matrix elements swell up to its maximum swelling strain, as defined in its isotropic material model input. The resultant internal stresses and the composite strain are homogenised for the RVE. The bottom left node is restrained in x and y directions to prevent rigid-body motions. The bottom right node is restrained in y direction to prevent rotations of the RVE. An example of a 7x7 RVE from the base model RVE mesh from sensitivity analysis is given with the boundary conditions in Figure 10.

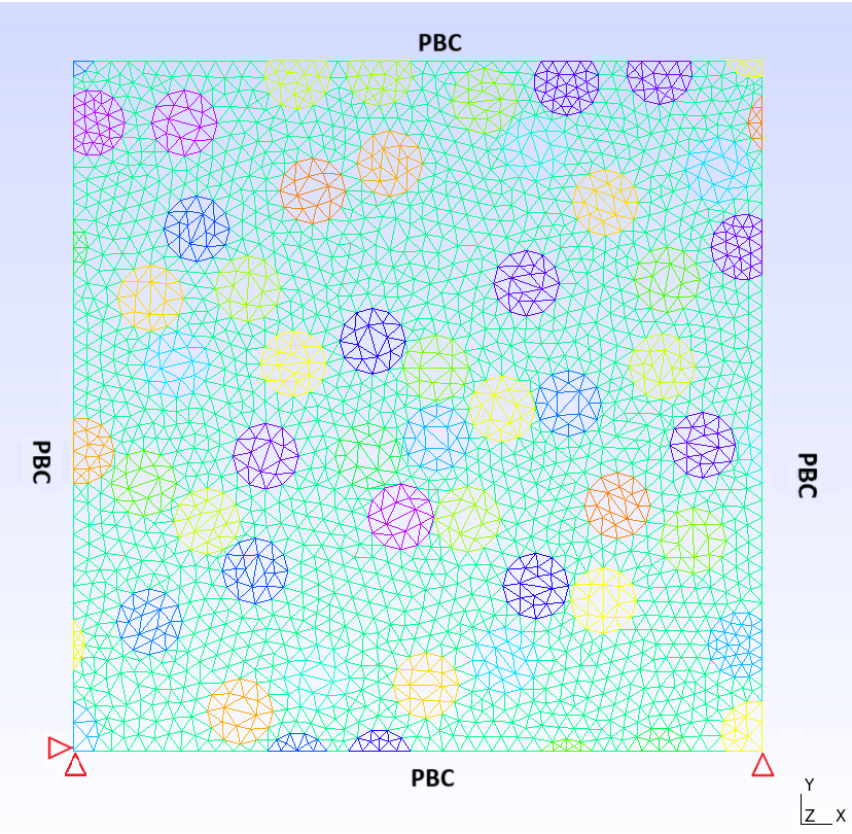

Figure 10: 7x7 RVE Mesh for the Base Model - Green colour indicates the matrix

Interfaces based on the Cohesive Interface Material are created at all the fiber-matrix interfaces. Periodic Boundary Conditions are ensured at all the RVE edges. The Boundary

Line element from the Jive package is used with the Newton-Cotes 2 integration scheme for the interface elements. The 'FlexArcLen' solver is used to solve for equllibrium in the swelling analysis. The solver traces complex equillibrium paths by switching between displacement control and energy-based arclength control methods. All respective solvers, models and modules are taken from [76] and the related research group.

4 Model Parameters

An experimental campaign is carried out to study and characterise the effects of moisture absorption in transverse flax-fiber composites. The swelling due to moisture absorption of both the epoxy and transverse flax composites was studied. Tensile tests were performed on transverse flax composite specimens and neat epoxy resin specimens. The tensile tests were conducted for both aged and pristine samples to get an idea about the material degradation. The main motivation of the experimental study was to extract the modelling parameters of importance for simulation of transverse tensile tests and swelling of the composite material that is missing from literature and that corresponds to the material being used. The degradation mechanisms of importance were studied with the experimental campaign.

4.1 Experimental Campaign

The epoxy resin used was the 2511-1AL, in combination with the hardener 2511-1BL, both from the manufacturer SWANCOR [93]. Natural flax fibers with no chemical treatment were used, as specified by the manufacturer. The fibers used were the L-FLAXTAPE-200 from EcoTechnilin [45].

The epoxy resin and hardener were mixed in the ratio of 100:30 as per manufacturer specification. The epoxy-hardener mixture was then de-gassed in the de-gassing vacuum chamber to remove air from the mixture. This mixture was then used to manufacture the neat epoxy resin specimens and the flax composite plates.

A 3D printed mould negative was created to make flexible moulds for epoxy resin. Dog bone shaped silicon moulds were prepared from the negatives to prepare the neat epoxy specimens. The epoxy-hardener mixture was poured in the silicon moulds. The epoxy resin specimens were allowed to cure Figure 12 for 48 hours in the moulds at room conditions. The neat epoxy resin specimens were removed from the moulds and then post-cured in the auto-clave at 70° Celsius for 48 hours.

It is important to note that the manufactured neat epoxy specimens had uneven thickness due to slight flow during curing and bends because of the flexible and inconsistent silicon mould geometry. The specimens were still sufficient to be used within the scope of this thesis work.

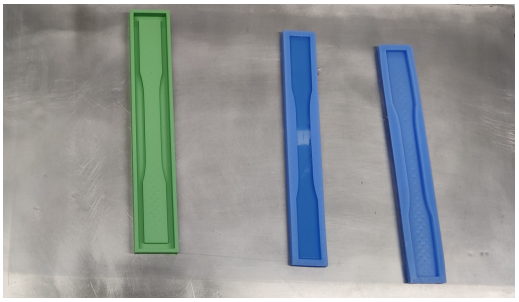

Figure 11: Neat Epoxy Resin Specimens Manufacturing

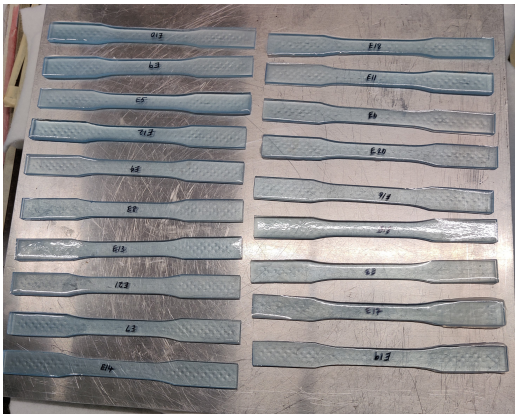

Figure 12: Manufactured Neat Epoxy Resin Specimens

8 plies of the flaxtape fiber mats Figure 13 were cut and stacked in between steel plates. The plates were confined to be vacuum-infused with epoxy-hardener mixture. Two plates of uni-directional flax-fiber composites were manufactured by the process of

vacuum infusion Figure 14 of resin along the fiber direction. The composite plates were post-cured in the auto-clave for 48 hours at 70° Celsius. Dog bone shaped cutouts of the composite were made using the water jet cutting process to obtain parallel-sided transverse specimens of the flax-fiber composites.

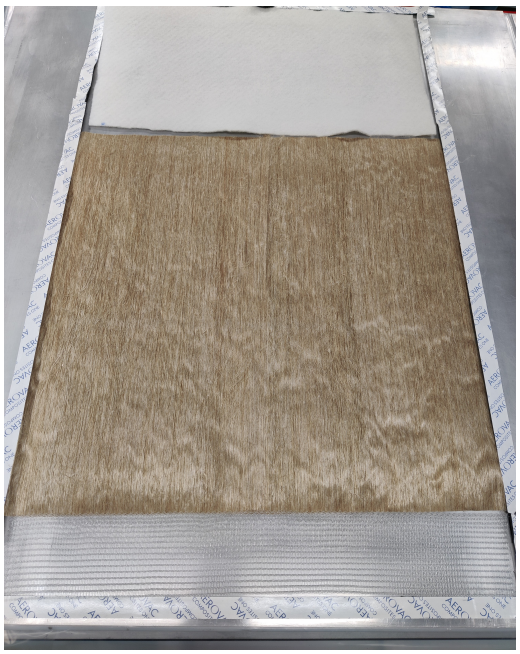

Figure 13: Flax Fiber Mats

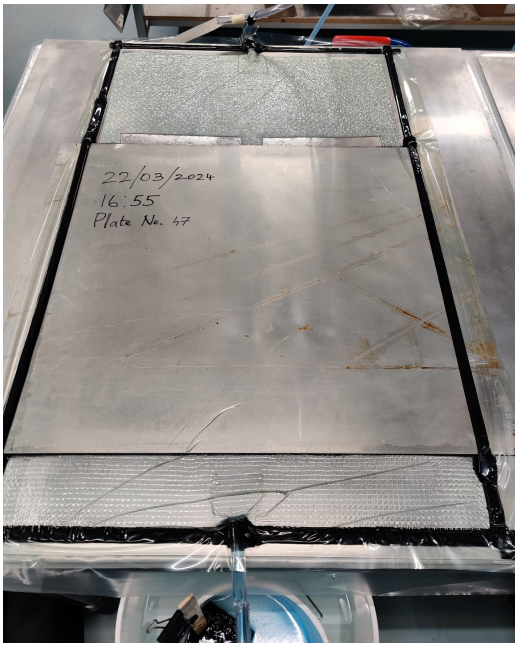

Figure 14: Vacuum Infusion Manufacturing of Flax Fiber Composites

4.1.1 Fiber Geometry, Distribution & Volume Fraction

First, the microscopy images of the cross-section are analysed to get the geometry distributions of the fibers. The geometry distributions pertaining to fibers in yarns, yarns, and fibers used for the manufacturing of composites in this thesis work is presented. The geometry parameters of fibers are also compared with, and taken from literature as necessary. Methods used for image analysis are discussed and suggestions are made for improvements in the same. With the results of the image analysis of the microscopy images of composite cross-sections, an idealized 2-D Representative Volume Element mesh is generated using the HADES module from Jive. Swelling of the composite is modelled at the micro-scale using necessary model ingredients such as Periodic Boundary Conditions, FE Homogenization and material model definitions for matrix and fiber. The assumptions for modelling, model ingredient definitions and results are discussed.

Microscopy images of the cross-section of [0-90-0]S flax yarn coupons (6 ply) were used to quantify of the areas of individual fibres and yarn bundles along with their respective area fractions. The focus of the geometry parameter quantification was restricted to only within the yarn bundles for yarn composites. Therefore, images with a scale length of 100 micrometer were found to be most suitable for the analyses. A reference image is presented in Figure 15. The black surfaces that can be seen in Figure 15 are possibly porosities/voids in the matrix or artefacts from polishing but it is still unclear what they are. The effects of porosities like lumen and voids in the matrix are not considered in the numerical models.

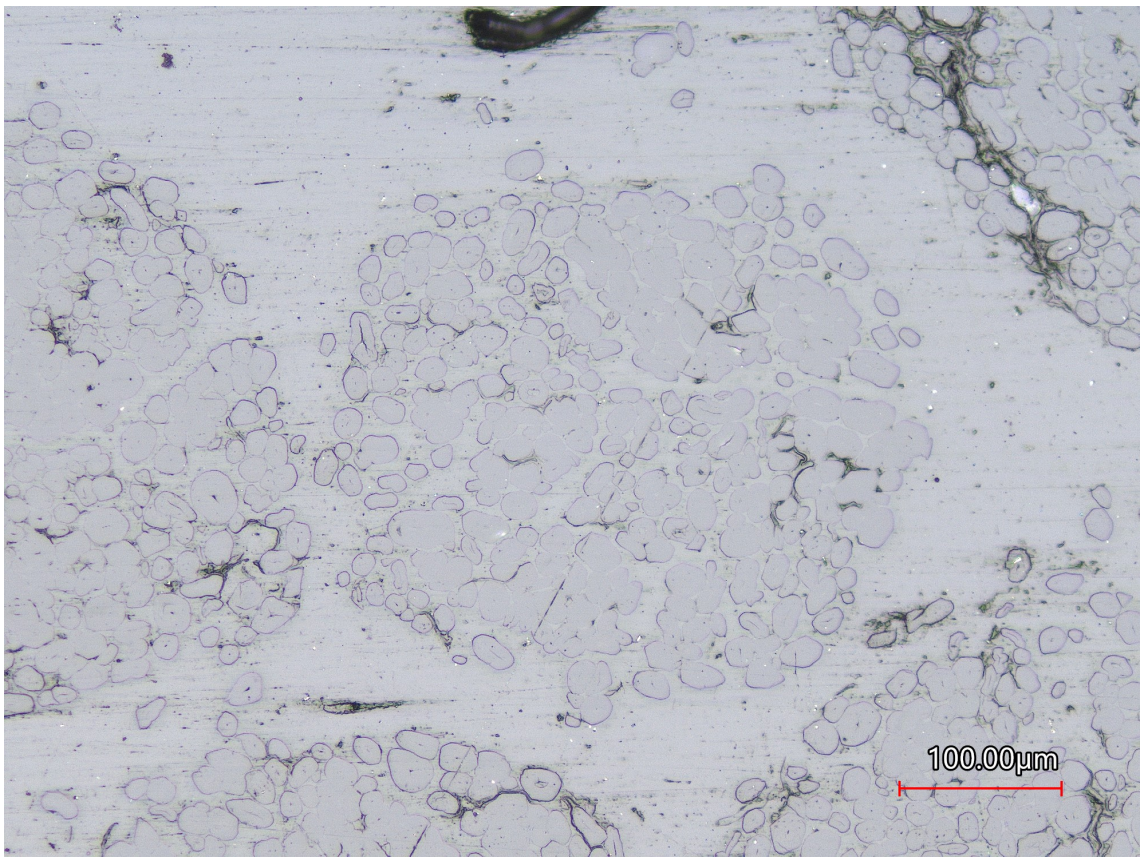

Figure 15: Reference Microscopy Image of a flax yarn composite cross-section

The tools used for image analysis are OpenCV [24] and ImageJ [81] and its derivatives. OpenCV is a Python package that provides general image manipulation and analysis functions based on pre-defined algorithms. OpenCV was found to be more suited for automating identified case-specific routines/workflows with a standardized input of images. On the other hand, ImageJ comes with a handy Graphical-User-Interface (GUI). It is a Java based, open source software. ImageJ is application oriented for use in microscopy image analysis. ImageJ is widely used for microscopy image analysis in fields like medical imaging and materials science. ImageJ has derivative software like Fiji [80] and plugins like ilastik [16] that expand its functionality and add specialized methods of analysis to the base software of ImageJ.

Image Basics and Input Images are generally discretized into pixels on computers, with each pixel representing a pre-defined color within a chosen color spectrum. The size of the image, or resolution (height, width) is measured in pixels. The microscopy images are originally captured in the RGB spectrum. In the RGB spectrum, the pixel values present in each color range (Red, Green and Blue) are in the range [0,255]. Different colors are obtained for each pixel by adjusting the red, green and blue color pallette values within the range. The entire image size is 32-bit which is made up by combining the red, green and blue 8-bit channels. Histograms of the image can be studied to observe the dominant pixel values in the images, that helps make an initial estimation of distinct features in the image. A cropped and resized version of Figure 15 and its histogram in the RGB spectrum is shown below in Figure 16 and Figure 17. The overlap of the color ranges already indicate that the features of the image do not have sufficient distinction in pixel color values.

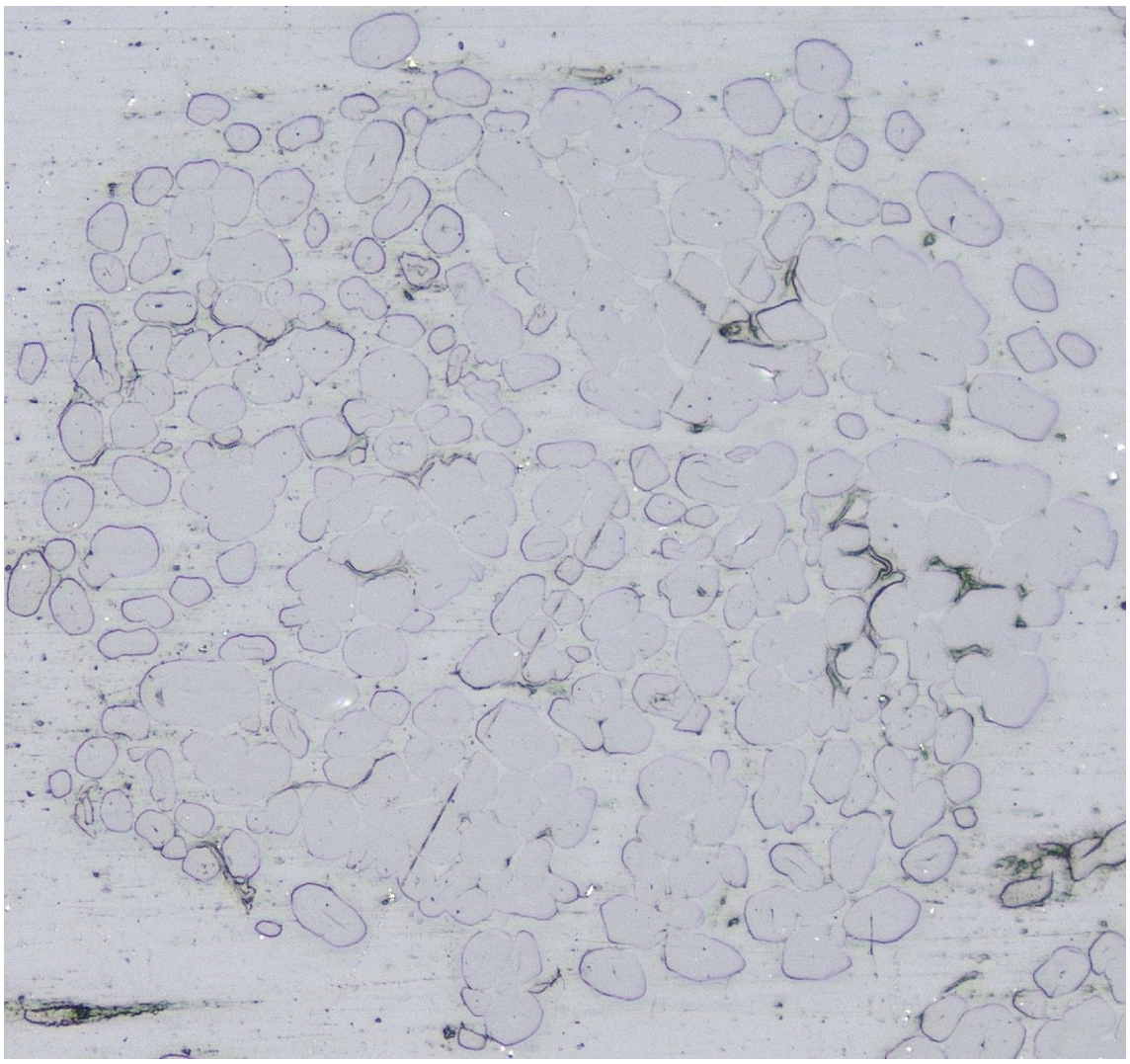

Figure 16: Reference Microscopy Image Figure 15 Cropped & Resized

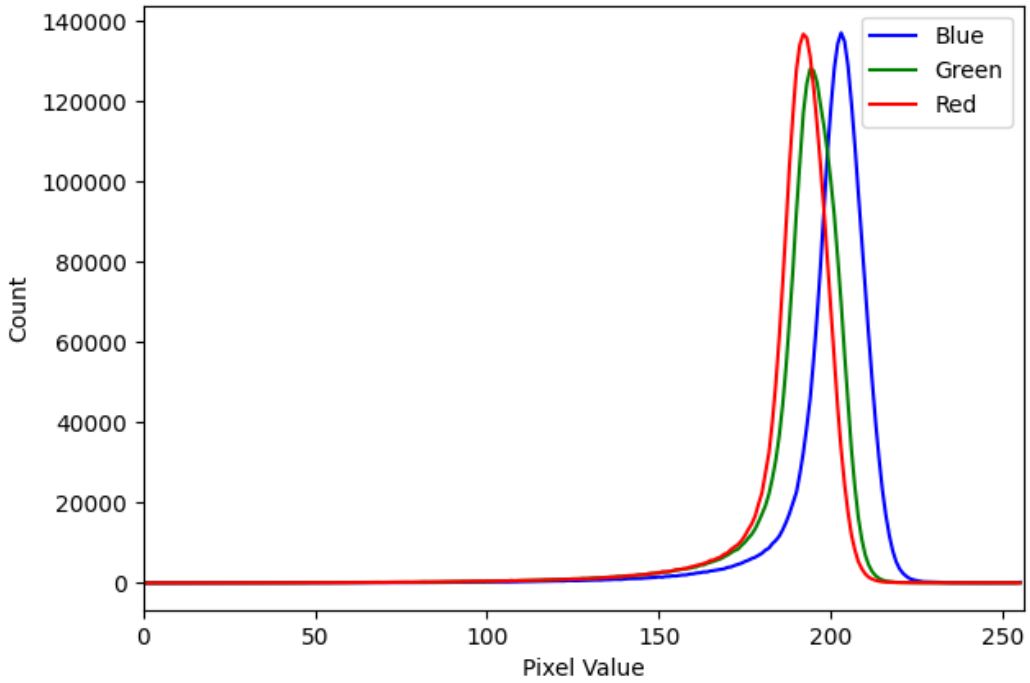

Figure 17: RGB Spectrum Histogram of Figure 16

Image Conversion and Pre-processing The images are first converted to grayscale for ease of processing. Grayscale conversion reduces the image size from a 32-bit RGB spectrum file to an 8-bit single spectrum image. The image software identifies the pixel value ranges of the image in the form of arrays and stores them in the memory of the computer for further manipulation. The images can also be split into each channel spectrum of the RGB range, which can then be used for further manipulation. Pre-processing algorithms such as Gaussian Blur, which smoothen the image are used to reduce noise and grain artefacts present within the image. Watershedding algorithms allow averaging of pixel values in the image based on the common pixel values in its vicinity. Pre-processing depends on user-choice, based on sound judgement with the goal of obtaining the best suited binary image when thresholded

Thresholding After pre-processing the image using pre-defined algorithms suitable for the specific use case, the final step is to use thresholding filters to convert the image to a binary image (black and white) that can be used to segment and measure area of the inclusions/features in the ImageJ software. The best possible thresholding is achieved when there is a significant distinction in pixel values of the features.

Area Of The Fibers The reference image from Figure 16 was used to analyse the area of the fibers. The RGB image was input into the software and converted to HSV (Hue, Saturation, Value) scale. The HSV spectrum was selected for the image after extensive testing on different color spectra to obtain a suitable binary image for segmentation, after pre-processing of the image. Finally, the pixel values were band-pass filtered in specific ranges chosen to obtain maximum distinction between inclusions and matrix. The image was smoothened using Gaussian Blur. After pre-processing using OpenCV, the image was input into ImageJ and thresholded using the default filter in order to segment the image using the 'Analyze Particles' function by specifying approximate circularity and size values based on an initial estimate of the areas of the inclusions. The areas of the fibers were

also measured by fitting ellipses to the inclusions manually and measuring with ImageJ. The resultant images are presented in Figure 18 and Figure 19.

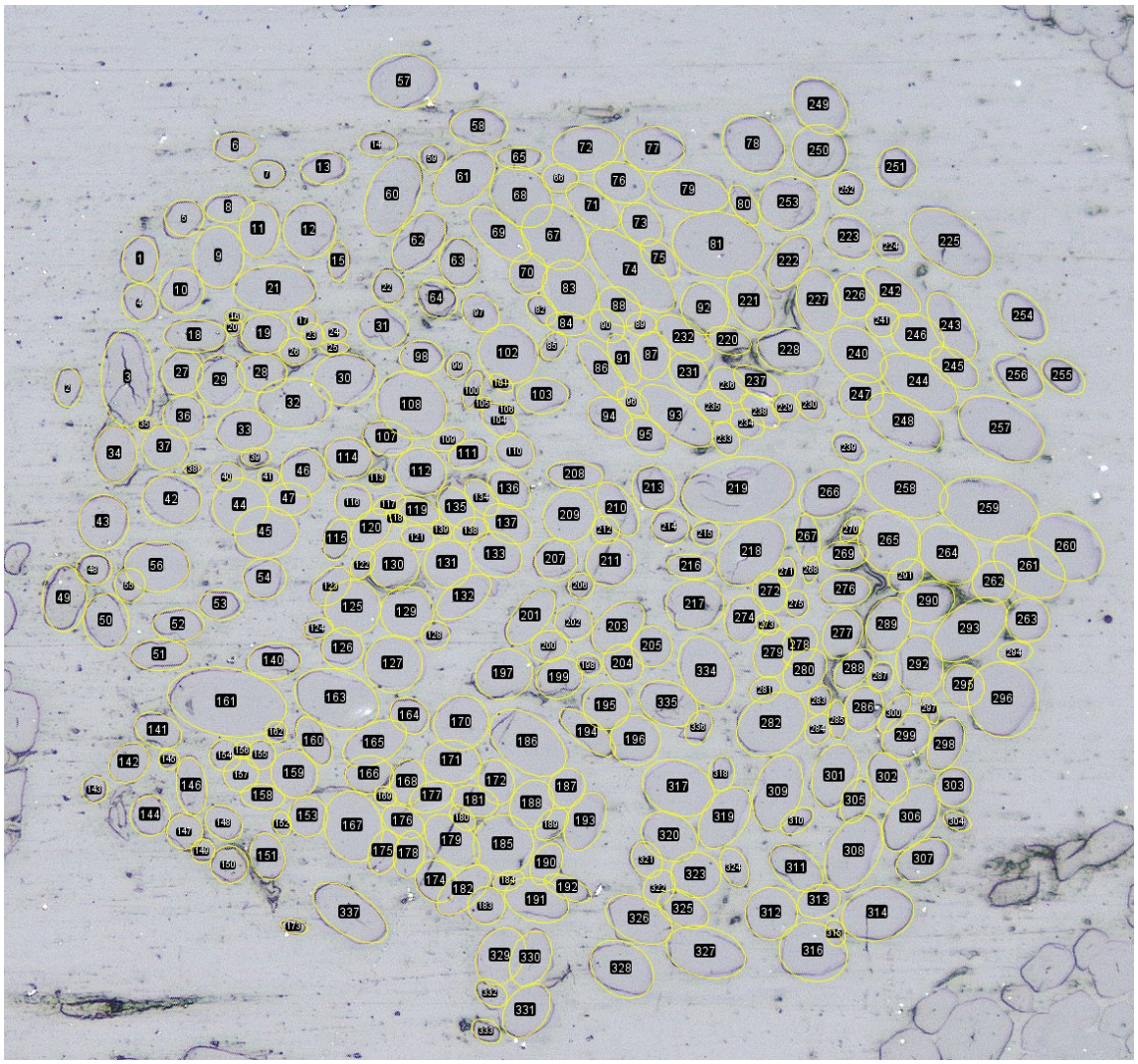

Figure 18: Manual Segmentation of Elementary Fibers of the Processed Image Figure 16

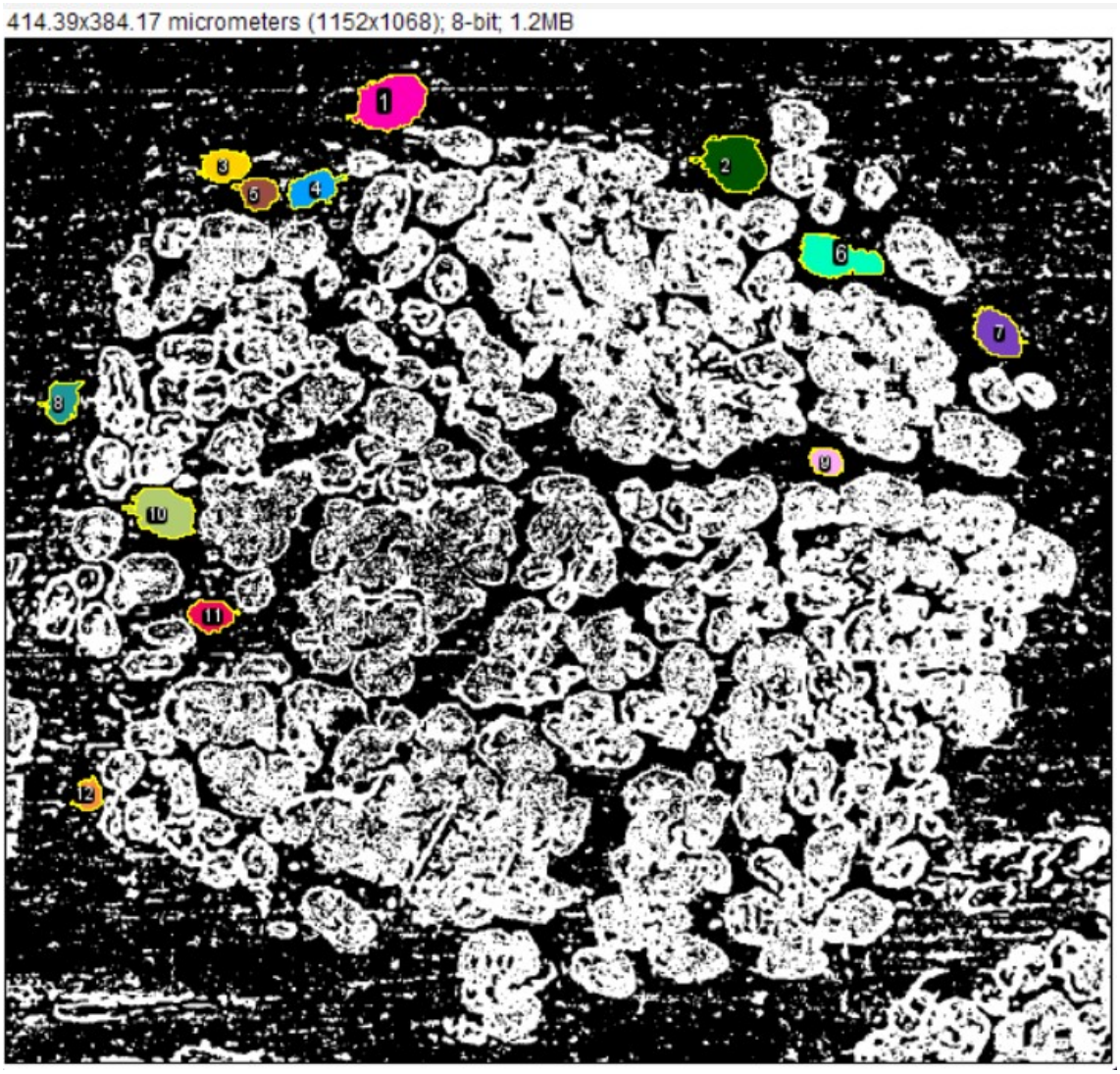

Figure 19: Automatic Segmentation of Elementary Fibers of the Processed Binary Image Figure 16

Statistical distributions of the diameters of fibers are derived for both automatic segmentation and manual fitting. The diameters of fibers are estimated to be the length of the minor axes of the fitted ellipses for both automatic segmentation as well as manual fitting. The statistical distributions of diameter and area of the fibers are presented in Figure 20 and Figure 21.

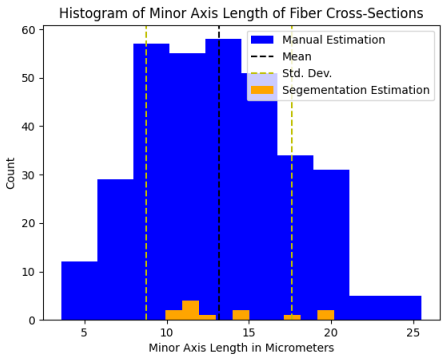

Figure 20: Histogram of Minor Axis Length of Fiber Cross-sections

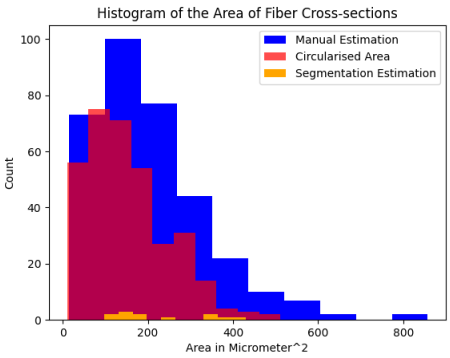

Figure 21: Histogram of the Area of Fiber Cross-sections

Area of the Yarns The area of the yarns was measured manually by drawing ellipses on microscopy images of uni-directional flax fabric reinforced composites using ImageJ. The binary image was obtained by thresholding after heavy pre-processing using erosion, dilatation, minimum value filters methods. Automatic segmentation of the binary image using the watershed algorithms proved unfeasible. Therefore, only the results from manual fitting are presented below in Figure 22. The histograms of the diameters and areas of yarns, similar to the fibers, are presented in Figure 23 and Figure 24, respectively.

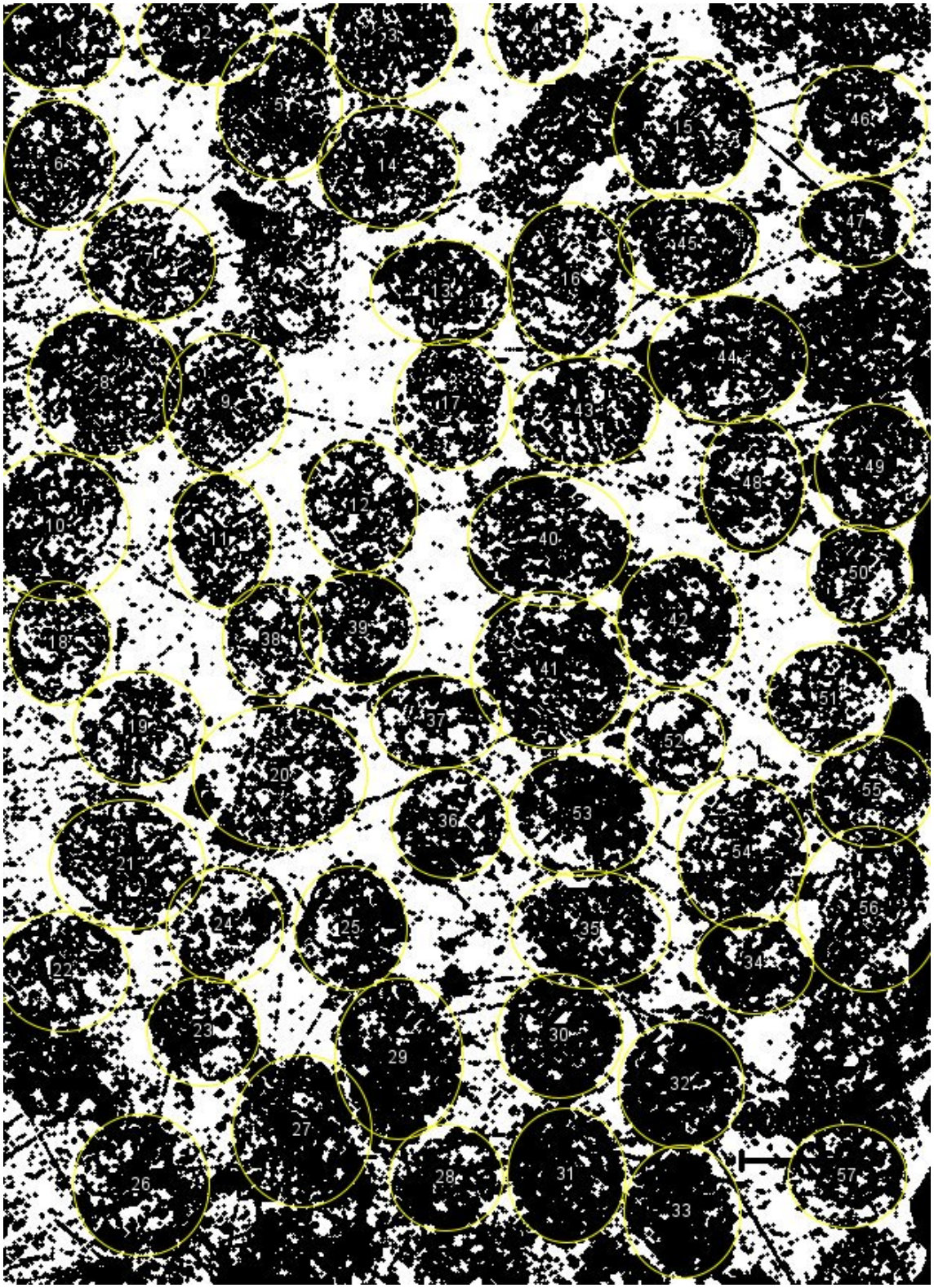

Figure 22: Manual Segmentation of Yarn Cross-sections

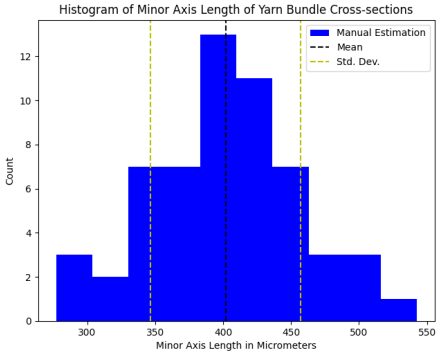

Figure 23: Histogram of Minor Axis Length of Yarn Bundle Cross-sections

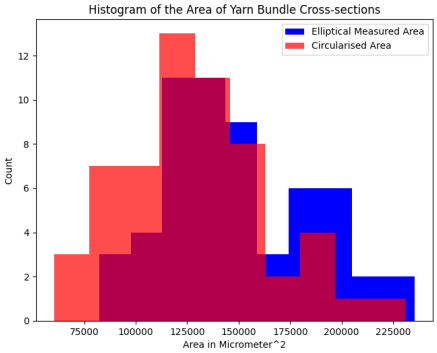

Figure 24: Histogram of the Area of Yarn Bundle Cross-sections

Area Fractions For the measurement of area fractions, the microscopy image from Figure 16 was used. More microscopy images of 6-ply, [0-90-0]s with a scale of 100 micrometers were used with ilastik [16], a pixel classification plugin with ImageJ to discern the fibers from matrix in a more consistent manner within a yarn. The segmentation involves labelling and marking individual constituent phases. The fibers and matrix from the images had to be classified using a marking tool and the AI model would then automatically classify the image between fibers and matrix based on the selections and its pixel value similarities. The batch classification option produced inconsistent classification of fibers from matrix for images as a batch so each image had to be individually segmented after marking the phases. The area fraction was measured as the percentage of the area of black marked inclusions with the area of the white matrix background, within the selected cross-section of each yarn as seen in Figure 25 and Figure 26. The area fractions were also estimated manually to compare with the automatic segmentation. The histogram for the measured area fractions of fiber content within the yarn can be seen in Figure 27

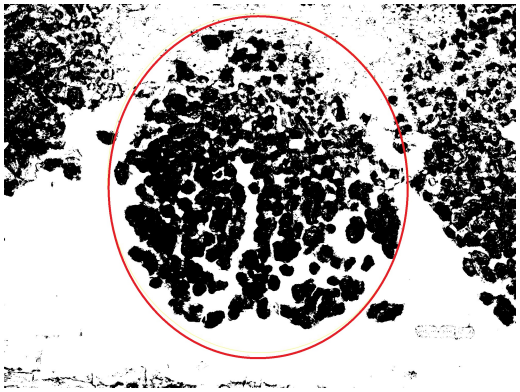

Figure 25: Area Fraction Measurement Binary Image 1 Ilastik

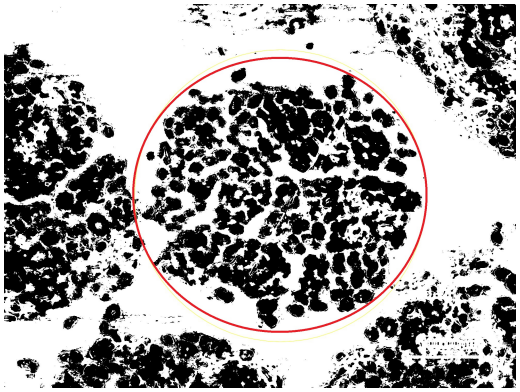

Figure 26: Area Fraction Measurement Binary Image 2 Ilastik

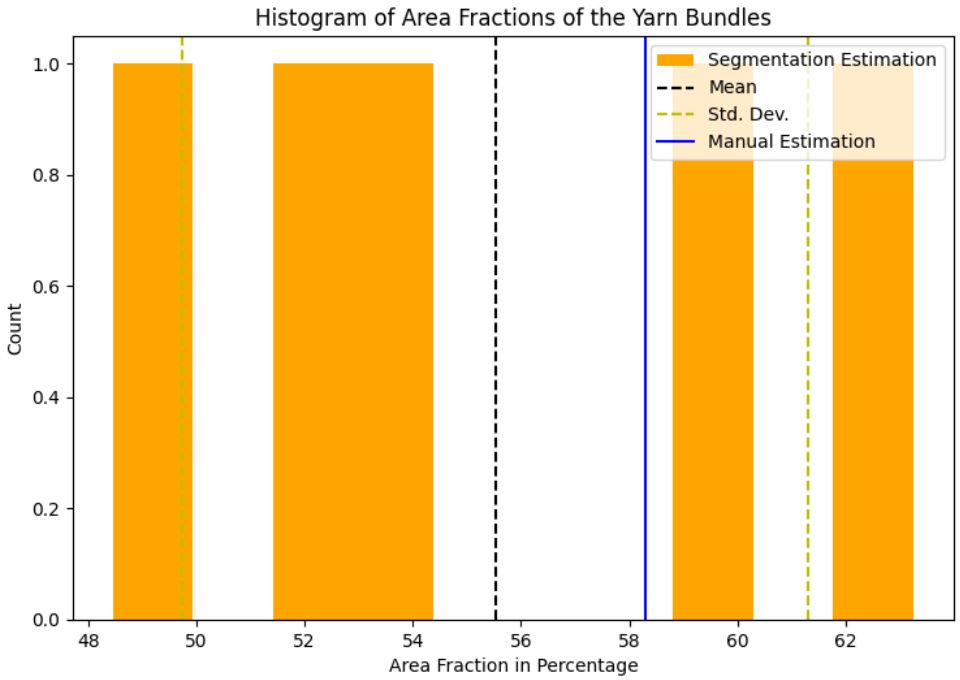

Figure 27: Histogram of Area Fractions of the Yarn Bundles

Microscopy Images of Transverse Flax Composite Specimens In order to validate the models, observe how failure occurs and to see the behaviour of composite due to moisture degradation, microscopy images were taken of the cross-sections of transverse flax composite specimens. Microscopy image analysis was performed on the transverse flax composite specimens to obtain a more accurate representation of the fibers for the RVE mesh. Samples were cut from pristine composite slabs and at the fracture surface of the tensile breaks. Pristine samples were embedded in resin and polished to view under the microscope. The cut composite samples were also moisture degraded till saturation and embedded in resin and polished before microscopy imaging. The fiber volume fraction is also compared with the microscopy images.

Pristine Composite Specimens The images of the pristine state composite are shown below in Figure 28. Here, pristine composite refers to the composite specimens cut from the slabs at room conditions.

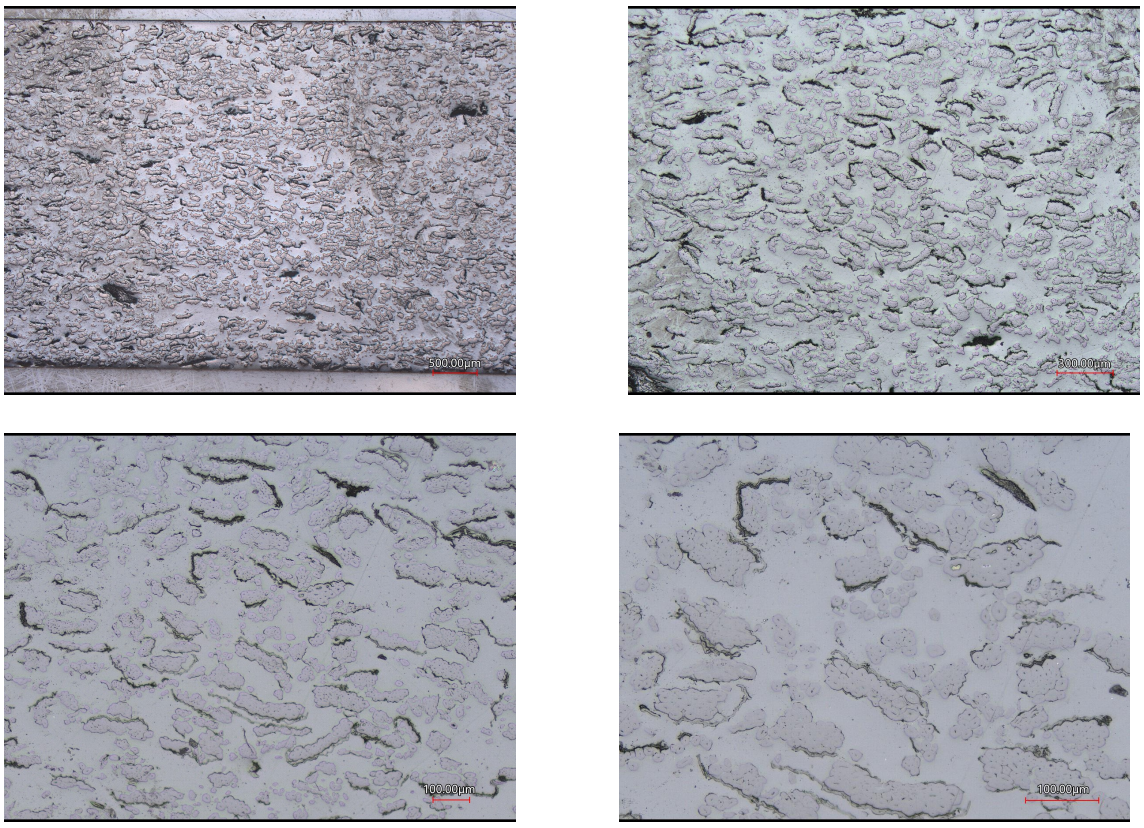

Figure 28: Pristine Flax-Epoxy Specimen Microscopy 1

The figures show that the composite has a really high fraction of technical fibers. There is a high local volume fraction of fibers within different zones of the cross-section. The lumen porosity is significant within the fibers. It is still unclear how the black spots seen on the cross-section of the composites from microscopy images arise. It could be from the polishing of epoxy embedded composite.

Fiber Diameters The fiber diameters were estimated for two images manually to compare the fiber diameters with literature and for modelling purposes.

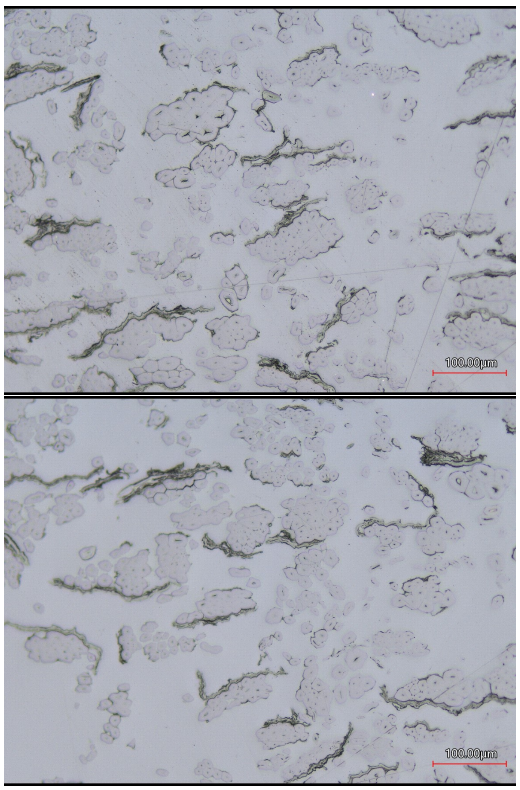

Figure 29: Microscopy Images For Fiber Ellipse Fit

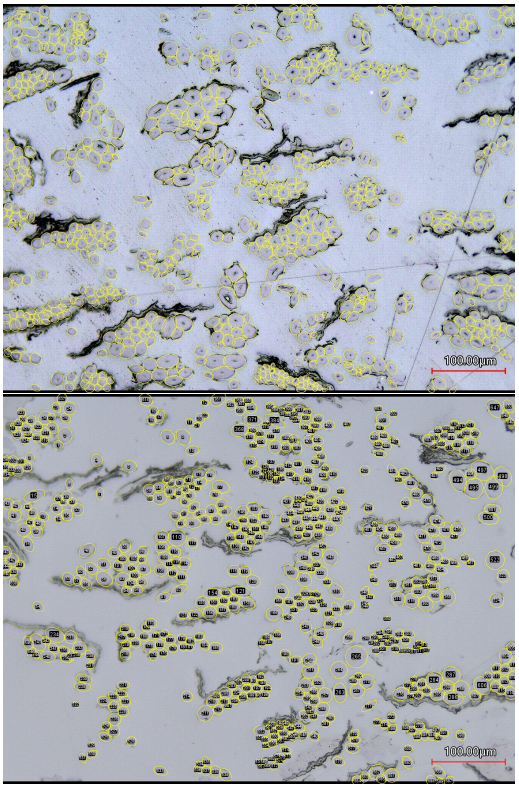

Figure 30: Fiber Elliptical Fit

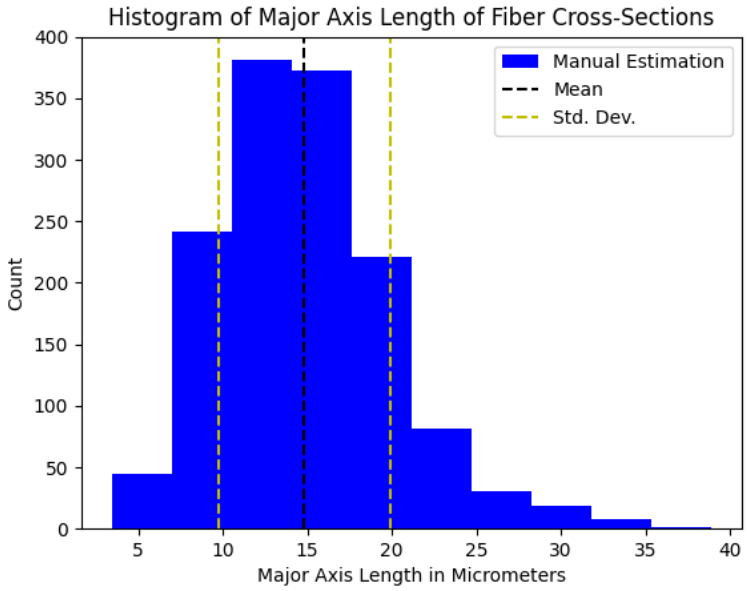

Figure 31: Major Axis Length Histogram of Fitted Ellipses from Figure 30

The fiber diameters have a mean of 10 µm with a standard deviation of around 5 µm which corresponds exactly to the sensitivity analysis fiber diameters taken from [57] as seen in 4.3.

Volume Fractions The Area fractions was estimated at different zones of binary microscopy images of the pristine composite.

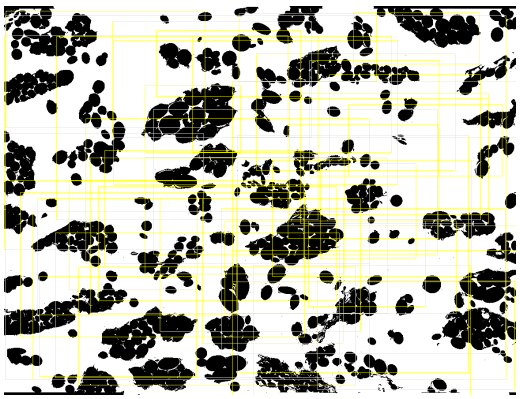

Figure 32: Fiber Area Fraction Zones

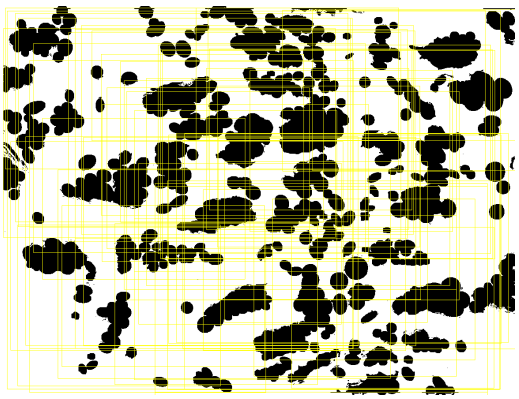

Figure 33: Fiber Area Fraction Zones

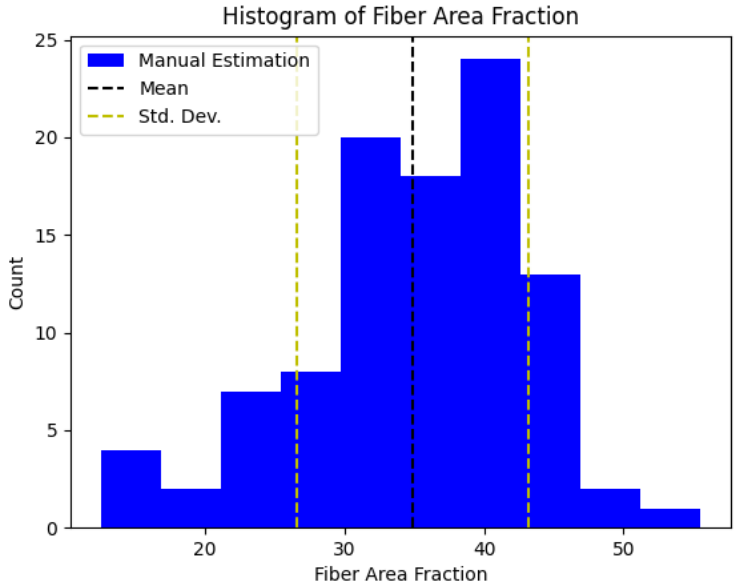

Figure 34: Area Fraction Histogram of Figure 32 & Figure 33

The histogram of area fractions for Figure 32 by itself had a mean of 28% but the histogram Figure 34 was plotted for both images combined. The local fiber area fraction due to the technical fibers is high and also in different zoomed areas of the flax composite cross-section which contributes to a change in the estimation of fiber area fractions when measuring matrix rich and fiber rich zones of the cross-section.

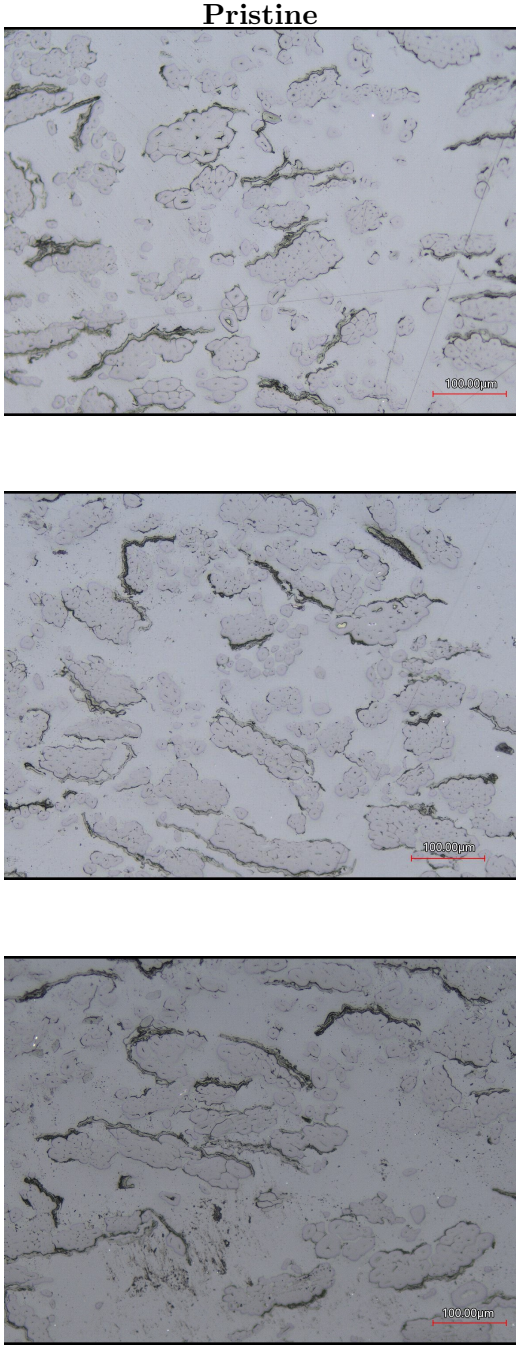

Figure 35: Pristine Flax-Epoxy Specimen Microscopy 2

Figure 36: Moisture Degraded Flax-Epoxy Specimen Microscopy

Moisture Degraded Composite Specimens The interface between fibers and between the fiber-matrix interface is opened due to moisture degradation. Although this phenomenon is seen in the pristine composite, possibly due to the moisture uptake at room conditions, it is heavily accentuated due to moisture degradation in the climate chamber. The moisture degraded composites undergo interface debonding possibly due to the differential swelling of fibers and matrix as also seen in literature.

Observations Regarding Microscopy Image Analysis

- Suitable thresholding levels isolating fibers were not achieved due to the inconsistent lighting, insufficient distinction in color (pixel values) between phases in the microscopy images which produce grainy and noisy binary images.
- Segmentation between fibers is insufficient for measurement of each fiber area but

suitable for area fractions. A better solution needs to be adopted for automatic fitting of ellipses to the segmented fibers using the ilastik plugin.

- Lumen area is ignored within the image analysis. Sometimes it can be seen to be significantly large within the fiber.
- The areas of circularized fibers are smaller than the actual elliptical areas.
- All technical fibers are separated into individual technical fibers in the manual measurements. There is no suitable segmentation adopted for technical fiber segmentation.
- The manual measurements are adopted for an arbitrary yarn bundle, therefore, only one estimate of area fraction of a yarn bundle can be produced without increasingly cumbersome effort to demarcate each elementary fiber manually.
- The pristine composite sometimes can contain cracks in the fibers and cracks and voids within the matrix, after manufacturing, which are not taken into consideration.

Conclusions Regarding Microscopy Image Analysis

- The machine learning trained ilastik plugin proves useful in thresholding images to distinguish between fiber and matrix when there is even minimal trend in pixel value distribution of features. Segmentation of fibers and batch classification of images can be explored further using ilastik.
- Segmentation of inclusions based on conventional watershed algorithms present in ImageJ are insufficient. Therefore, macros or suitable algorithms can be designed to segment the individual phases.
- The technical and elementary fiber phases could be distinguished based on the measure of contact between fibers while segmenting the inclusions. Nearest neighbour distances could be defined to ensure sufficient differentiation between technical and elementary fibers.
- The fiber inclusions could possibly be tainted with color to obtain suitable distinction between phases before microscopy.

Calculation of Fiber Volume Fraction The volume fraction of the composites was calculated using 2 methods. The first method involves calculating the volume fraction of fibers as the volume difference between composite and matrix and using weight-specific weight relations.

$$V_f = V_c - V_m \tag{10}$$

The weight of matrix is calculated as the difference between the weights of composite and fibers. The weight of fibers can be calculated as the product of areal weight of the fibers, surface area of one ply within the composite and number of plies. The areal weight of the fibers is obtained from the manufacturer datasheet and the other values were measured from the manufactured epoxy and composite specimens. The fiber volume fraction is calculated as the ratio between volume of fiber and composite.

$$V_f = V_c - \frac{W_c - (GSM_f \cdot A_f \cdot n)}{\gamma_m} \tag{11}$$

where,
W_c = Weight of the composite in g
GSM_f = Areal weight of the fibers in $\frac{g}{cm^2}$

A_f = Surface area of the fiber plies within composite in cm^2
n = Number of plies
γ_m = Specific weight of the matrix in $\frac{g}{cm^3}$

The fiber volume fraction was alternatively also calculated according to [57], with the following formulation:

$$V_f = \frac{n \cdot GSM_f}{\rho_f \cdot t} \tag{12}$$

where,
n = Number of plies
ρ_f = Density of the fiber in $\frac{g}{cm^2}$
t = Thickness of the laminate in cm

The areal weight of the fibers used is $200 * 10^{-4} \frac{g}{cm^2}$, as from the manufacturer [45]. The surface area of the flax composite was estimated to be 42.42 cm^2 from composite cutting specifications. The number of plies is 8. The specific weight of flax fiber is taken as 1.45 $\frac{g}{cm^2}$. The thickness of the laminate is 0.4 cm. The specific weight of epoxy is calculated as 1.608 $\frac{g}{cm^2}$. The density of flax fibers ρ_f is between 1.4 to 1.5 $\frac{g}{cm^2}$ in literature [21] [11].

It is important to note that the areal weight was measured to be 177.708 $\frac{g}{m^2}$ for the flax fiber mats used which is 11.5% lesser compared to what the manufacturer states. Also, the specific weight of the epoxy was measured for a single epoxy specimen, by measuring the dimensions using a micrometer, to obtain the specific weight using volume and weight relations. The calculated fiber volume fraction is therefore considered to be a rough estimate. The fiber volume fraction was estimated as 29% from Equation 11 and 27.5% using Equation 12.

4.1.2 Swelling Co-efficients

The manufactured transverse flax composite specimens and epoxy specimens were placed in the climate chamber to undergo moisture absorption under controlled temperature and relative humidity conditions. A set of epoxy specimens were also immersed in water before tensile tests to observe moisture absorption effects on the material behaviour. Swelling and moisture absorption characteristics were studied of both neat epoxy and transverse flax specimens. Tensile tests were performed on moisture degraded, oven-dried flax specimens and at room condition.

The moisture absorption is estimated as the weight gain at regular time intervals as a percentage of the initial weight of the samples Equation 13. This gives an estimate of the increase in water content in the samples. This is the most followed method in literature [57] [56] [64] [10] [83] [76]. The weight was measured on a weighing scale with least count of 0.0001 g

$$M_t(\%) = \left(\frac{W_t - W_0}{W_0} \cdot 100 \right) \tag{13}$$

The swelling of the samples is calculated in a similar manner to Equation 13 by replacing the weight for thickness. By measuring percentage increase of thickness from the initial thickness at initial water content, the swelling corresponding to the increase in water content is measured. The swelling co-efficient β is defined as the percentage increase in swelling per percentage increase in moisture content in the sample [57]. The thickness was measured with a micro-meter with a least count of 0.001 mm.

Hygrothermal Aging of Composites The transverse flax composite specimens were placed in the climate chamber which was set to 50° Celsius and 90% Relative Humidity (RH) Figure 37. The thickness variation of the samples was studied at three locations of the specimen. Thickness change was measured at the center of the sample and at an offset distance to the left and right of the centre to get an average estimate (also considering anisotropy in fiber swelling). The measurements taken were still within the central tapered width of the dog-bone specimens. The moisture content variation was obtained by measuring the weight of the samples at regular time intervals. The flax composite specimens reached saturation at around 12 days of ageing.

Figure 37: Hygrothermal Aging of the Transverse Flax Composites

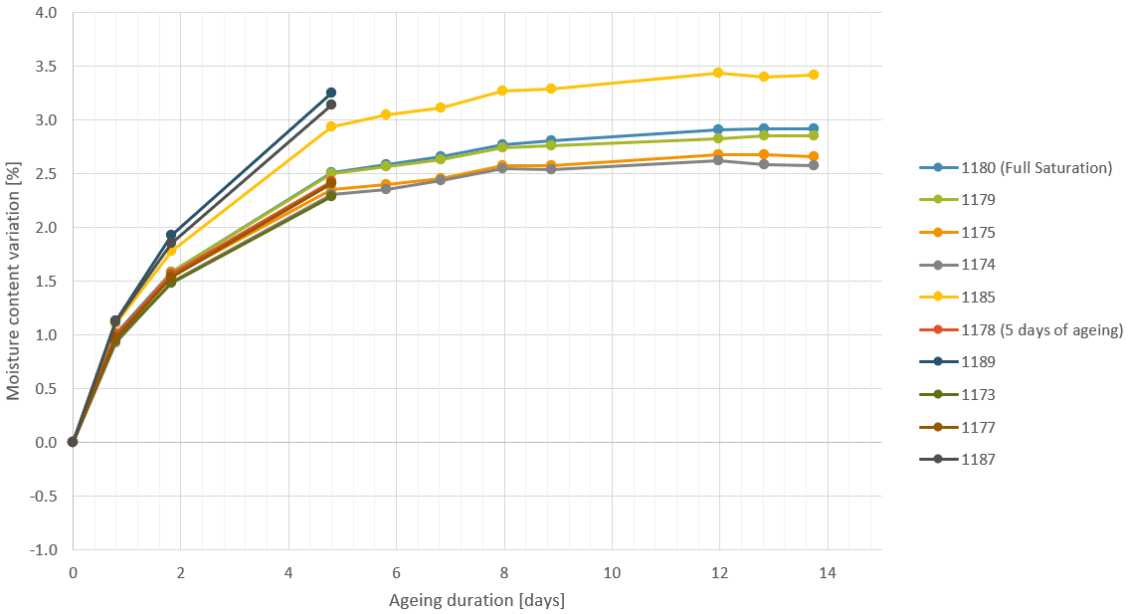

Figure 38: Moisture Absorption of Transverse Flax Fiber Composite Specimens at 50° Celsius and 90% RH

The rate of moisture uptake is rapid initially, for the first 5 days Figure 38, and then slows down to reach equillibrium after 12 days. The moisture absorption can be assumed to follow Fick's model [37] upto the observed absorption duration. It is assumed that the fiber does not plasticize here, as is also seen in literature for the given climate conditions.

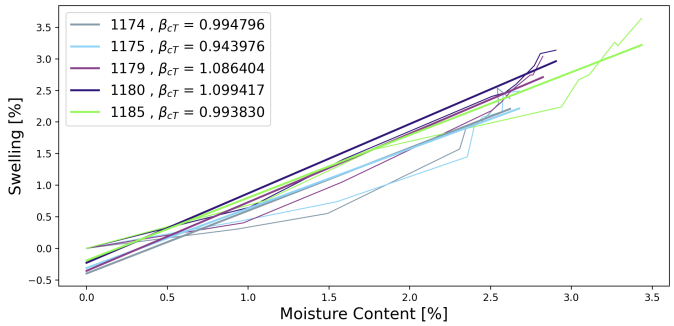

Figure 39: Linear Regression Fit of Swelling Curves of Transverse Flax Fiber Composites Specimens at 50° Celsisus and 90% RH at the Left Side

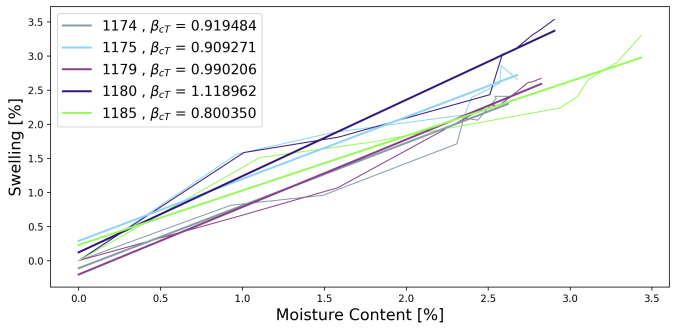

Figure 40: Linear Regression Fit of Swelling Curves of Transverse Flax Fiber Composites Specimens at 50° Celsisus and 90% RH at the Center

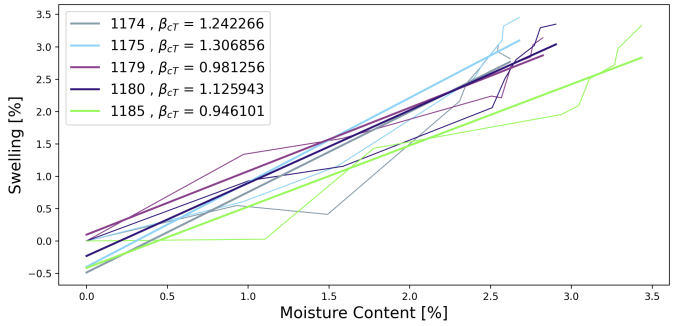

Figure 41: Linear Regression Fit of Swelling Curves of Transverse Flax Fiber Composites Specimens at 50° Celsisus and 90% RH at the Right Side

The swelling curves Figure 39, Figure 40 and Figure 41 are plotted till the point that the composite specimens reach equillibrium. The swelling at different points of the cross-section is bound to have some variation due to the anisotropy of flax fibers. The thickness swelling co-efficients of the composites β_{cT} (refers to the transverse or thickness swelling of composite) were computed as the slope of the linear regression fit on the experimental swelling curves. The obtained thickness swelling co-efficient values are higher than for longitudinal flax composites cited in literature [57], which is around 0.6 to 0.85 [3]. To the author's best knowledge, there are presently no transverse (thickness) swelling co-efficients found in literature for parallel-sided flax composite specimens for comparison.

Hygrothermal Aging of Epoxy The swelling of epoxy of different geometries was studied to get an idea of the corresponding swelling strain of epoxy at flax composite saturation to be used as model input. The epoxy samples 2 Figure 46 were broken from the dog-bone specimens. The epoxy samples 3 Figure 47 were cut at equal spacing within the tapered width dog-bone specimen cross-section.

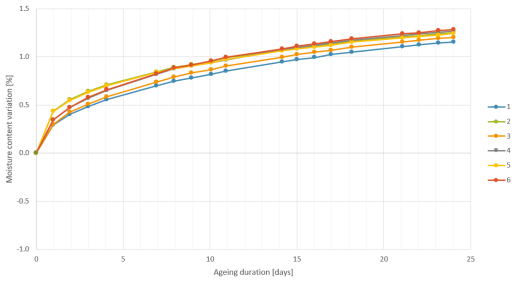

Figure 42: Moisture Absorption Curves for Epoxy Samples 2 at 50° Celsius and 90% RH

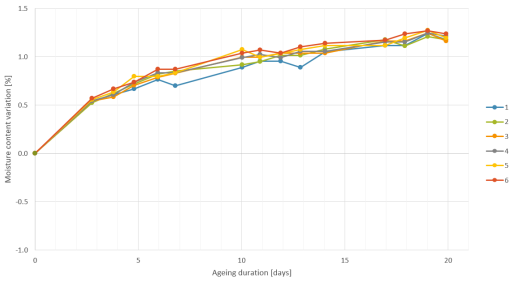

Figure 43: Moisture Absorption Curves for Epoxy Samples 3 at 50° Celsius and 90% RH

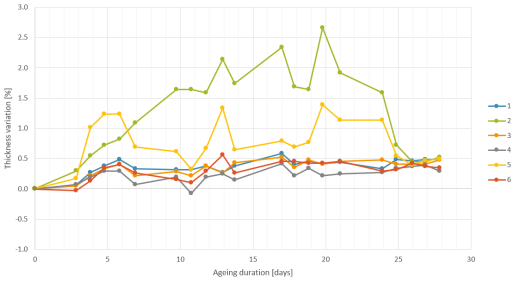

Figure 44: Thickness Variation Curves for Epoxy Samples 2 at 50° Celsius and 90% RH

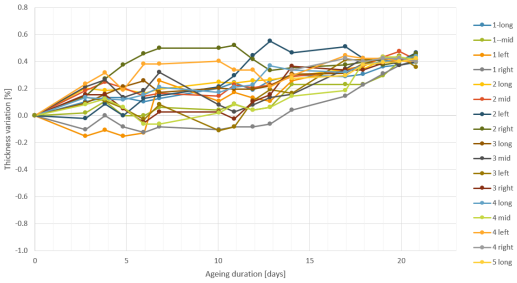

Figure 45: Strain Variation Curves for Epoxy Samples 3 at 50° Celsius and 90% RH

Figure 46: Epoxy Samples 2

Figure 47: Epoxy Samples 3

The moisture content variation was measured as weight gain at regular time intervals along with the thickness measurement. For epoxy samples 3 the swelling measurement was taken along the longitudinal direction of the sample and at 3 points in the thickness direction to get an accurate measurement of the swelling. The swelling curves for the epoxy samples 3 give a less varied and more accurate measure for swelling co-efficent, around 0.3 and for the epoxy samples 2 it was more varied, between 0.1 to 0.9.

The input for modelling is taken as the strain of epoxy at around 12 days of saturation. The value of swelling strain corresponding to the ageing duration that the composite reaches saturation is around 0.2% as the mean value. The epoxy and composites were started to be aged from room conditions respectively. It is expected that the difference in moisture uptake due to the geometry variation of the epoxy samples has an effect on the moisture absorption, but for the same ageing condition, the difference in moisture uptake does not have a significant effect Figure 48. It is clear that the fibers are responsible for a majority of the moisture absorption as also seen in [57].

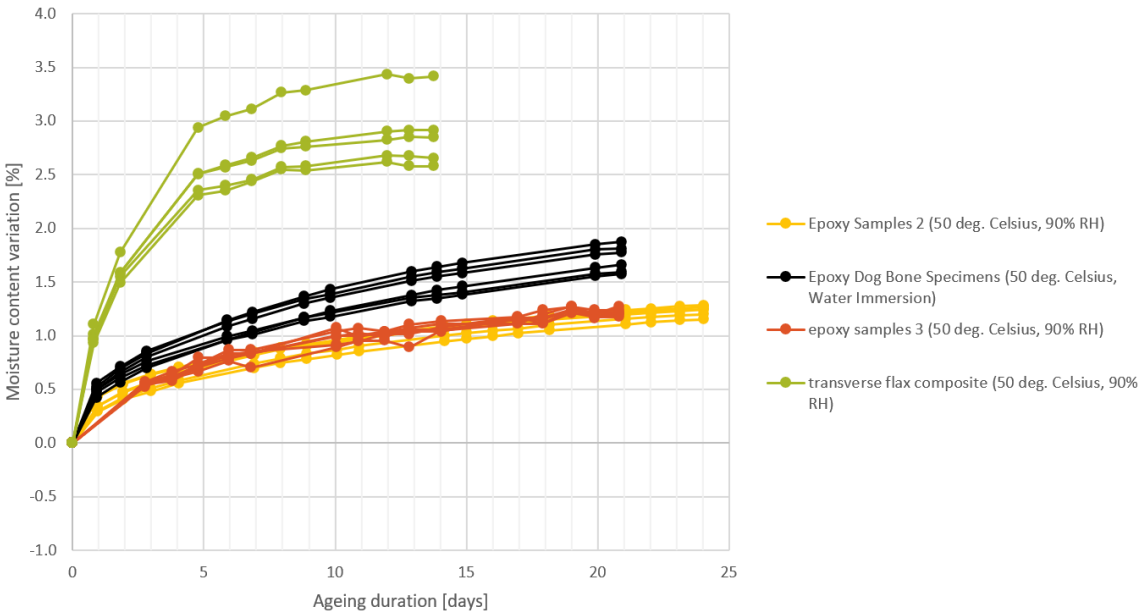

Figure 48: Moisture Uptake of Epoxy Samples

4.1.3 Transverse Fiber Swelling Co-efficient

The transverse swelling co-efficient of fiber can be calculated according to [44] as Equation 14

$$\beta_{cT} = \frac{E_m}{E_{cT}} \left(\left(1 - \sqrt{V_f}\right) \beta_m + \frac{\sqrt{Vf} \cdot \beta_m - V_f \left(\beta_m - \beta_{fT}\right)}{1 - \sqrt{V_f} \left(1 - \frac{E_m}{E_{fT}}\right)} \right) \tag{14}$$

β_m = Isotropic Swelling Co-efficient of Matrix
β_{fT} = Transverse Swelling Co-efficient of Fiber

The transverse swelling co-efficient of fiber β_{fT} is found to be 2.652. The values for calculation are taken from the epoxy swelling and composite swelling in the climate chamber at 50° Celsius and 90% RH as in Figure 45 and from back-calculation from experiments. The Equation 14 is highly sensitive to the fiber volume fraction. A V_f of 40% gives a swelling co-efficient of fiber equal to technical fibers from literature using room condition composite and epoxy modulus values. The back-calculated fiber swelling co-efficients possibly indicate that there is a dominating presence of fiber bundles giving rise to high fiber volume fractions.

4.1.4 Epoxy/Fiber Modulus

The stiffness of composite materials is described using both macro-mechanics and micro-mechanics by taking into account orientation, geometry, mechanical properties and distri-

bution of the individual phases within the composite. At the macro-scale, the composite stiffness is homogenized based on the anisotropy of the individual lamina, considering them as quasi-homogenous and using their average stiffnesses. For a uni-directional laminate, the material properties of the phases can be back-calculated using the rule of mixtures [49]. The Young's Modulus of the unidirectional lamina in the longitudinal direction, i.e parallel to the fibers, is then given as:

$$E_1 = E_f \cdot V_f + E_m \cdot V_m \tag{15}$$

where,
E_1 : Longitudinal Young's Modulus of the Uni-directional Laminate
E_f : Longitudinal Young's Modulus of the Reinforcement Fiber
E_m : Young's Modulus of the Matrix
V_f : Volume Fraction of the Fiber
V_m : Volume Fraction of the Matrix

The average stiffness can be estimated for the lamina and critical failure mechanisms such as fatigue and interface debonding can be studied extensively [49] [35] based on the Representational Volume Element definition. The smallest part of the heterogenous composite material that represents the whole material is defined as the Representational Volume Element. An overview of micro-mechanical analysis principles and its methods is delineated in [40] [95].

The distribution of the phases such as the fiber, matrix and the interface at the micro-scale induce heterogenous material behaviour under complex loading mechanisms. To model damage initiation and propagation due to complex loading mechanisms, and to simulate the failure mechanisms, the micro-structural effects between phases need to be accounted for. The micro-structural effects are not apparent at the macro-scale but affect the macro-scale properties. Composites exhibit significant heterogenous material behaviour where the distribution and phases significantly influence macroscopic properties. Therefore, micro-mechanical definitions of the material require the use of numerical techniques to compute the field variables and model the homogenized composite material response at the macro-scale.

The element stiffness matrices for truss and beam elements for relatively simple geometric configurations can be computed directly using physical reasoning but more complicated geometries require consistent formulation through variational methods or weighted residual methods [33]. The early and popularized Ritz formulation [75] involves the discretization of a continuum from an integral functional spanning line, area or volume to a function of finite degrees of freedom. From a structural mechanics standpoint, the boundary value problem is solved for finite element discretization domain Ω_e to obtain an approximate solution $u|_{\Omega_e} = \sum_{i=1}^{n} N_i \bar{u}_i$ for the nodal displacements $\bar{u}_i$ using shape functions N_i [76]. The weak form of the integrals can be solved numerically.

The stress equillibrium definition for a continuum related to the finite element formulation across discontinuities such as the phase interface to simulate debonding and crack growth and the respective constitutive stress strain models can be found in [76]. In order to treat multiple physics based differential equations such as diffusion, and stress equillibrium, a multiscale/multiphysics modelling approach is adopted in [76] to take into account the homogenized micro-scale stress field using the FE^2 computational homogenization method [68]. This approach is carried out in combination with reduced order modelling techniques which decrease computational expense by reducing the number of degrees of freedom and integration points where material response is computed. Model ingredients are defined by numerical algorithms to simulate constituent material behaviour

of the phases within the composite micro-structure to model tensile, fatigue, hygrothermal aging behaviour of glass fiber composites in [76]. The model ingredients of the phases are characterized and modelled through extensive experiments with the resulting numerical and experimental response of the composite validated under different testing conditions.

Tensile Tests on Neat Epoxy Specimens The neat epoxy specimens were immersed in a bucket of distilled water in the climate chamber at 50° Celsius. The epoxy specimens were immersed in water to speed up the moisture absorption process. The degradation mechanisms such as hydrolysis and plasticization are accentuated due to immersion aging. The water immersed epoxy samples were used for tensile tests in order to obtain an upper bound for material degradation behaviour in the given time. The swelling and moisture absorption was measured at regular intervals. The strain rate for the tensile tests was 2 mm/min. A load cell was used to capture the load in the specimen. A linear regression fit was performed on the curves to find the modulus of stress-strain graphs from the tensile tests between 0 and 0.2% strain values to obtain the tensile stiffness of the specimens. The initial length of the extensometer was 25 mm, over which the strain was calculated. The epoxy was tested at 24° Celsius room temperature.

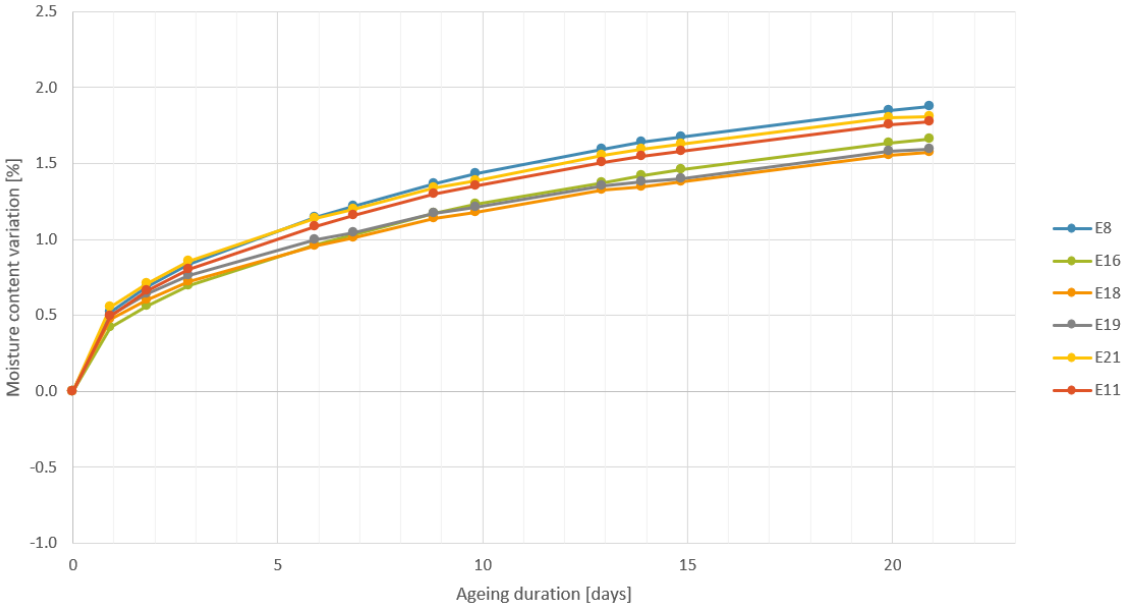

Figure 49: Moisture Absorption of Neat Epoxy Specimens immersed in distilled water at 50° Celsius

Water immersion is possibly causing an increase in the equillibrium moisture content of the specimens. It is also possible that the increase in the rate of moisture uptake in the specimens is due to water immersion.

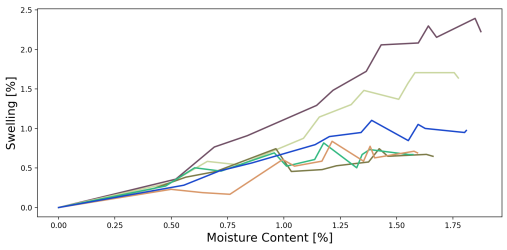

Figure 50: Immersion Swelling of Neat Epoxy Specimens at 50° Celsius

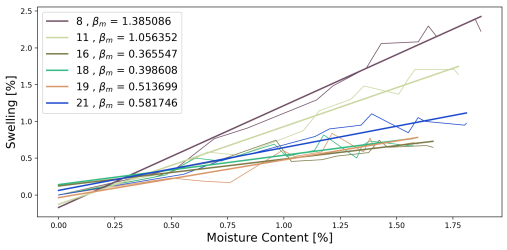

Figure 51: Linear Regression Fit of Swelling Curves of Figure 50

The swelling characteristics as seen in Figure 51 shows a spread in the swelling curves.

There is also seen higher swelling co-efficients. This is possibly due to the water immersion aging. The uncertainty seen is possibly due to the the shifting of placement of specimens within the narrow bucket causing non-uniform water intake in the specimens during water immersion aging, geometric inconsistencies from manufacturing resulting in uneven uptake of moisture within the composite.

The tensile tests were performed on the water immersion aged neat epoxy resin dog-bone specimens. The water immersion aging was done to accelerate degradation. The tensile tests on water immersion samples provide an estimate of the upper bound of material degradation behaviour in the given time of the thesis work. The stress values were computed for each individual specimen by dividing the cross-section area at the tapered width of the specimen, and by using the area at break for breaks near the clamp. The individual areas were used because of the inconsistency in thickness of specimen from manufacturing. Some specimens failed at the clamps. The specimens with the clamps near breaks still give an acceptable qualitative representation of the stress-strain behaviour in tension but the specimens broken at clamps are not reported here.

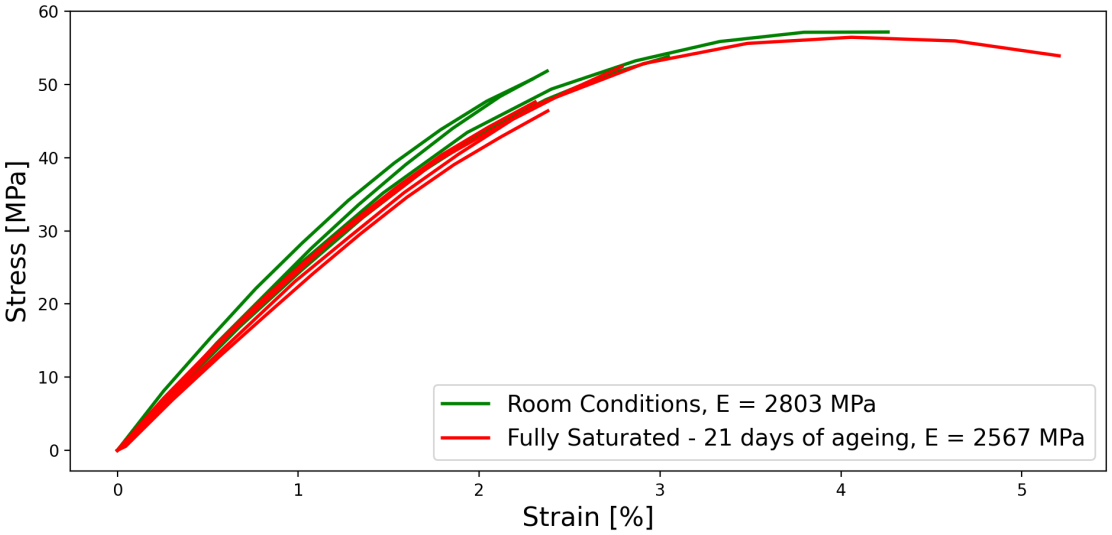

Figure 52: Transverse Tensile Tests of Neat Epoxy Specimens

It can be seen in Figure 52 that the degradation of material under water immersion is not too significant. Although this is true, the plasticization effect seen in the curves at higher strain is quite significant. The epoxy seems to fail between a stress of 40 to 60 MPa. Due to the slight inconsistency in thickness of specimens from manufacturing, the failure stress values seen here should be considered an approximate indication of the same. The temperature difference from the climate chamber to testing could also have an impact on the plasticization effect seen in the tensile tests of the matrix. The epoxy silicon moulds could also be improved to get a more consistent epoxy sample after manufacturing.

Fiber Tensile Modulus When the composite is stressed in the transverse direction, assuming that the stresses in the phases are equal as opposed to the deformation in the traditional rule of mixtures, the following formulation can be used to estimate the transverse modulus of the fibers [49]. Transverse tensile tests of flax composite can be found in 5.2.

$$\frac{1}{E_2} = \frac{V_f}{E_{fT}} + \frac{V_m}{E_m} \tag{16}$$

The transverse fiber properties modulus can be back-calculated using the Halpin-Tsai equation. Transverse tensile tests on flax composites Figure 80 were performed and the

fiber modulus was back-calculated using the Halpin-Tsai equation [13] and an alternative by Hopkins and Chamins [44]. A shape factor value of 2 is adopted according to [4]. The mean linear composite modulus from 0 to 0.2 % strain from the stress-strain graphs of the tensile tests Figure 80 was used to back-calculate the fiber properties.

$$\frac{E_{cT}}{E_m} = \frac{1 + \xi * \eta * V_f}{1 - \eta * V_f} \tag{17}$$

where,

$$\eta = \frac{\frac{E_{fT}}{E_m} - 1}{\frac{E_f}{E_m} + \xi} \tag{18}$$

E_{cT} = Transverse Tensile Modulus of Composite
E_{fT} = Transverse Tensile Modulus of the Fiber
E_m = Isotropic Tensile Modulus of Matrix
V_f = fibre volume content
ξ = shape factor [4]

The formulation to determine the transverse modulus by Hopkins and Chamins [44] is as follows:

$$E_{cT} = E_m \left(\left(1 - \sqrt{V_f}\right) + \frac{\sqrt{V_f}}{1 - \sqrt{V_f \left(1 - \frac{E_m}{E_{fT}}\right)}} \right) \tag{19}$$

The back-calculated fiber tensile modulus is given as seen in Table 1.

Formulation	**Transverse Fiber Modulus [MPa]**
Modified Rule of Mixtures	25932
Halpin-Tsai [4] [13]	7466
Hopkins & Chamins [44]	5996

Table 1: Back-calculated Fiber Properties

Elasto-Plastic Material Model Calibration The elasto-plastic material model [62] as also used in [76] uses the compressive and tensile yield functions σ_c and σ_t respectively to define the paraboloidal yield criterion to define hardening of the material.

The stress-strain evolution of the epoxy from the tensile tests Figure 52 are used to fit the tensile yield function σ_t. An initial estimate for the tensile yield function was made by fitting 2 exponential functions to the hardening part of one of the curves from Figure 52. For the initial fit, the hardening was assumed to start from a stress of 27.5 MPa. The elastic modulus was recalculated for the assumed elastic part of the curve. The equivalent plastic strain is then estimated for each point in the curve. The initial fit for the tensile yield function is given in Figure 53.

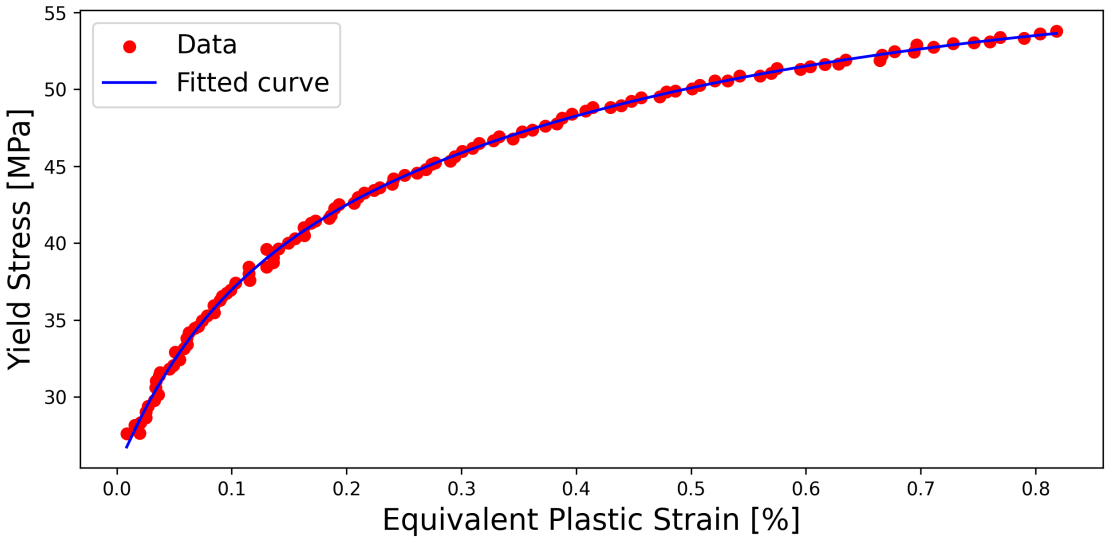

Figure 53: Initial Tensile Yield Function fit for Epoxy Elasto-Plastic Material

The obtained parameters for the 2 exponential functions from Figure 53 was used to perform one-element validation as also seen in [62]. The fine-tuning of the fit was made for tensile yield function σ_t by simulating uni-axial tensile one-element test. A square 'Quadrilateral 4' element with sides of unit length is used to calibrate the material with one integration point (Gauss 1x1 integration scheme) at the center of the element Figure 54. PBCs are ensured at all edges of the one element. The 'Nonlin' module with a 'SkylineLU' solver from Jive is used to apply displacement increments of 0.00001 at the right edge. The solver is set to a tolerance of $1 \cdot 10^{-6}$ for a maximum of 100 iterations per step.

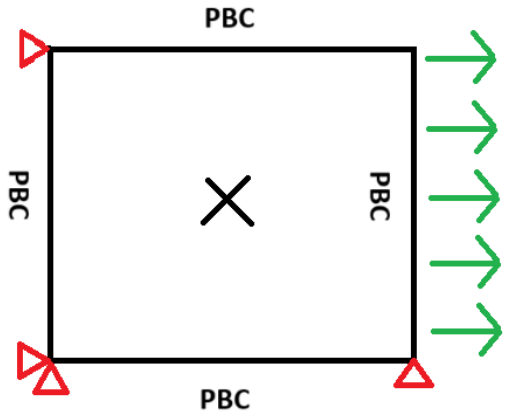

Figure 54: One Element for Elasto-Plastic Material Calibration

The yield function σ_t was adapted further with the one element tests to obtain an overall fit when compared with the stress-strain curves from epoxy tensile test experiments at room conditions. The fit for the elasto-plastic material model is given in Figure 55. The compression yield function σ_c was inputted as $1.25 * \sigma_t$ to ensure a higher threshold in compression. The expressions found for σ_t is Equation 20 and σ_c is Equation 21

$$\sigma_t = 53.73 - 25.1 \cdot e^{x/-0.00318} - 9.37 \cdot e^{x/-0.00612} \tag{20}$$

$$\sigma_c = 1.25 \cdot \left(53.73 - 25.1 \cdot e^{x/-0.00318} - 9.37 \cdot e^{x/-0.00612}\right) \tag{21}$$

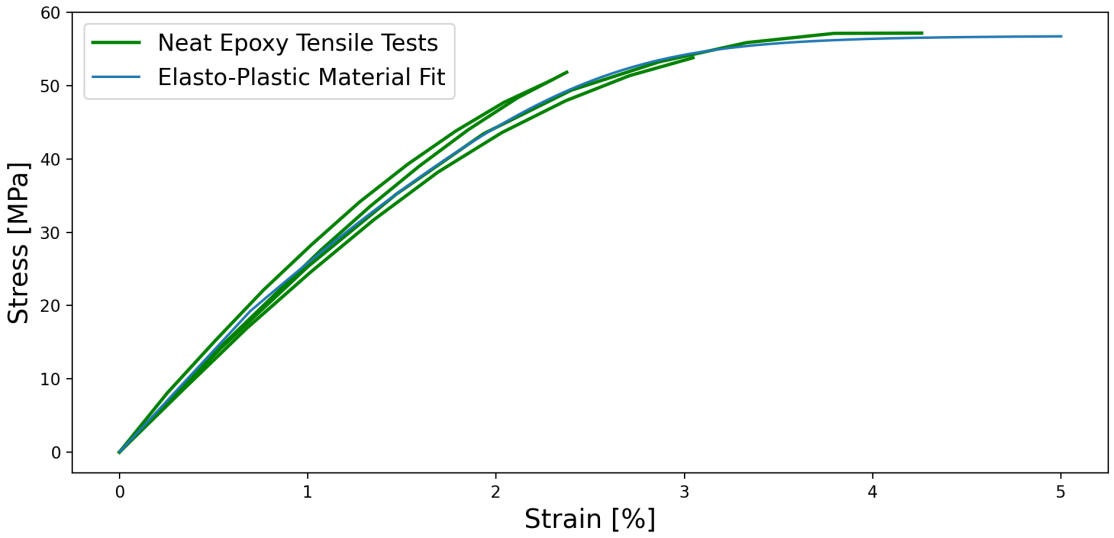

Figure 55: One element Uni-axial Tension Fit to Experiments

The slope of the linear part of the curve is higher than the experiments but still within the global range of the experimental curves. The obtained fit was sufficiently accurate for the required modelling effort. Further fine-tuning can be done to achieve greater accuracy at the linear slope. The damage variables (tension and compression fracture and fracture toughness) are set to really high values, therefore fracture damage is not modelled. The degradation factor can also be adjusted in the model to fit to the degraded epoxy.

4.2 Literature

4.2.1 Interface Properties

[36] identified and validated the significant contribution of hygroscopic expansion of fibers in flax fiber composites with a micro-mechanical concentric cylindrical model, which predicts the residual stresses at the interface of fiber and matrix, based on the mechanical properties and experimentally determined expansion co-efficients of the fiber. The obtained residual stresses accurately predict static friction co-efficients found in literature, of other composite systems. Experimentally determined curvature values of thin assymetric flax fiber composite laminates are used to compare the hygroscopic and thermal residual stress contribution before and after compression molding process.

Microbond tests were performed on flax fibre/ Poly(lactic) acid composites to study the interface between fiber and matrix in [52]. Micro-mechanical analysis was performed to estimate and compare the inter-facial properties to experiments for samples subjected to different thermal treatments. Dynamic Scanning Calorimetry was used to characterize the thermal phases of the matrix. Polarization and Scanning Electron Microscopy were used to study interfacial morphology and fracture. The estimation of contact angle measurements was also carried out. Microbond tests used to characterize fiber/matrix interface are extensively outlined in [63].

While studying the predominant zone of the interface in flax-fibre composites in Hermes and Electra flax fibre variants, [53] quantified the influence of resin penetration near the interphase zone of fiber using Laser Confocal Microscopy by delineating fiber and resin zones with colors. The chemical constitution of the fibers is characterized using Fourier Transform Infrared Spectroscopy. The fibre surface in microbond test samples is characterized using X-ray Photo-electron Spectroscopy.

Single Fiber Fragmentation tests, Pull-out tests and microbond tests are carried out on different plant fibre composites in [39]. Qualitative and quantitative characterization of the interface is performed. [28] provides Interfacial Shear Strength (IFSS) values from tests by various authors. The interphase thickness is measured by a novel two fiber tensile test experimentally, and a contact width model based on fiber diameter is derived and compared with literature. The inter-phase thickness is also measured using Transmission Electron Microscopy.

The interface properties were studied at the microscopic scale and compared at macroscopic scale for aligned flax fibre composites in [61] using Rule of Mixtures. Extensive experiments are performed at both scales to characterize the mechanical behaviour of the composite specimens for some bio-based resins, making the composite fully bio-based.

[47] performs single fiber fragmentation tests on treated and untreated single fibers embedded in matrix to test the adhesion characteristics for both. SFFT is used to characterize both the adhesion and strength characteristics of the flax fibers. [94] studies the strength and adhesion parameters of single yarn and fabric reinforced composites with and without surface alkali treatment. SEM micrographs are used to depict the surface morphology of the yarns. The strength of the interface between elementary fibers in a technical bundle was studied with novel fiber shearing experiments in [28] to characterize the force displacement graphs and derive mechanical properties to be used to describe cohesive zone numerical models between fibers in a bundle.

For modelling the interface in this thesis work, all the parameters were obtained from literature.

4.3 Parameters Summary

Epoxy		**Interface**		**Fiber**	
E [MPa][a]	2803	K_d [MPa][b]	$5 \cdot 10^7$	E [MPa][b]	6958
ν [−][76]	0.37	X_n [MPa][53]	13.2	ν [−][82]	0.498
$\varepsilon_{e,max}$ [−][57]	0.008	X_s [MPa][53]	13.2	$\varepsilon_{f,max}$ [−][57]	0.15
		G_{Ic} [N/mm][72]	1.96		
		G_{IIc} [N/mm][72]	1.405		
		η [−][b]	1.0		

[a] Experimentally obtained values
[b] Assumed values

Table 2: Material Properties Variation Models 1 to 8

Epoxy		Interface		Fiber	
E [MPa][b]	2390	K_d [MPa][b]	$5 \cdot 10^7$	E [MPa][b]	6958
ν [−][76]	0.37	X_n [MPa][53]	13.2	ν [−][82]	0.498
ν_p [−][76]	0.32	X_s [MPa][53]	13.2	$\varepsilon_{f,max}$ [−][57]	0.15
X_t [MPa][b]	$1 \cdot 10^3$	G_{Ic} [N/mm][72]	1.96		
X_c [MPa][b]	$1 \cdot 10^3$	G_{IIc} [N/mm][72]	1.405		
G_c [MPa][b]	$1 \cdot 10^3$	η [−][b]	1.0		
σ_t [MPa][b]	Equation 20				
σ_c [MPa][b]	Equation 21				
$\varepsilon_{e,max}$ [−][57]	0.008				

[a] Experimentally obtained values
[b] Assumed values

Table 3: Material Properties Variation 9 Model

Epoxy		Interface		Fiber	
E [MPa][b]	2390	K_d [MPa][b]	$5 \cdot 10^7$	E [MPa][b]	5996
ν [−][76]	0.37	X_n [MPa][53]	13.2	ν [−][82]	0.498
ν_p [−][76]	0.32	X_s [MPa][53]	13.2	$\varepsilon_{f,max}$ [−][57]	0.15
X_t [MPa][b]	$1 \cdot 10^3$	G_{Ic} [N/mm][72]	1.96		
X_c [MPa][b]	$1 \cdot 10^3$	G_{IIc} [N/mm][72]	1.405		
G_c [MPa][b]	$1 \cdot 10^3$	η [−][b]	1.0		
σ_t [MPa][b]	Equation 20				
σ_c [MPa][b]	Equation 21				
$\varepsilon_{e,max}$ [−][a]	0.002				

[a] Experimentally obtained values
[b] Assumed values

Table 4: Material Properties Benchmark Model

NOTE: $\varepsilon_{f,max}$ and $\varepsilon_{e,max}$ in the context of this thesis work is the maximum swelling strain percentage point of the flax fiber and epoxy matrix attained at the final concentration step.

5 Numerical Results, Experimental Benchmark & Discussion

5.1 Flax FRP Swelling

Swelling analysis is performed on the micro-scale RVE meshes. A sensitivity analysis is performed for swelling to understand the influence of modelling parameters in the swelling analysis. The Moisture Uptake Model as seen in 3.4 is used but with updated RVE mesh representative of each analysis. A final iteration of the swelling analysis with the experimental values is presented. The differences between modelling and experimental benchmark are discussed. Swelling of epoxy was measured under similar conditions as the composite to be used for the model as seen in 4.1.2. Transverse tensile test simulations are briefly discussed. Microscopy images are presented that show the differences between model assumptions and reality that need to be addressed.

5.1.1 Sensitivity Analysis

A sensitivity analysis is performed based on literature parameters to get an understanding of the influence of geometry and material parameters in the swelling model and to compare the obtained results with the results in literature. Concentration dependent degradation is taken into account through the sensitivity analysis by decreasing stiffness values of the phases. Geometry influence is estimated by adjusting the diameter of fibers and the volume fraction. The diameter also varies within a range as mentioned in [57]. The sensitivity analysis is performed by keeping the swelling parameters constant.

For the initial sensitivity analysis, the parameters for swelling and geometry are obtained from [57]. The meshes are generated according to the parameters of each variation. The parameters for the first 8 variations of the sensitivity analysis is given in Table 2. The initial modulus for epoxy is assumed from the experiments performed since it the corresponding value for the same is not given in [57]. The transverse flax fiber modulus is back-calcuated using the transverse composite modulus in [57] and epoxy modulus from experiments, using the formulation in [44]. The swelling co-efficient of each phase is taken as the final strain due to swelling from [57]. The rest of the properties are obtained from cited literature sources as necessary. The values used for the variations 1 to 8 are given in Table 2.

The Base Model and the Variations 5 to 8 use the same mesh with varying material parameters to ensure consistency in the comparison between variations with regards to mesh generation.

Model Variation	**Variables**				Output Variables		
	$\mathbf{D_f}$ [µm]	$\mathbf{V_f}$ [%]	$\mathbf{E_m}$ [MPa]	$\mathbf{E_f}$ [MPa]	$\epsilon_{\mathbf{xx}}$ [%]	$\sigma_{\mathbf{xx}}$	$\sigma_{\mathbf{yy}}$
Base Model	15	35	$1 \cdot E_m$	$1 \cdot E_f$	6.641	Figure 56	Figure 57
Variation 1	10	35	$1 \cdot E_m$	$1 \cdot E_f$	6.244	Figure 58	Figure 59
Variation 2	20	35	$1 \cdot E_m$	$1 \cdot E_f$	6.436	Figure 60	Figure 61
Variation 3	15	20	$1 \cdot E_m$	$1 \cdot E_f$	4.129	Figure 62	Figure 63
Variation 4	15	50	$1 \cdot E_m$	$1 \cdot E_f$	8.723	Figure 64	Figure 65
Variation 5	15	35	$1.2 \cdot E_m$	$1 \cdot E_f$	6.587	Figure 66	Figure 67
Variation 6	15	35	$0.8 \cdot E_m$	$1 \cdot E_f$	6.708	Figure 68	Figure 69
Variation 7	15	35	$1 \cdot E_m$	$1.2 \cdot E_f$	6.690	Figure 70	Figure 71
Variation 8	15	35	$1 \cdot E_m$	$0.8 \cdot E_f$	6.582	Figure 72	Figure 73

Table 5: Swelling Sensitivity Analysis Variations

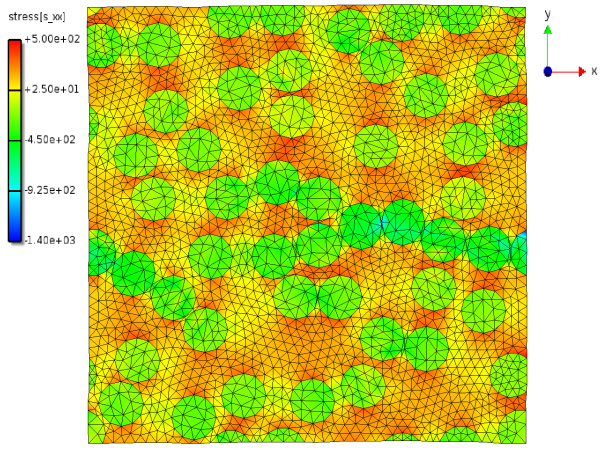

Figure 56: Base Model Internal Stresses σ_{xx}

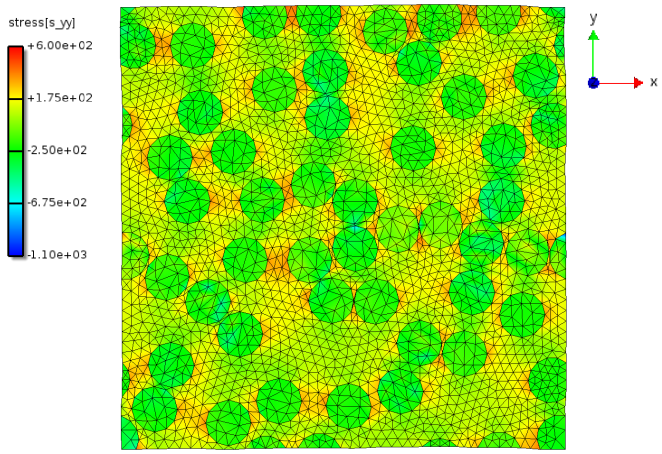

Figure 57: Base Model Internal Stresses σ_{yy}

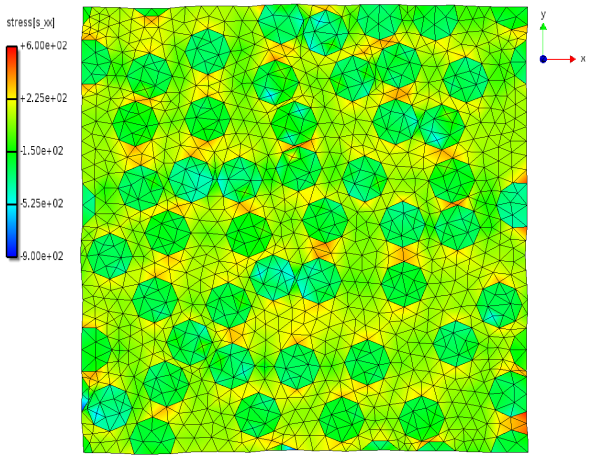

Figure 58: Variation 1 Model Internal Stresses σ_{xx}

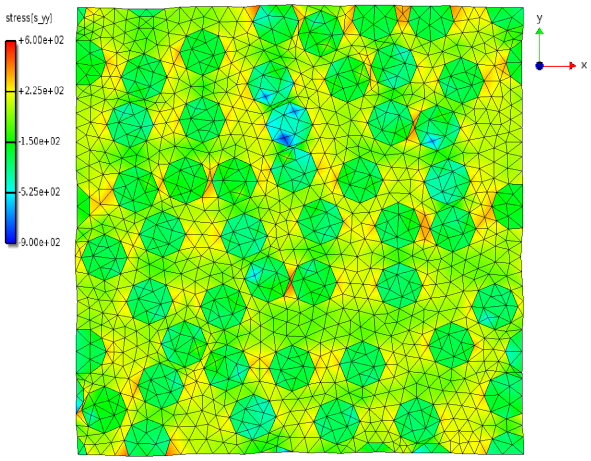

Figure 59: Variation 1 Model Internal Stresses σ_{yy}

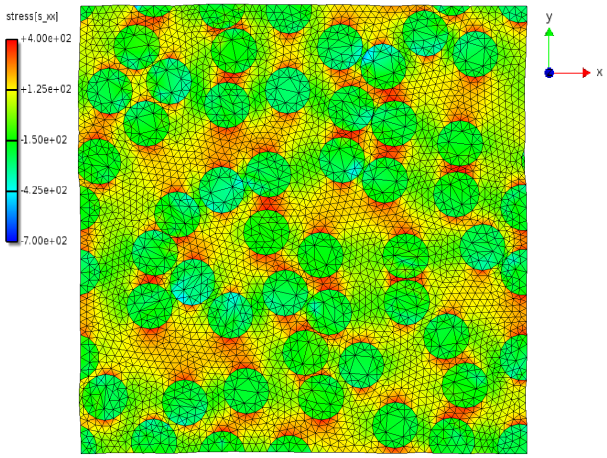

Figure 60: Variation 2 Model Internal Stresses σ_{xx}

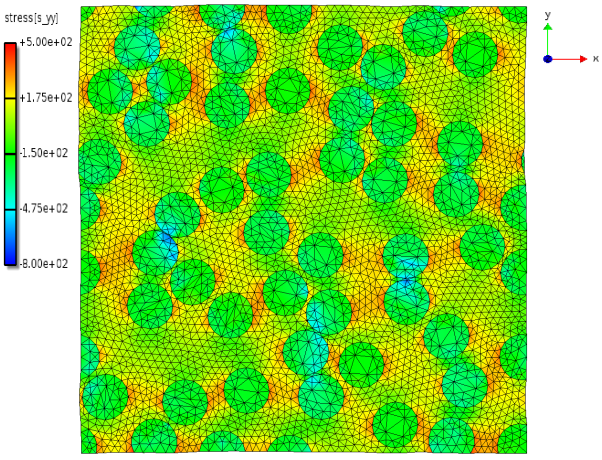

Figure 61: Variation 2 Model Internal Stresses σ_{yy}

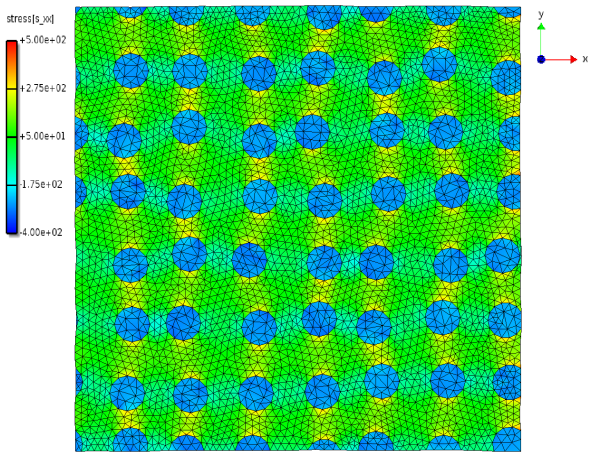

Figure 62: Variation 3 Model Internal Stresses σ_{xx}

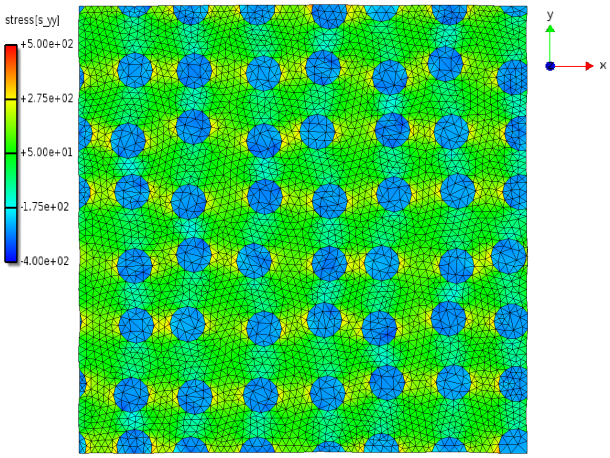

Figure 63: Variation 3 Model Internal Stresses σ_{yy}

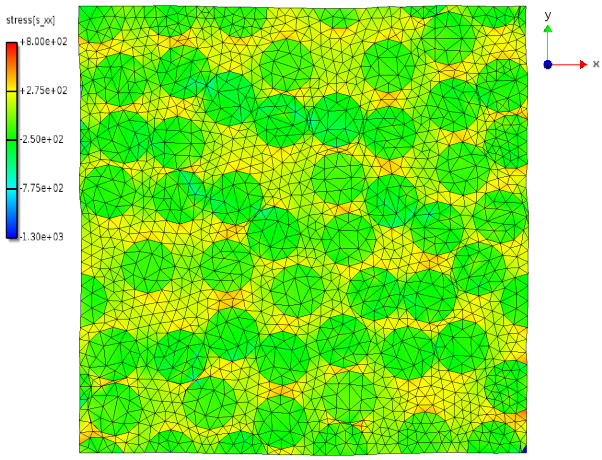

Figure 64: Variation 4 Model Internal Stresses σ_{xx}

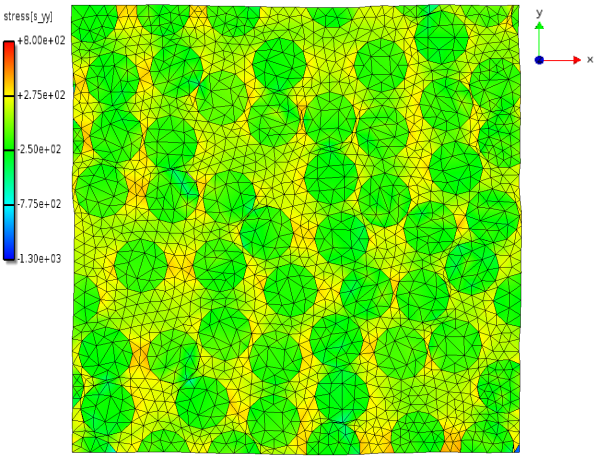

Figure 65: Variation 4 Model Internal Stresses σ_{yy}

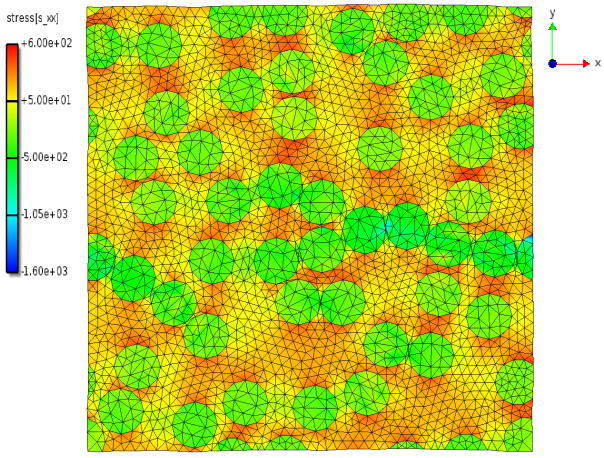

Figure 66: Variation 5 Model Internal Stresses σ_{xx}

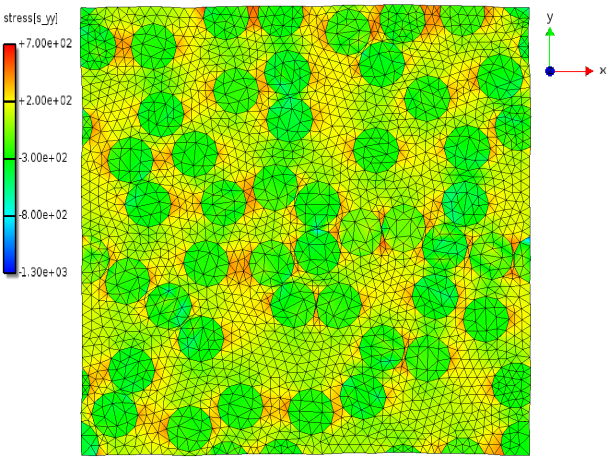

Figure 67: Variation 5 Model Internal Stresses σ_{yy}

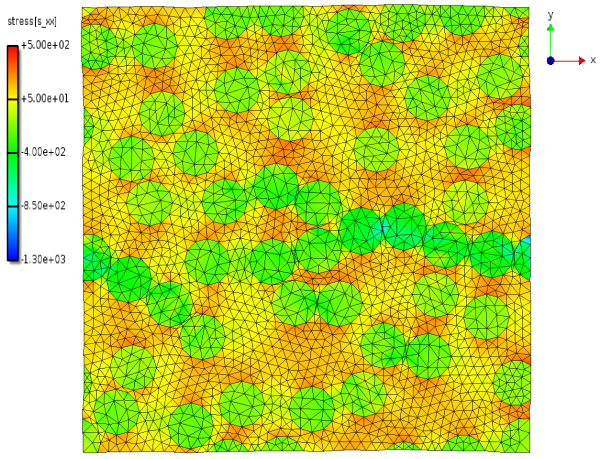

Figure 68: Variation 6 Model Internal Stresses σ_{xx}

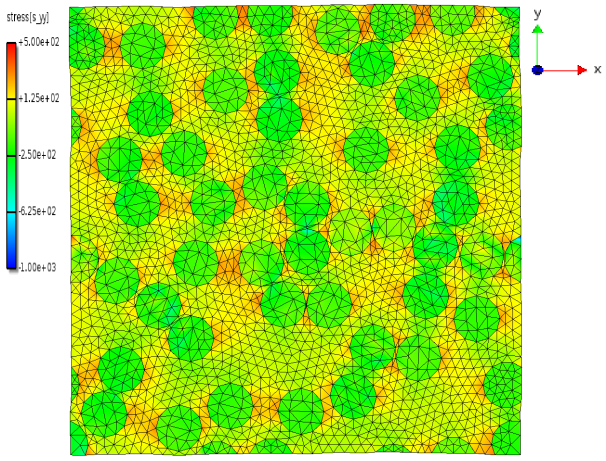

Figure 69: Variation 6 Model Internal Stresses σ_{yy}

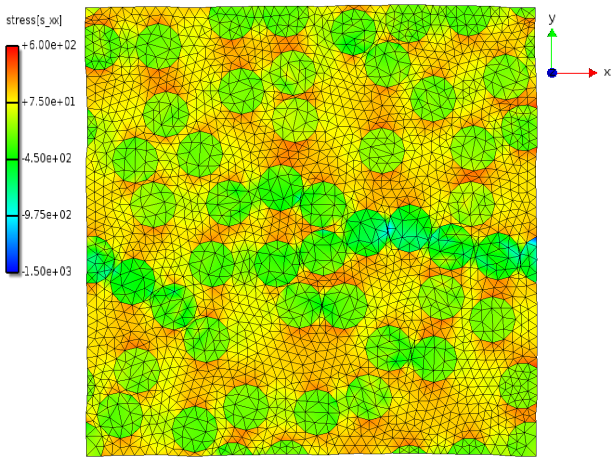

Figure 70: Variation 7 Model Internal Stresses σ_{xx}

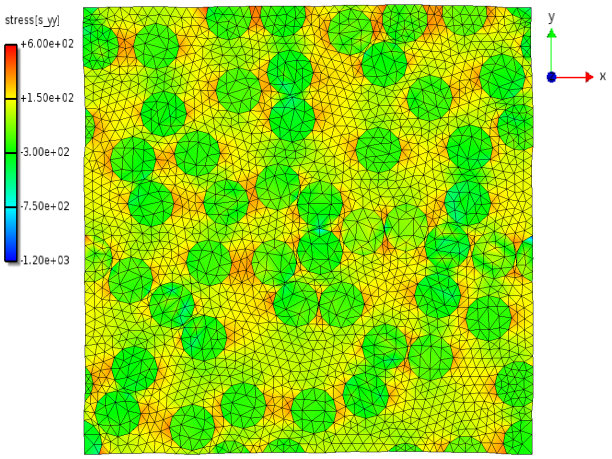

Figure 71: Variation 7 Model Internal Stresses σ_{yy}

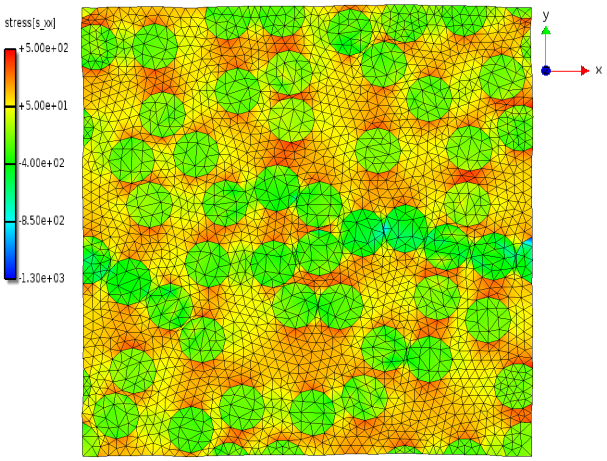

Figure 72: Variation 8 Model Internal Stresses σ_{xx}

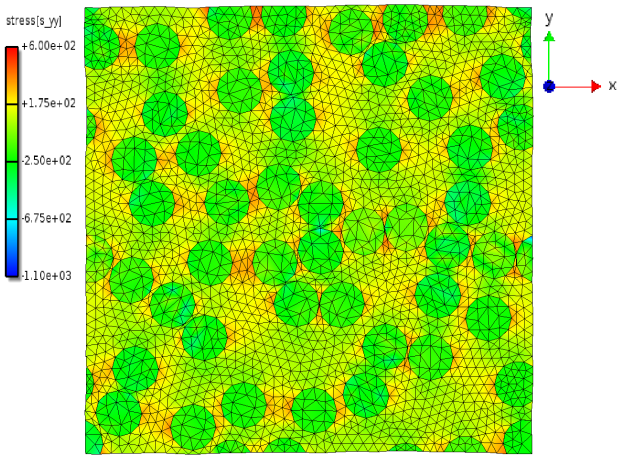

Figure 73: Variation 8 Model Internal Stresses σ_{yy}

The composite strains are estimated to be between 4% to 6.7% at the final concentration step. The composite strain obtained in [57] is 3.5% for flax-epoxy composites. The internal stresses are in the range 800 MPa (tensile) to 1600 MPa (compressive). The high internal stresses could owe to the linear assumptions for the material models of the

phases, constraining effect of the matrix, and lack of damage modelling in the interface and phases. The free fiber swelling co-efficient is used from [57] but there is an estimated constrained moisture absorption of fiber due to its surrounding of matrix in the composite, which leads to a reduction in the fiber swelling co-efficient.

A reduction in diameter of the fibers leads to a decrease in the composite strain. There is an increase in the tensile stresses in the matrix and interface but a decrease in the compressive stresses between the fibers due to increased spacing of the fibers. An increase in the fiber diameter leads to a slight decrease in the composite strain and a reduction in the internal stresses when compared to the base model. This can be attributed to the increase in load bearing of the fibers, reduced stress concentrations around fiber, higher homogenized modulus of composite, reduced interfacial area due to the increase in fiber diameter. The difference in fiber packing has a drastic influence on the microstructure of the composite. Furthermore, the change in volume fraction drastically influences the composite strain in a proportional manner. There is an increase of composite strain by 60% for a 40% increase in the fiber volume fraction and similarly vice-versa. The geometry has a significant effect on the resultant composite strain.

An increase in the matrix modulus in Variation 5 results in a reduction in the resultant composite strain and similar inverse trend is seen vice-versa in Variation 6. The compressive and tensile internal stresses follow a similar trend. The stiffer matrix results in greater magnitude of internal stresses for the same input strain for the phases due to greater share of load sharing and stress concentration. The opposite holds true for a change in fiber stiffness. Stiffer fibers lead to greater composite strain and internal stresses and weaker fibers lead to lower composite strain and internal stresses than the base model. This could be attributed to increased load sharing and the diffferential swelling effect of stiffer/weaker fibers on the homogenized composite strain for the same input swelling strain.

Variation 9 The elasto-plastic material model [62] and as used in [76] is used for epoxy in the swelling analysis. The material properties of the model are given in Table 3. The calibration of the elasto-plastic material is given in 4.1.4 A lower epoxy stiffness value was used to fit the model with the one element tests. The base model variation is re-analysed with the new elasto-plastic material for epoxy. The plastic hardening behaviour of epoxy is taken into account with the use of the elasto-plastic material model. Damage reduction in tensile stress-strain behaviour is not so significant even with water immersion as seen in Figure 52. Therefore, material stiffness reduction of matrix is not included.

The resultant composite strain in the x-x direction is 6.533 %. This is lesser compared to the linear elastic base model. The hardening of the epoxy causes re-distribution of stresses causing a reduction in the internal stresses and strains within the epoxy. Figure 76 shows the Equivalent Plastic Strains in the epoxy material due to hardening.

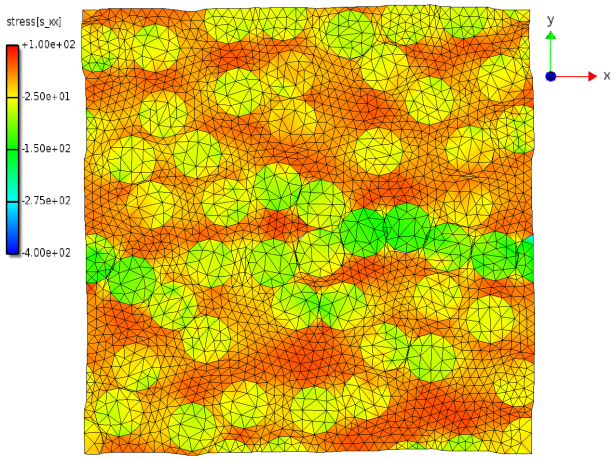

Figure 74: Variation 9 Model Internal Stresses σ_{xx}

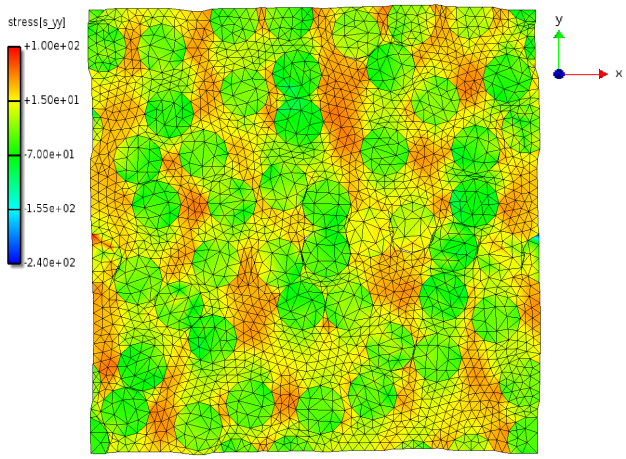

Figure 75: Variation 9 Model Internal Stresses σ_{yy}

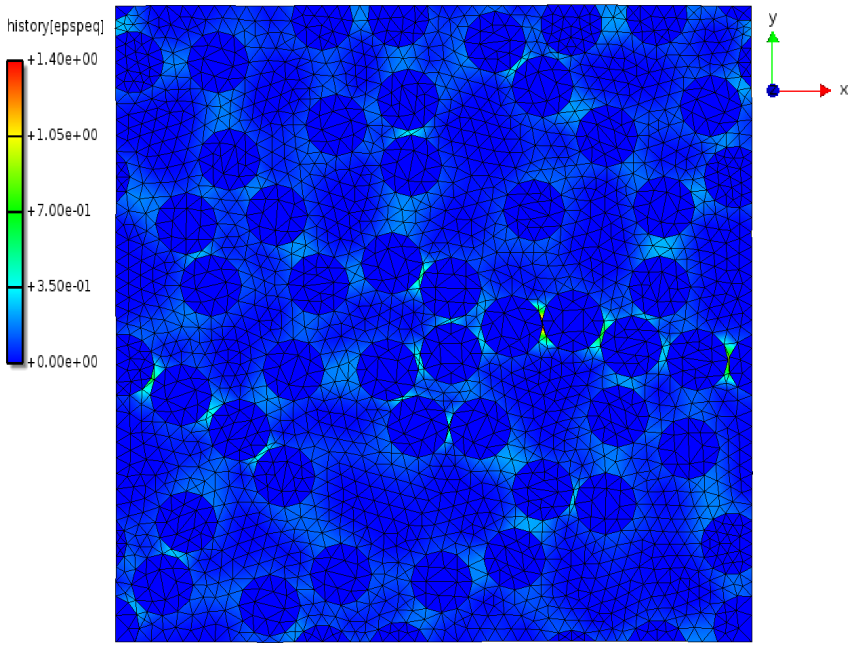

Figure 76: Variation 9 Model Equivalent Plastic Strains $\epsilon_{p,eq}$

There are high tensile stresses seen within fibers and matrix in the internal stress plots in the x-x direction Figure 74. This could indicate potential plasticization of the fibers as well as the matrix. The equivalent plastic strains Figure 76 shows hardening between the fibers, with hardening increasing with decreasing proximity between fibers. High stress concentrations can be observed in the matrix between closer fibers and in the fibers with farther spaced fibers.

5.1.2 Benchmark

An RVE mesh representative of the experiments was created, with 28% fiber volume fraction. The diameters of fibers corresponding to the mean of the microscopy image study of 15 µm was adopted. The resultant composite strain from the analysis was 4.96%. The material properties used are provided in Table 4. The input values are taken as seen in the experiments for epoxy and back-calculated for the fiber from epoxy values.

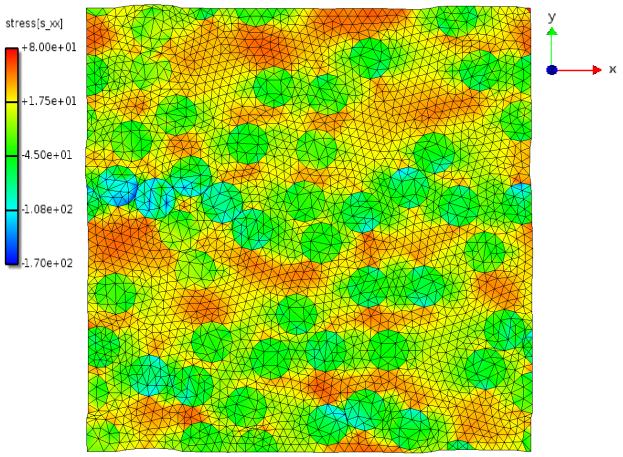

Figure 77: Benchmark Model Internal Stresses σ_{xx}

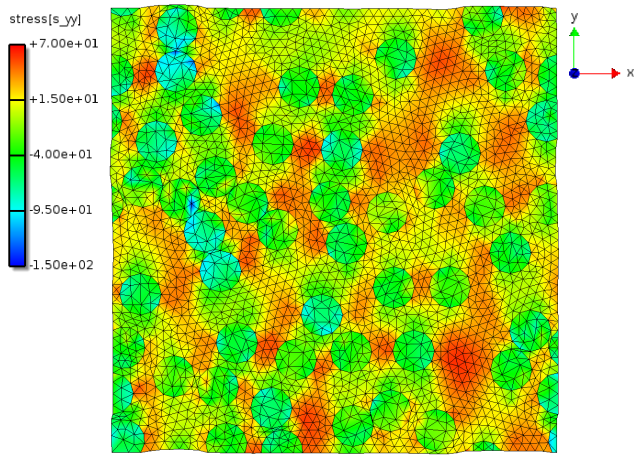

Figure 78: Benchmark Model Internal Stresses σ_{yy}

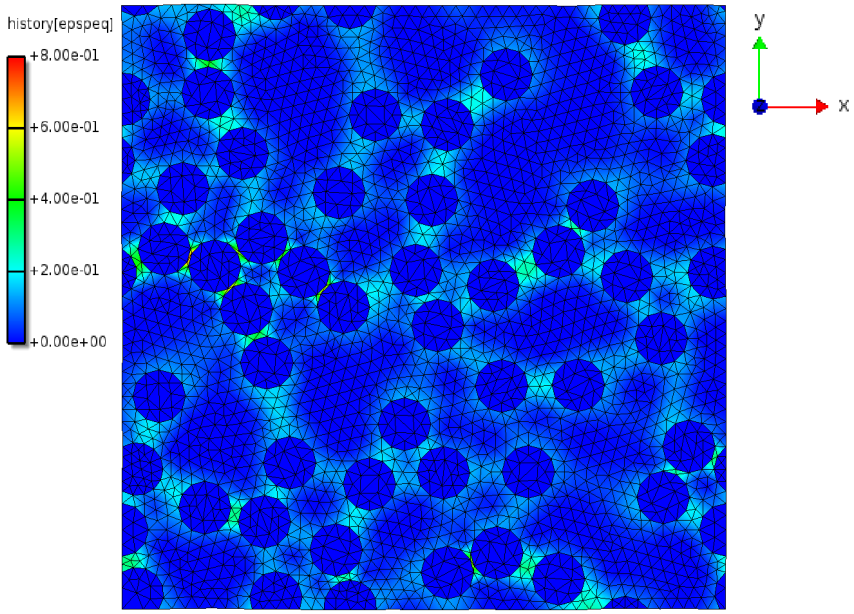

Figure 79: Benchmark Model Equivalent Plastic Strains $\epsilon_{p,eq}$

In Figure 79 there are high localized plastic strains between closely packed fibers. The model uses linear isotropic fibers with an elasto-plastic material for matrix. The differential swelling causing compressive stresses between closely packed fibers could potentially explain the high plasticization of the matrix between these fibers. Although the bulk material behaviour of the matrix is well represented, interface debonding is not seen in the model.

5.2 Flax FRP Transverse Tensile Loading

Tensile tests were performed on transverse flax-epoxy composite specimens to study its transverse tensile behaviour and the interface loading in this configuration. The tests were performed at around 18° Celsius as recorded by the temperature sensor. The specimens were tested at room conditions, after oven-drying, after 5 days of aging days and after reaching saturation in the climate chamber. The aging of the specimens was carried out at 50° Celsius and 90% RH in the climate chamber. There was negligible difference in moisture conditions between testing environmental conditions and the climate chamber.

The specimens were dog-bone shaped to ensure failure at the tapered width and to ensure uniform strength distribution. The strain rate for the tensile tests was 2 mm/min. A load cell was used to capture the load in the specimen. A linear regression fit was performed on the curves to find the modulus of stress-strain graphs from the tensile tests between 0 and 0.2% strain values to obtain the tensile stiffness of the specimens.

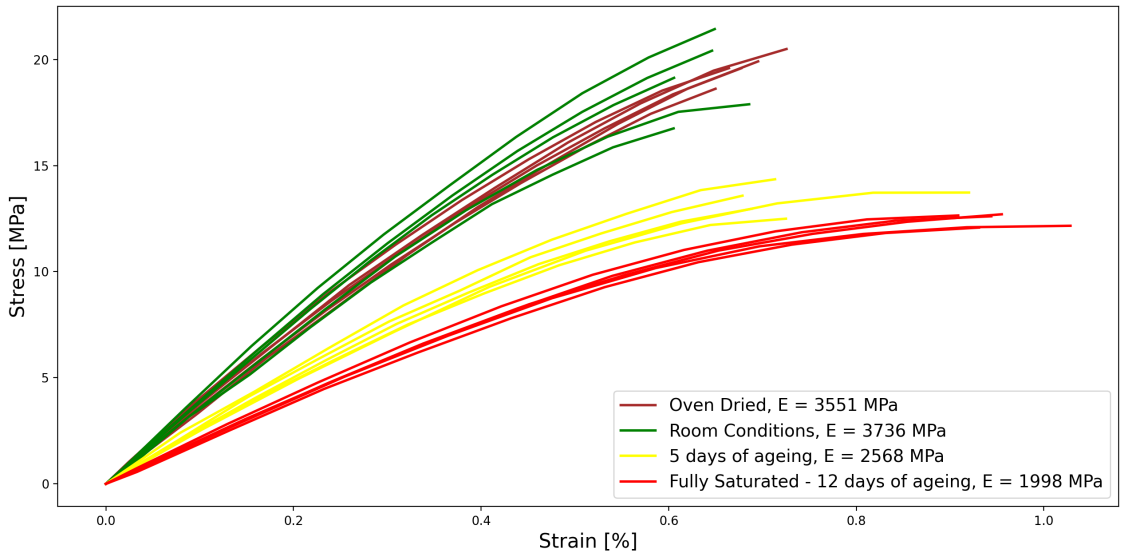

Figure 80: Transverse Tensile Tests of Flax Fiber Composite Specimens

The mean area of the samples at the tapered width of the dog-bone specimens was used to calculate the stress values for the stress-strain tensile test graph shown in Figure 80. The local strain where mean area is measured is taken as the ratio between the change in extensometer length versus the initial extensometer length which is 25 mm.

It can be seen by comparing Figure 52 and Figure 80 that the stress at break is significantly lower for the flax composites than the epoxy. The composite specimens at room condition have higher stress values and lower strain values at break showing less ductile behaviour. Meanwhile, with increasing moisture degradation, there is increased ductility, higher strain at break and lower stress at break for the flax composites.

Transverse tensile testing was performed on the micro-RVE model. The benchmark model was adapted to include linear fiber and matrix with the cohesive interface. The same values as Table 2 for the base model was used. The second analysis uses elasto-plastic model for matrix with linear isotropic fibers with properties as in Table 4. The boundary conditions are the same as for swelling as seen in Figure 10. The load is applied using displacement control at a strain rate of 2 mm/min normalized according the experiments and at the bottom right node in the 'x' direction. The 'FlexArclen' solver is used from Jive.

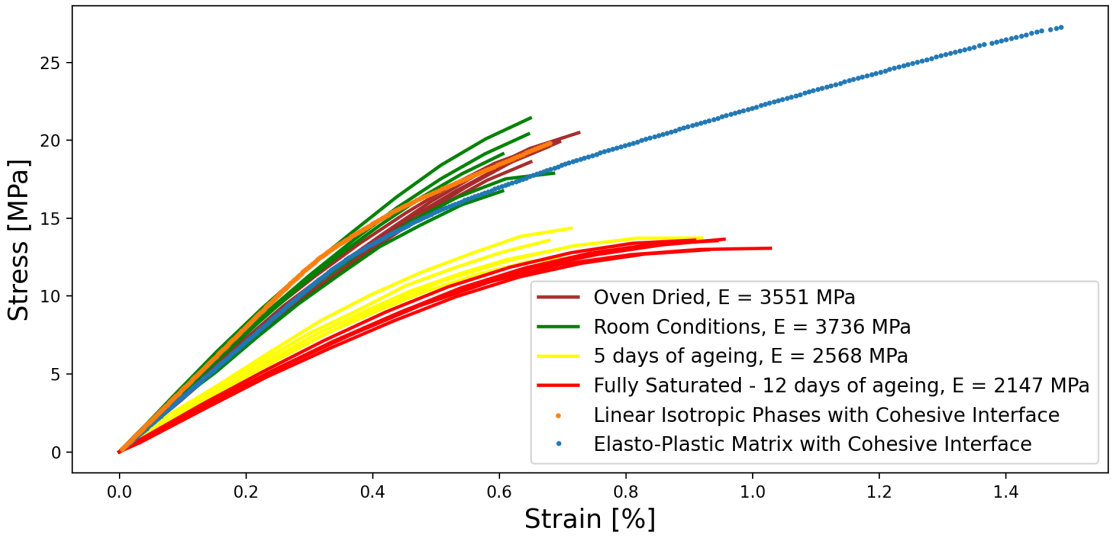

Figure 81: Transverse Tensile Test Stress-Strain Plots

The interface already opens in the linear analysis. The model converges to an equillibrium solution for 248 steps and then fails to reach convergence. The interface opening contributes highly to the transverse tensile behaviour. This phenomenon was already of significance when observed in the comparison between tensile text experiments of epoxy and composite. Whereas the plasticization of matrix is less significant at the pristine state. Introducing material degradation in the elasto-plastic model could represent the behaviour of the degraded transverse composite well and modelling plasticity in matrix and fibers in correlation to the degraded composite with consistent physics. The plasticity matrix model tensile test simulation converges to an equillibrium solution for 334 steps and fails to reach convergence.

5.2.1 Tensile Fracture

Pristine The composite is possibly failing at the interface between fibers and between the fiber and matrix. It is not highly prevalent in the microscopy images but it is the expected failure mode. In Figure 82 the fracture surface does not clearly depict where failure occurs. Although there are few interface fracture zones seen in Figure 83 (near fracture surface), it is still unclear from the images whether fiber interface is where fracture is occurring.

Figure 82: Pristine Composite Tensile Test Fracture Surface

Moisture Degraded The effect of interface failure is more accentuated for the moisture degraded tensile break specimens. Near the fracture surface, the failure crack follows the

fibers. Due to uniform stress distribution, it can be deduced that the fracture surface also behaves similarly but further experiments are required to be performed to affirm the same.

Pristine Tensile Test

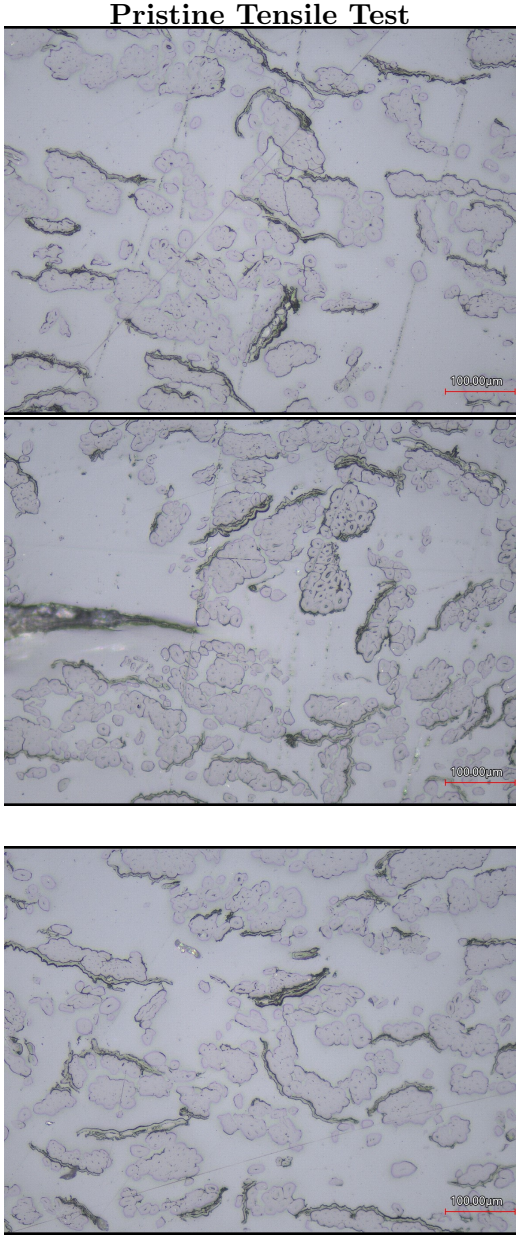

Figure 83: Pristine Composite After Tensile Test

Moisture Degraded Tensile Test

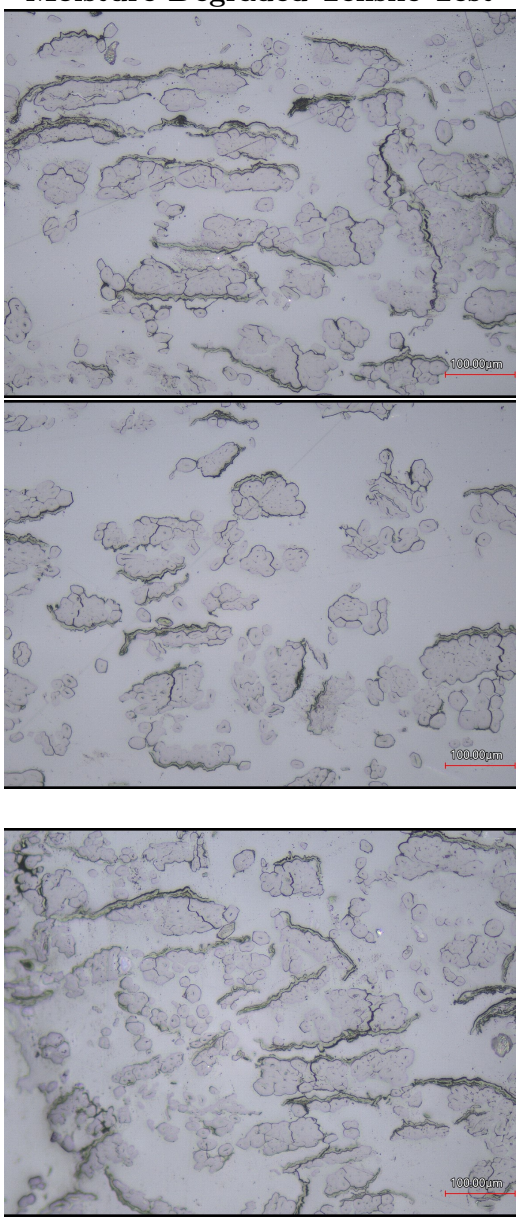

Figure 84: Moisture Degraded Composite After Tensile Test

5.3 Capabilities & Shortcomings Of The Model

Constrained Moisture Absorption of Fibers The fiber swelling co-efficients and strains taken from [57] are measured for free fibers. [57] states that there may be a reduction in moisture absorption by fibers due to the matrix constraining effect. Therefore, although the swelling co-efficient for free fibers may be a good indication of the rate of absorption of moisture in general for flax fibers, the final saturation points may not be sufficiently representative of the same seen in experiments. This phenomenon could also be potentially explained by accounting for realistic moisture uptake within each phase in the composite material. The moisture uptake within the fibers may be constrained due to the matrix. The internal stresses are also significantly lower as seen in [30] [36] when compared to the results from the numerical models.

For simplicity, the rule of mixtures can be used to estimate the moisture content of fibers embedded in the composites by using the experimentally obtained values for neat epoxy moisture absorption and composite. At 12 days of ageing, the mean moisture uptake of flax composite is 2.8%. For the same duration of moisture uptake for the same ageing conditions and similar initial conditions, assuming the difference in diffusion is negligible, the epoxy moisture uptake is around 0.8%. The fiber moisture content is back-calculated to be around 8% for the volume fraction of 28%. Using the elementary fiber swelling co-efficient as in [57] Figure 85, a $\varepsilon_{f,max}$ of 0.096 (final strain of fiber) is obtained. Using this as input for the model with the same properties as the Benchmark Model Table 4, a composite strain of around 3.1% is achieved which is well within the range of the transverse composite strain due to swelling observed in experiments. The internal stresses are obtained for this analysis are similar to the Benchmark Model.

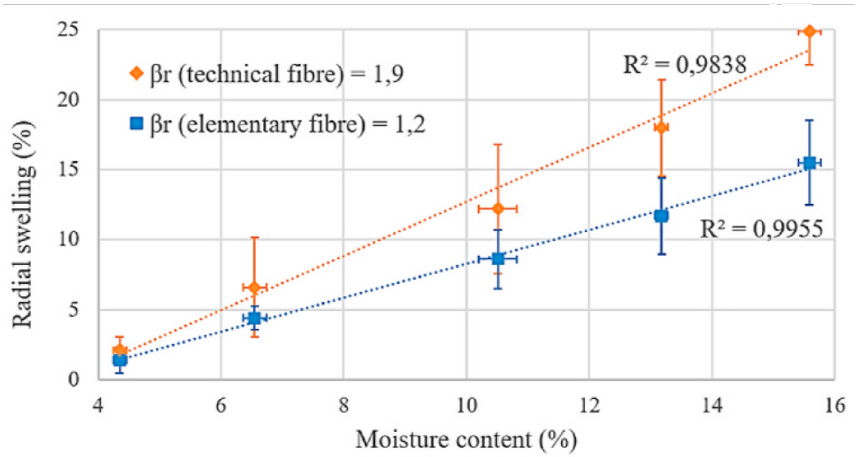

Figure 85: Free Fiber Swelling Co-efficient [57]

Although, the reduction in moisture absorption of fibers embedded in matrix gives a more accurate measurement of composite swelling, it is an over-simplified technique using the Rule Of Mixtures to modify input swelling values for the model which still does not accurately represent the complex mechanical processes and geometry variation within the model.

Model Comparison The damage in the cohesive zone model at the interface is not activated in the numerical model for swelling. Interface opening is seen but not captured clearly unless deformation is exaggerated at the post-processing stage. The microscopy image shows interface debonding between the fibers in the bundle and between fiber and matrix. The physical swelling is not clear from the microscopy images because of absence of images of the cross-section prior to moisture aging.

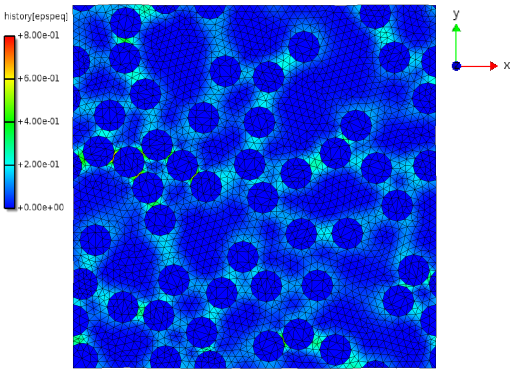

Figure 86: Numerical Model Equivalent Plastic Strains $\epsilon_{p,eq}$

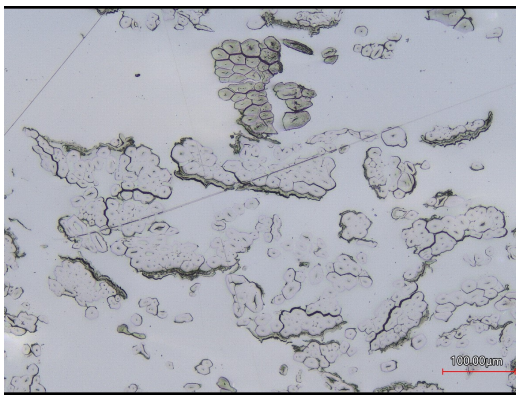

Figure 87: Microscopy Image Swelling

For the tensile tests, although the behaviour of the interface opening is captured qualitatively, the failure is not captured by the cohesive zone model. Also, softening of the matrix or damage is not simulated. The parameters taken from literature offer a qualitative analysis but the interface and matrix parameters should be characterized properly with experiments. It is in whole unclear what the failure mode in transverse tension is or how it occurs. It is expected that the interface between fibers or fiber-matrix is where failure occurs so far. [13] lists the parameters influencing the transverse tensile tests. These include the fiber diameter variation, fiber rich zones, matrix failure strain, quality of the interface and interphase.

6 Conclusions & Recommendations

A micro-scale RVE swelling model is created that is able simulate swelling of flax fiber composites and model transverse tensile behaviour. The swelling strain from experiments is replicated but with shortcomings. Interface opening is seen in the microscopy images that is not captured accurately in the swelling model. Material degradation is not simulated in the models. A preliminary tensile test simulation offers insight into the model's capabilities and shortcomings. The interface, matrix and fiber could be parametrised with experiments and suitable material models for more reliability in modelling. The microscopy images offer initial insight into the failure behaviour in transverse tension and the degradation mechanisms due to moisture uptake. The observed behaviour could be verified further and quantised using more advanced imagery techniques. The size distribution of the elementary fibers are estimated using image analysis techniques with sufficient accuracy. The observed elementary fiber sizes correspond well with literature but the effects of the high local volume fraction in the form of technical fiber bundles, and other influential geometrical features such as the lumen and interface between the fibers in a bundle should be studied and characterized with suitable experiments in order for increased consistency in the modelling efforts. The main conclusions and recommendations derived from this thesis work are presented below.

6.1 Conclusions

- There is high local volume fraction in the form of technical fiber bundles that affect swelling and tensile behaviour. The models currently only use elementary fibers modelled as circles with the same diameter. Porosity within the fibers is not modelled currently. It is increasingly clear with the sensitivity analysis that the geometry variation has a significant effect on the modelling.

- The interface between fibers in a flax bundle and between fiber bundles and matrix seems to be the crucial zone where failure occurs due to fracture in transverse tension. Sometimes the fracture surface is seen to pass through the fiber through the lumen.

- The high internal stresses in the models are redistributed within the matrix by calibrating an elasto-plastic material using tensile tests on the epoxy. Swelling strain seen in the experiments are simulated with sufficient accuracy considering the constrained moisture absorption of fiber.

- When comparing both epoxy and transverse flax composite tensile tests, it seems increasingly possible that the contribution of interface loading and interface degradation in the transverse configuration is predominant in governing the transverse tensile behaviour, especially after moisture aging.

- Although matrix material stiffness reduction due to moisture degradation is not considered in this thesis work, the material stiffness reduction of the flax fibers may be significant because the transverse stiffness of the flax composite is reduced significantly due to moisture degradation as seen in the tensile tests Figure 80. The stiffness reduction seen in the composite could be predominantly due to the contribution of the flax fiber stiffness degradation.

- There are significant artefacts that hinder the quality of the microscopy images that arise from polishing. Embedding the composite in resin is too time consuming. Another disadvantage is that the same sample, once embedded cannot be analysed before and after undergoing moisture degradation.

- Damage is not considered or adapted to the material through experiments in the numerical models. Therefore, fracture or failure of matrix/interface is not simulated.

The failure in transverse tensile tests could be due to a combination of damage evolution within interface and matrix together with other influencing parameters [13].

- Poisson ratio of fiber is highly sensitive in the model. Although linear isotropic model could be sufficient for swelling models, effects such as plasticization of the fiber and micro-fibrillar re-orientation could have an influence in the tensile behaviour, especially of significance in the longitudinal direction.

6.2 Recommendations

The technical fiber bundles could be generated using nearest neighbour distribution functions [89] to define packing of fibers within the bundles. When it comes to improving the geometry, it becomes crucial to model the interface between the fibers in bundles since there is interface debonding seen within the fiber bundles. Although it could be that moisture aging drastically increases the involvement of the interface in transverse tensile behaviour, Baley lists all the possible parameters influencing the transverse tensile test behaviour [13], of which the interface is a part. The modelling of the matrix failure strain, fiber rich zones, fiber diameter variation and interface with accurate characterization according to experiments becomes crucial. Further exploration of damage evolution and moisture degradation can be carried out using MicroCT imaging, so that the contribution of interface and matrix in the fracture surface and failure can be accurately captured in the numerical models.

Tainting the fibers with dye could drastically ease the automatic segmentation process of the microscopy images obtained from the resin embedded composites. An alternative to the arduous process of preparing specimens for microscopy could be potentially overcome using MicroCT imaging. The added advantages of MicroCT imaging is non-destructive and in-situ imaging. This could help with realistic mesh generation [58] and to clearly see the evolution of damage of the same sample before and after aging [14]. The parameters for the interface model should be adapted with experiments such as three point bending tests and microbond tests. The hypothesis of interface loading in transverse configuration could be further affirmed through microCT images and accurate modelling of the interface. The high compressive stresses seen in the fibers in the models could indicate potential plastic deformations in the fiber. Further experiments conducted to parametrize the fiber material model taking into account the degradation mechanisms seen in the fiber micro-structure and its influence on tensile behaviour would improve the modelling accuracy [50] [90]. The micro-fibrils play an important role in the tensile behaviour of the flax composite, especially in the longitudinal direction [27]. Experimental methods could be used to quantify internal stresses and to identify evolution of damage [69], to compare with numerical models.

The swelling parameters could be consistently modelled while taking into account the degradation of material for achieving further accuracy in modelling. The swelling coefficients offer a more accurate swelling strain-moisture concentration relationship for the composite and epoxy. The free fiber swelling parameters from literature possibly results in an overestimation of the fiber swelling. MicroCT imaging could also confirm the effect of the constrained moisture absorption of the fiber and help identify the exact swelling strain of embedded fibers. This could also help in identifying the moisture uptake of embedded fibers as opposed to analytical back-calculation of fiber moisture uptake.

Appendix

Benchmark Model Code Based on Experiments (Variation 10)

```
mFile = "var10RVE.msh";

log =
{
pattern = "*.info";
file = "-$(CASE_NAME).log";
};

control =
{
runWhile = "i<101";
fgMode = true;
};

    userinput =
{
modules = [ "input", "interface", "ngroups", "pbcinput" ];

interface =
{
type = "InterfaceNodes";
nodeGroups = [ "int" ];

int.intersection = [ "gmsh1", "gmsh2" ];
int.makeElements = true;
};

pbcinput =
{
type = "PBCGroupInput";
duplicatedNodes = "int.interface.newNodes";
};

input =
{
type = "GmshInput";
file = mFile;
doElemGroups = "true";
};

ngroups =
{
type = "GroupInput";
nodeGroups = ["r","l"];

r.xtype = "max";
l.xtype = "min";
};
};
```

```
model =
{
type = "Matrix";

model =
{
type = "Multi";
models = [ "fibers", "fixed", "epoxy", "interface", "pbc", "lodiR", "lodiL" ];

fibers =
{
type = "Stress";
elements = "gmsh1";

material =
{
type = "Isotropic";
rank = 2;
anmodel = "PLANE_STRAIN";
E = 5.996e3; // exp.
nu = 0.498; // Scida et. al (2017)
swelling_coeff = 0.15; // Morissa Lu et. al (2022) - radial fiber swelling
//maxConcDegradation = 0.;
//maxWaterConc = 0.;
};

shape =
{
type = "Triangle3";
intScheme = "Gauss1";
};
};

epoxy =
{
type = "Stress";
elements = "gmsh2";

material =
{
type = "Melro";
rank = 2;

E = 2.390e3;
nu = 0.37;
anmodel = "PLANE_STRAIN";

poissonP = 0.32;
sigmaT = "53.73-25.1*exp(x/-3.18e-3)-9.37*exp(x/-6.12e-3)";
sigmaC = "1.25*(56.73-21.89*exp(x/-4.18e-3)-9.57*exp(x/-6.12e-3))";
//minEpsPT = 0.04;
//minEpsPC = 0.01;
```

```
xT = "10.e3";
xC = "10.e3";
G = 10.e3;

swelling_coeff = 0.002;
//maxConcDegradation = 0.2;
//maxWaterConc = 0.034;
};

shape =
{
type = "Triangle3";
intScheme = "Gauss1";
};
};

interface =
{
type = "Interface";
elements = "int.interface.newElems";

shape =
{
type = "BLine2";
intScheme = "NewtonCotes2";
};

coheMat =
{
type = "AlfanoTuron";

dim = 2;
dummy = 5.e7;

f2t = 13.2; // Le Duigou et. al (2014)
f6 = 13.2;

gI = 1.96; // Vishnu Prasad et. al (2019)
gII = 1.405; //
eta = 1.0;

mu = 100.;
dilatancy = 0.;
};
};

pbc =
{
type = "PeriodicBC";
duplicatedNodes = "int.interface.newNodes";
};

fixed =
```

```
{
type = "BasicConstrainer";
nodeGroups = [ "cornerx"];
dofs = ["dy"];
values = [0.];
};

lodiR =
{
type = "LoadDisp";
group = "r";
};

lodiL =
{
type = "LoadDisp";
group = "l";
};

};
};

usermodules =
{
modules = [ "water_age", "sample", "solver", "graph", "view", "output" ];

water_age =
{
type = "multiphysics";
water = "true";
maxStep = 10;
concStep = 0.1;
};

output =
{
type = "Output";

file = "$(CASE_NAME).out";

vectors = [ "state = solution" ];

tables = [ "nodes/nodalStress" ];

};

sample =
{
type = "Sample";
file = "var10Swell-curve.dat";
dataSets = [ "model.model.lodiR.load[0]", "model.model.lodiR.disp[0] - model.model.lodiL.disp[0]"
];
sampleWhen = "accepted";
```

```
};

solver =
{
type = "FlexArclen";
};

graph =
{
type = "Graph";
sampleWhen = "accepted";

graph =
{
showKey = false;
xLabel = "Displacement";
yLabel = "Internal Force";
};

dataSets = [ "loadDisp" ];

loadDisp =
{
xData = "model.model.lodiR.disp[0] - model.model.lodiL.disp[0]";
yData = "model.model.lodiR.load[0]";
lineColor = "red";
lineWidth = 2.0;
};
sampleWhen = "accepted";
};

view =
{
type = "FemView";

updateWhen = "accepted";
snapWhen = false;
snapFile = "$(CASE_NAME)configFile = "$(CASE_NAME).view";

dataSets = [ "state", "history", "stress" ];

state =
{
type = "Vector";
vector = "nodes/state";
};

history =
{
type = "Table";
table = "nodes/nodalHistory";
};
```

```
stress =
{
type = "Table";
table = "nodes/nodalStress";
};

mesh =
{
elements = "int.interface.oldElements";
deformation = "0.25 * state";

plugins = "colors";

colors =
{
type = "MeshColorView";
//data = "stress[s_xx]"; // Use for viewing internal stresses in xx direction
//data = "stress[s_yy]"; // Use for viewing internal stresses in yy direction
data = "history[epspeq]";
//data = "history[d]";
palette = "rainbow";
autoScale = true;
};
};
palettes.rainbow.maxValue = 0.3;
palettes.rainbow.minValue = 0.;
};

};
```

References

[1] Baley C." "Le Duigou A. Davies Peter. ""Seawater ageing of flax/poly(lactic acid) biocomposites"". In: *"Polymer Degradation and Stability"* "94"."7" ("2009"), "1151–1162". DOI: "https://doi.org/10.1016/j.polymdegradstab.2009.03.025". URL: https://archimer.ifremer.fr/doc/00000/6639/.

[2] W Hall A S Virk and J Summerscales. "Modulus and strength prediction for natural fibre composites". In: *Materials Science and Technology* 28.7 (2012), pp. 864–871. DOI: https://doi.org/10.1179/1743284712Y.0000000022. URL: https://journals.sagepub.com/doi/abs/10.1179/1743284712Y.0000000022?journalCode=msta.

[3] Marwa Abida et al. "Hygro-mechanical coupling and multiscale swelling coefficients assessment of flax yarns and flax / epoxy composites". In: *Composites Part A: Applied Science and Manufacturing* 136 (2020), p. 105914. ISSN: 1359-835X. DOI: https://doi.org/10.1016/j.compositesa.2020.105914. URL: https://www.sciencedirect.com/science/article/pii/S1359835X20301536.

[4] J. C. Halpin Affdl and J. L. Kardos. "The Halpin-Tsai equations: A review". In: *Polymer Engineering & Science* 16.5 (1976), pp. 344–352. DOI: https://doi.org/10.1002/pen.760160512. URL: https://4spepublications.onlinelibrary.wiley.com/doi/abs/10.1002/pen.760160512.

[5] Souher Aldroubi et al. "Multi-scale investigation of morphological, physical and tensile properties of flax single fiber, yarn and unidirectional fabric". In: *Composites Part B: Engineering* 259 (2023), p. 110732. ISSN: 1359-8368. DOI: https://doi.org/10.1016/j.compositesb.2023.110732. URL: https://www.sciencedirect.com/science/article/pii/S1359836823002354.

[6] J Andersons, J Modniks, and E Spārniņš. "Modeling the nonlinear deformation of flax-fiber-reinforced polymer matrix laminates in active loading". In: *Journal of Reinforced Plastics and Composites* 34.3 (2015), pp. 248–256. DOI: https://doi.org/10.1177/0731684414568043. URL: https://journals.sagepub.com/doi/10.1177/0731684414568043.

[7] J. Andersons, E. Poriķe, and E. Spārniņš. "The effect of mechanical defects on the strength distribution of elementary flax fibres". In: *Composites Science and Technology* 69.13 (2009). Smart Composites and Nanocomposites Special Issue with Regular Papaers, pp. 2152–2157. ISSN: 0266-3538. DOI: https://doi.org/10.1016/j.compscitech.2009.05.010. URL: https://www.sciencedirect.com/science/article/pii/S0266353809002139.

[8] A. Arbelaiz et al. "Mechanical properties of short flax fibre bundle/polypropylene composites: Influence of matrix/fibre modification, fibre content, water uptake and recycling". In: *Composites Science and Technology* 65.10 (2005), pp. 1582–1592. ISSN: 0266-3538. DOI: https://doi.org/10.1016/j.compscitech.2005.01.008. URL: https://www.sciencedirect.com/science/article/pii/S0266353805000370.

[9] Alireza Ashori. "Wood–plastic composites as promising green-composites for automotive industries!" In: *Bioresource Technology* 99.11 (2008). Exploring Horizons in Biotechnology: A Global Venture, pp. 4661–4667. ISSN: 0960-8524. DOI: https://doi.org/10.1016/j.biortech.2007.09.043. URL: https://www.sciencedirect.com/science/article/pii/S0960852407007560.

[10] M. Assarar et al. "Influence of water ageing on mechanical properties and damage events of two reinforced composite materials: Flax–fibres and glass–fibres". In: *Materials Design* 32.2 (2011), pp. 788–795. ISSN: 0261-3069. DOI: https://doi.org/10.1016/j.matdes.2010.07.024. URL: https://www.sciencedirect.com/science/article/pii/S0261306910004590.

[11] C. Baley. "Analysis of the flax fibres tensile behaviour and analysis of the tensile stiffness increase". In: *Composites Part A: Applied Science and Manufacturing* 33.7 (2002), pp. 939–948. ISSN: 1359-835X. DOI: https://doi.org/10.1016/S1359-835X(02)00040-4. URL: https://www.sciencedirect.com/science/article/pii/S1359835X02000404.

[12] Christophe Baley and Alain Bourmaud. "Average tensile properties of French elementary flax fibers". In: *Materials Letters* 122 (2014), pp. 159–161. ISSN: 0167-577X. DOI: https://doi.org/10.1016/j.matlet.2014.02.030. URL: https://www.sciencedirect.com/science/article/pii/S0167577X14002420.

[13] Christophe Baley et al. "Transverse tensile behaviour of unidirectional plies reinforced with flax fibres". In: *Materials Letters* 60.24 (2006), pp. 2984–2987. ISSN: 0167-577X. DOI: https://doi.org/10.1016/j.matlet.2006.02.028. URL: https://www.sciencedirect.com/science/article/pii/S0167577X06002023.

[14] R. Barbière et al. "Influence of moisture and drying on fatigue damage mechanisms in a woven hemp/epoxy composite: Acoustic emission and micro-CT analysis". In: *International Journal of Fatigue* 136 (2020), p. 105593. ISSN: 0142-1123. DOI: https://doi.org/10.1016/j.ijfatigue.2020.105593. URL: https://www.sciencedirect.com/science/article/pii/S0142112320301249.

[15] Alexis Beakou and Karine Charlet. "Mechanical properties of interfaces within a flax bundle—Part II: Numerical analysis". In: *International Journal of Adhesion and Adhesives* 43 (2013), pp. 54–59. ISSN: 0143-7496. DOI: https://doi.org/10.1016/j.ijadhadh.2013.01.013. URL: https://www.sciencedirect.com/science/article/pii/S0143749613000146.

[16] Stuart Berg et al. "ilastik: interactive machine learning for (bio)image analysis". In: *Nature Methods* 16 (2019), pp. 1226–1232. ISSN: 1548-7105. DOI: https://doi.org/10.1038/s41592-019-0582-9. URL: https://www.nature.com/articles/s41592-019-0582-9.

[17] J.M.F.A. Blanchard, A.J. Sobey, and J.I.R. Blake. "Multi-scale investigation into the mechanical behaviour of flax in yarn, cloth and laminate form". In: *Composites Part B: Engineering* 84 (2016), pp. 228–235. ISSN: 1359-8368. DOI: https://doi.org/10.1016/j.compositesb.2015.08.086. URL: https://www.sciencedirect.com/science/article/pii/S1359836815005260.

[18] A. K. Bledzki, S. Reihmane, and J. Gassan. "Properties and modification methods for vegetable fibers for natural fiber composites". In: *Journal of Applied Polymer Science* 59.8 (1996), pp. 1329–1336. DOI: https://doi.org/10.1002/(SICI)1097-4628(19960222)59:8<1329::AID-APP17>3.0.CO;2-0. URL: https://onlinelibrary.wiley.com/doi/abs/10.1002/%28SICI%291097-4628%2819960222%2959%3A8%3C1329%3A%3AAID-APP17%3E3.0.CO%3B2-0.

[19] H. L. Bos, M. J. A. Van Den Oever, and O. C. J. J. Peters. "Tensile and compressive properties of flax fibres for natural fibre reinforced composites". In: *Journal of Materials Science* 37 (2002), pp. 1683–1692. DOI: https://doi.org/10.1023/A:1014925621252. URL: https://link.springer.com/article/10.1023/A:1014925621252.

[20] H.L. Bos and A.M. Donald. "In situ ESEM study of the deformation of elementary flax fibres". In: *Journal of Materials Science* 34.13 (1999), pp. 3029–3034. ISSN: 0022-2461. DOI: https://doi.org/10.1023/A:1004650126890. URL: https://link.springer.com/article/10.1023/A:1004650126890.

[21] A. Bourmaud and C. Baley. "Investigations on the recycling of hemp and sisal fibre reinforced polypropylene composites". In: *Polymer Degradation and Stability* 92.6 (2007), pp. 1034–1045. ISSN: 0141-3910. DOI: https://doi.org/10.1016/j.polymdegradstab.2007.02.018. URL: https://www.sciencedirect.com/science/article/pii/S0141391007000729.

[22] A. Bourmaud et al. "Observation of the structure of a composite polypropylene/flax and damage mechanisms under stress". In: *Industrial Crops and Products* 43 (2013), pp. 225–236. ISSN: 0926-6690. DOI: https://doi.org/10.1016/j.indcrop.2012.07.030. URL: https://www.sciencedirect.com/science/article/pii/S0926669012004050.

[23] Alain Bourmaud et al. "Relationships between micro-fibrillar angle, mechanical properties and biochemical composition of flax fibers". In: *Industrial Crops and Products* 44 (2013), pp. 343–351. ISSN: 0926-6690. DOI: https://doi.org/10.1016/j.indcrop.2012.11.031. URL: https://www.sciencedirect.com/science/article/pii/S0926669012006206.

[24] G. Bradski. "The OpenCV Library". In: *Dr. Dobb's Journal of Software Tools* 25.11 (2000), pp. 120–125. ISSN: 1044-789X. URL: http://www.ddj.com/ftp/2000/2000_11/opencv.txt.

[25] Harris G. Carter and Kenneth G. Kibler. "Langmuir-Type Model for Anomalous Moisture Diffusion In Composite Resins". In: *Journal of Composite Materials* 12.2 (1978), pp. 118–131. DOI: https://doi.org/10.1177/002199837801200201. URL: https://journals.sagepub.com/doi/10.1177/002199837801200201.

[26] Júlio César dos Santos et al. "Ageing of autoclaved epoxy/flax composites: Effects on water absorption, porosity and flexural behaviour". In: *Composites Part B: Engineering* 202 (2020), p. 108380. ISSN: 1359-8368. DOI: https://doi.org/10.1016/j.compositesb.2020.108380. URL: https://www.sciencedirect.com/science/article/pii/S1359836820334284.

[27] K. Charlet et al. "Tensile deformation of a flax fiber". In: *Procedia Engineering* 1.1 (2009). Mesomechanics 2009, pp. 233–236. ISSN: 1877-7058. DOI: https://doi.org/10.1016/j.proeng.2009.06.055. URL: https://www.sciencedirect.com/science/article/pii/S1877705809000563.

[28] Karine Charlet and Alexis Béakou. "Mechanical properties of interfaces within a flax bundle – Part I: Experimental analysis". In: *International Journal of Adhesion and Adhesives* 31.8 (2011), pp. 875–881. ISSN: 0143-7496. DOI: https://doi.org/10.1016/j.ijadhadh.2011.08.008. URL: https://www.sciencedirect.com/science/article/pii/S0143749611001266.

[29] Karine Charlet et al. "Scattering of morphological and mechanical properties of flax fibres". In: *Industrial Crops and Products* 32.3 (2010), pp. 220–224. ISSN: 0926-6690. DOI: https://doi.org/10.1016/j.indcrop.2010.04.015. URL: https://www.sciencedirect.com/science/article/pii/S0926669010001068.

[30] Abderrazak Chilali et al. "Analysis of the hydro-mechanical behaviour of flax fibre-reinforced composites: Assessment of hygroscopic expansion and its impact on internal stress". In: *Composite Structures* 206 (2018), pp. 177–184. ISSN: 0263-8223. DOI: https://doi.org/10.1016/j.compstruct.2018.08.037. URL: https://www.sciencedirect.com/science/article/pii/S0263822318314752.

[31] C.P.L. Chow, X.S. Xing, and R.K.Y. Li. "Moisture absorption studies of sisal fibre reinforced polypropylene composites". In: *Composites Science and Technology* 67.2 (2007), pp. 306–313. ISSN: 0266-3538. DOI: https://doi.org/10.1016/j.compscitech.2006.08.005. URL: https://www.sciencedirect.com/science/article/pii/S026635380600296X.

[32] European Commission and Directorate-General for Climate Action. *Going climate-neutral by 2050 – A strategic long-term vision for a prosperous, modern, competitive and climate-neutral EU economy*. Publications Office, 2019. DOI: https://doi.org/10.2834/02074.

[33] Robert D Cook et al. *Concepts and applications of finite element analysis*. John Wiley & Sons, 2007.

[34] Guillaume Coroller et al. "Effect of flax fibres individualisation on tensile failure of flax/epoxy unidirectional composite". In: *Composites Part A: Applied Science and Manufacturing* 51 (2013), pp. 62–70. ISSN: 1359-835X. DOI: https://doi.org/10.1016/j.compositesa.2013.03.018. URL: https://www.sciencedirect.com/science/article/pii/S1359835X13001000.

[35] Isaac M. Daniel and Ori Ishai. *Engineering Mechanics of Composite Materials*. Second. Oxford University Press, 2006.

[36] Antoine le Duigou et al. "Hygroscopic expansion: A key point to describe natural fibre/polymer matrix interface bond strength". In: *Composites Science and Technology* 151 (2017), pp. 228–233. ISSN: 0266-3538. DOI: https://doi.org/10.1016/j.compscitech.2017.08.028. URL: https://www.sciencedirect.com/science/article/pii/S0266353817300477.

[37] Adolph Fick. "V. On liquid diffusion". In: *The London, Edinburgh, and Dublin Philosophical Magazine and Journal of Science* 10.63 (1855), pp. 30–39. DOI: https://doi.org/10.1080/14786445508641925. URL: https://www.tandfonline.com/doi/abs/10.1080/14786445508641925.

[38] Jayamol George, S.S. Bhagawan, and Sabu Thomas. "Effects of environment on the properties of low-density polyethylene composites reinforced with pineapple-leaf fibre". In: *Composites Science and Technology* 58.9 (1998), pp. 1471–1485. ISSN: 0266-3538. DOI: https://doi.org/10.1016/S0266-3538(97)00161-9. URL: https://www.sciencedirect.com/science/article/pii/S0266353897001619.

[39] Nina Graupner et al. "Fibre/matrix adhesion of cellulose fibres in PLA, PP and MAPP: A critical review of pull-out test, microbond test and single fibre fragmentation test results". In: *Composites Part A: Applied Science and Manufacturing* 63 (2014), pp. 133–148. ISSN: 1359-835X. DOI: https://doi.org/10.1016/j.compositesa.2014.04.011. URL: https://www.sciencedirect.com/science/article/pii/S1359835X14001134.

[40] Z. Hashin. "Analysis of Composite Materials—A Survey". In: *Journal of Applied Mechanics* 50.3 (Sept. 1983), pp. 481–505. ISSN: 0021-8936. DOI: https://doi.org/10.1115/1.3167081. URL: https://asmedigitalcollection.asme.org/appliedmechanics/article-abstract/50/3/481/389153/Analysis-of-Composite-Materials-A-Survey.

[41] J. W. S. Hearle. "The structural mechanics of fibers". In: *Journal of Polymer Science Part C: Polymer Symposia* 20.1 (1967), pp. 215–251. DOI: https://doi.org/10.1002/polc.5070200118. URL: https://onlinelibrary.wiley.com/doi/abs/10.1002/polc.5070200118.

[42] Callum A. S. Hill, Andrew Norton, and Gary Newman. "The water vapor sorption behavior of natural fibers". In: *Journal of Applied Polymer Science* 112.3 (2009), pp. 1524–1537. DOI: https://doi.org/10.1002/app.29725. URL: https://onlinelibrary.wiley.com/doi/abs/10.1002/app.29725.

[43] R. Hill. "Elastic properties of reinforced solids: Some theoretical principles". In: *Journal of the Mechanics and Physics of Solids* 11.5 (1963), pp. 357–372. ISSN: 0022-5096. DOI: https://doi.org/10.1016/0022-5096(63)90036-X. URL: https://www.sciencedirect.com/science/article/pii/002250966390036X.

[44] Dale A. Hopkins and Christos C. Chamis. "A Unique Set of Micromechanics Equations for High-Temperature Metal Matrix Composites". In: 1988. URL: https://api.semanticscholar.org/CorpusID:136915924.

[45] Ecotechnilin. URL: https://eco-technilin.com/en/flaxtape/68-L-FLAXTAPE-200-26.html.

[46] H. M. A. E. El-Behery J. W. S. Hearle and V. M. Thakur. "6—THE MECHANICS OF TWISTED YARNS : TENSILE PROPERTIES OF CONTINUOUS-FILAMENT YARNS". In: *Journal of the Textile Institute Transactions* 50.1 (1959), T83–T111. DOI: https://doi.org/10.1080/19447025908662487. URL: https://www.tandfonline.com/doi/abs/10.1080/19447025908662487.

[47] Roberts Joffe, Jānis Andersons, and Lennart Wallström. "Strength and adhesion characteristics of elementary flax fibres with different surface treatments". In: *Composites Part A: Applied Science and Manufacturing* 34.7 (2003), pp. 603–612. ISSN: 1359-835X. DOI: https://doi.org/10.1016/S1359-835X(03)00099-X. URL: https://www.sciencedirect.com/science/article/pii/S1359835X0300099X.

[48] Thomas Joffre et al. "Swelling of cellulose fibres in composite materials: Constraint effects of the surrounding matrix". In: *Composites Science and Technology* 74 (2013), pp. 52–59. ISSN: 0266-3538. DOI: https://doi.org/10.1016/j.compscitech.2012.10.006. URL: https://www.sciencedirect.com/science/article/pii/S0266353812003600.

[49] Autar K. Kaw. *Mechanics of Composite Materials*. CRC Press, 2005.

[50] V. Keryvin et al. "Analysis of flax fibres viscoelastic behaviour at micro and nano scales". In: *Composites Part A: Applied Science and Manufacturing* 68 (2015), pp. 219–225. ISSN: 1359-835X. DOI: https://doi.org/10.1016/j.compositesa.2014.10.006. URL: https://www.sciencedirect.com/science/article/pii/S1359835X14003169.

[51] M. Knight and D. Curliss. "Composite Materials". In: *Encyclopedia of Physical Science and Technology (Third Edition)*. Ed. by Robert A. Meyers. Third Edition. New York: Academic Press, 2003, pp. 455–468. ISBN: 978-0-12-227410-7. DOI: https://doi.org/10.1016/B0-12-227410-5/00128-9. URL: https://www.sciencedirect.com/science/article/pii/B0122274105001289.

[52] Antoine Le Duigou, Peter Davies, and Christophe Baley. "Interfacial bonding of Flax fibre/Poly(l-lactide) bio-composites". In: *Composites Science and Technology* 70.2 (2010), pp. 231–239. ISSN: 0266-3538. DOI: https://doi.org/10.1016/j.compscitech.2009.10.009. URL: https://www.sciencedirect.com/science/article/pii/S0266353809003728.

[53] Antoine Le Duigou et al. "Interfacial properties of flax fibre–epoxy resin systems: Existence of a complex interphase". In: *Composites Science and Technology* 100 (2014), pp. 152–157. ISSN: 0266-3538. DOI: https://doi.org/10.1016/j.compscitech.2014.06.009. URL: https://www.sciencedirect.com/science/article/pii/S0266353814002024.

[54] Nicolas Lesaffre et al. "Recent advances on the ageing of flame retarded PLA: Effect of UV-light and/or relative humidity". In: *Polymer Degradation and Stability* 139 (2017), pp. 143–164. ISSN: 0141-3910. DOI: https://doi.org/10.1016/j.polymdegradstab.2017.04.007. URL: https://www.sciencedirect.com/science/article/pii/S0141391017300903.

[55] Mi Li et al. "Recent advancements of plant-based natural fiber–reinforced composites and their applications". In: *Composites Part B: Engineering* 200 (2020), p. 108254. ISSN: 1359-8368. DOI: https://doi.org/10.1016/j.compositesb.2020.108254. URL: https://www.sciencedirect.com/science/article/pii/S1359836820333047.

[56] Yan Li and Bing Xue. "Hydrothermal ageing mechanisms of unidirectional flax fabric reinforced epoxy composites". In: *Polymer Degradation and Stability* 126 (2016), pp. 144–158. ISSN: 0141-3910. DOI: https://doi.org/10.1016/j.polymdegradstab.2016.02.004. URL: https://www.sciencedirect.com/science/article/pii/S0141391016300271.

[57] Maria Morissa Lu, Carlos A. Fuentes, and Aart Willem Van Vuure. "Moisture sorption and swelling of flax fibre and flax fibre composites". In: *Composites Part B: Engineering* 231 (2022), p. 109538. ISSN: 1359-8368. DOI: https://doi.org/10.1016/j.compositesb.2021.109538. URL: https://www.sciencedirect.com/science/article/pii/S1359836821009045.

[58] Anna Madra et al. "A clustering method for analysis of morphology of short natural fibers in composites based on X-ray microtomography". In: *Composites Part A: Applied Science and Manufacturing* 102 (2017), pp. 184–195. ISSN: 1359-835X. DOI: https://doi.org/10.1016/j.compositesa.2017.07.028. URL: https://www.sciencedirect.com/science/article/pii/S1359835X17302968.

[59] Bo Madsen, Preben Hoffmeyer, and Hans Lilholt. "Hemp yarn reinforced composites – II. Tensile properties". In: *Composites Part A: Applied Science and Manufacturing* 38.10 (2007), pp. 2204–2215. ISSN: 1359-835X. DOI: https://doi.org/10.1016/j.compositesa.2007.06.002. URL: https://www.sciencedirect.com/science/article/pii/S1359835X07001030.

[60] Bo Madsen et al. "Hemp yarn reinforced composites – I. Yarn characteristics". In: *Composites Part A: Applied Science and Manufacturing* 38.10 (2007), pp. 2194–2203. ISSN: 1359-835X. DOI: https://doi.org/10.1016/j.compositesa.2007.06.001. URL: https://www.sciencedirect.com/science/article/pii/S1359835X07001029.

[61] L. Marrot et al. "Multi-scale study of the adhesion between flax fibers and biobased thermoset matrices". In: *Materials Design (1980-2015)* 62 (2014), pp. 47–56. ISSN: 0261-3069. DOI: https://doi.org/10.1016/j.matdes.2014.04.087. URL: https://www.sciencedirect.com/science/article/pii/S0261306914003628.

[62] A.R. Melro et al. "Micromechanical analysis of polymer composites reinforced by unidirectional fibres: Part I – Constitutive modelling". In: *International Journal of Solids and Structures* 50.11 (2013), pp. 1897–1905. ISSN: 0020-7683. DOI: https://doi.org/10.1016/j.ijsolstr.2013.02.009. URL: https://www.sciencedirect.com/science/article/pii/S0020768313000747.

[63] Bernard Miller, Pierre Muri, and Ludwig Rebenfeld. "A microbond method for determination of the shear strength of a fiber/resin interface". In: *Composites Science and Technology* 28.1 (1987), pp. 17–32. ISSN: 0266-3538. DOI: https://doi.org/10.1016/0266-3538(87)90059-5. URL: https://www.sciencedirect.com/science/article/pii/0266353887900595.

[64] Abdul Moudood et al. "Flax fiber and its composites: An overview of water and moisture absorption impact on their performance". In: *Journal of Reinforced Plastics and Composites* 38.7 (2019), pp. 323–339. DOI: https://doi.org/10.1177/0731684418818893. URL: https://journals.sagepub.com/doi/10.1177/0731684418818893.

[65] Malladi Nagalakshmaiah et al. "Chapter 9 - Biocomposites: Present trends and challenges for the future". In: *Green Composites for Automotive Applications*. Ed. by Georgios Koronis and Arlindo Silva. Woodhead Publishing Series in Composites Science and Engineering. Woodhead Publishing, 2019, pp. 197–215. ISBN: 978-0-08-102177-4. DOI: https://doi.org/10.1016/B978-0-08-102177-4.00009-4. URL: https://www.sciencedirect.com/science/article/pii/B9780081021774000094.

[66] Chi Nguyen-Thanh et al. “Jive: An open source, research-oriented C++ library for solving partial differential equations”. In: *Advances in Engineering Software* 150 (2020), p. 102925. ISSN: 0965-9978. DOI: https://doi.org/10.1016/j.advengsoft.2020.102925. URL: https://www.sciencedirect.com/science/article/pii/S0965997820309716.

[67] Fatma Omrani et al. “Mechanical properties of flax-fibre-reinforced preforms and composites: Influence of the type of yarns on multi-scale characterisations”. In: *Composites Part A: Applied Science and Manufacturing* 93 (2017), pp. 72–81. ISSN: 1359-835X. DOI: https://doi.org/10.1016/j.compositesa.2016.11.013. URL: https://www.sciencedirect.com/science/article/pii/S1359835X16303943.

[68] I. Özdemir, W.A.M. Brekelmans, and M.G.D. Geers. “FE2 computational homogenization for the thermo-mechanical analysis of heterogeneous solids”. In: *Computer Methods in Applied Mechanics and Engineering* 198.3 (2008), pp. 602–613. ISSN: 0045-7825. DOI: https://doi.org/10.1016/j.cma.2008.09.008. URL: https://www.sciencedirect.com/science/article/pii/S0045782508003277.

[69] Patricia P. Parlevliet, Harald E.N. Bersee, and Adriaan Beukers. “Residual stresses in thermoplastic composites—A study of the literature—Part II: Experimental techniques”. In: *Composites Part A: Applied Science and Manufacturing* 38.3 (2007), pp. 651–665. ISSN: 1359-835X. DOI: https://doi.org/10.1016/j.compositesa.2006.07.002. URL: https://www.sciencedirect.com/science/article/pii/S1359835X06002223.

[70] Vincent Placet, Ousseynou Cissé, and M. Lamine Boubakar. “Nonlinear tensile behaviour of elementary hemp fibres. Part I: Investigation of the possible origins using repeated progressive loading with in situ microscopic observations”. In: *Composites Part A: Applied Science and Manufacturing* 56 (2014), pp. 319–327. ISSN: 1359-835X. DOI: https://doi.org/10.1016/j.compositesa.2012.11.019. URL: https://www.sciencedirect.com/science/article/pii/S1359835X12003533.

[71] C. Poilâne et al. “Polymer reinforced by flax fibres as a viscoelastoplastic material”. In: *Composite Structures* 112 (2014), pp. 100–112. ISSN: 0263-8223. DOI: https://doi.org/10.1016/j.compstruct.2014.01.043. URL: https://www.sciencedirect.com/science/article/pii/S0263822314000567.

[72] Vishnu Prasad et al. “Enhancing Mode I and Mode II interlaminar fracture toughness of flax fibre reinforced epoxy composites with nano TiO2”. In: *Composites Part A: Applied Science and Manufacturing* 124 (2019), p. 105505. ISSN: 1359-835X. DOI: https://doi.org/10.1016/j.compositesa.2019.105505. URL: https://www.sciencedirect.com/science/article/pii/S1359835X19302544.

[73] Arnaud Regazzi et al. “Modeling of hydrothermal aging of short flax fiber reinforced composites”. In: *Composites Part A: Applied Science and Manufacturing* 90 (2016), pp. 559–566. ISSN: 1359-835X. DOI: https://doi.org/10.1016/j.compositesa.2016.08.011. URL: https://www.sciencedirect.com/science/article/pii/S1359835X16302676.

[74] Arnaud Regazzi et al. “Reversible and irreversible changes in physical and mechanical properties of biocomposites during hydrothermal aging”. In: *Industrial Crops and Products* 84 (2016), pp. 358–365. ISSN: 0926-6690. DOI: https://doi.org/10.1016/j.indcrop.2016.01.052. URL: https://www.sciencedirect.com/science/article/pii/S092666901630053X.

[75] Walter Ritz. “Über eine neue Methode zur Lösung gewisser Variationsprobleme der mathematischen Physik.” In: *Journal für die reine und angewandte Mathematik* 135 (1909), pp. 1–61. URL: http://eudml.org/doc/149295.

[76] I.B.C.M. Rocha. "Numerical and Experimental Investigation of Hygrothermal Aging in Laminated Composites". PhD thesis. Delft University of Technology, 2019. DOI: https://doi.org/10.4233/uuid:0eab23c7-9ba4-4d27-91ee-58f9f140dd34. URL: https://repository.tudelft.nl/islandora/object/uuid:0eab23c7-9ba4-4d27-91ee-58f9f140dd34?collection=research.

[77] Min Zhi Rong et al. "The effect of fiber treatment on the mechanical properties of unidirectional sisal-reinforced epoxy composites". In: *Composites Science and Technology* 61.10 (2001), pp. 1437–1447. ISSN: 0266-3538. DOI: https://doi.org/10.1016/S0266-3538(01)00046-X. URL: https://www.sciencedirect.com/science/article/pii/S026635380100046X.

[78] A. Rubio-López, T. Hoang, and C. Santiuste. "Constitutive model to predict the viscoplastic behaviour of natural fibres based composites". In: *Composite Structures* 155 (2016), pp. 8–18. ISSN: 0263-8223. DOI: https://doi.org/10.1016/j.compstruct.2016.08.001. URL: https://www.sciencedirect.com/science/article/pii/S0263822316313770.

[79] El Hadi Saidane et al. "Assessment of 3D moisture diffusion parameters on flax/epoxy composites". In: *Composites Part A: Applied Science and Manufacturing* 80 (2016), pp. 53–60. ISSN: 1359-835X. DOI: https://doi.org/10.1016/j.compositesa.2015.10.008. URL: https://www.sciencedirect.com/science/article/pii/S1359835X15003541.

[80] J. Schindelin et al. "Fiji: an open-source platform for biological-image analysis". In: *Nature Methods* 9.7 (2012), pp. 676–682. DOI: https://doi.org/10.1038/nmeth.2019. URL: https://www.nature.com/articles/nmeth.2019.

[81] C. Schneider, W. Rasband, and K. Eliceiri. "NIH Image to ImageJ: 25 years of image analysis". In: *Nature Methods* 9 (7 2012), pp. 671–675. DOI: https://doi.org/10.1038/nmeth.2089. URL: https://www.nature.com/articles/nmeth.2089.

[82] Daniel Scida, Alain Bourmaud, and Christophe Baley. "Influence of the scattering of flax fibres properties on flax/epoxy woven ply stiffness". In: *Materials Design* 122 (2017), pp. 136–145. ISSN: 0264-1275. DOI: https://doi.org/10.1016/j.matdes.2017.02.094. URL: https://www.sciencedirect.com/science/article/pii/S0264127517302368.

[83] Daniel Scida et al. "Influence of hygrothermal ageing on the damage mechanisms of flax-fibre reinforced epoxy composite". In: *Composites Part B: Engineering* 48 (2013), pp. 51–58. ISSN: 1359-8368. DOI: https://doi.org/10.1016/j.compositesb.2012.12.010. URL: https://www.sciencedirect.com/science/article/pii/S1359836812007883.

[84] Janis Sliseris, Libo Yan, and Bohumil Kasal. "Numerical modelling of flax short fibre reinforced and flax fibre fabric reinforced polymer composites". In: *Composites Part B: Engineering* 89 (2016), pp. 143–154. ISSN: 1359-8368. DOI: https://doi.org/10.1016/j.compositesb.2015.11.038. URL: https://www.sciencedirect.com/science/article/pii/S1359836815007222.

[85] Xuefeng TENG et al. "Experimental, analytical and numerical investigation on tensile behavior of twisted fiber yarns". In: *Chinese Journal of Aeronautics* 34.5 (2021), pp. 278–288. ISSN: 1000-9361. DOI: https://doi.org/10.1016/j.cja.2020.08.006. URL: https://www.sciencedirect.com/science/article/pii/S1000936120303617.

[86] S. Thomas et al. "Natural Fibres: Structure, Properties and Applications". In: *Cellulose Fibers: Bio- and Nano-Polymer Composites: Green Chemistry and Technology*. Ed. by Susheel Kalia, B. S. Kaith, and Inderjeet Kaur. Springer Berlin Heidelberg, 2011, pp. 3–42. ISBN: 978-3-642-17370-7. DOI: https://doi.org/10.1007/978-3-

642-17370-7_1. URL: https://link.springer.com/chapter/10.1007/978-3-642-17370-7_1.

[87] Moe Moe Thwe and Kin Liao. "Durability of bamboo-glass fiber reinforced polymer matrix hybrid composites". In: *Composites Science and Technology* 63.3 (2003), pp. 375–387. ISSN: 0266-3538. DOI: https://doi.org/10.1016/S0266-3538(02)00225-7. URL: https://www.sciencedirect.com/science/article/pii/S0266353802002257.

[88] Wenlong Tian et al. "Periodic boundary condition and its numerical implementation algorithm for the evaluation of effective mechanical properties of the composites with complicated micro-structures". In: *Composites Part B: Engineering* 162 (2019), pp. 1–10. ISSN: 1359-8368. DOI: https://doi.org/10.1016/j.compositesb.2018.10.053. URL: https://www.sciencedirect.com/science/article/pii/S1359836818319838.

[89] S Torquato, B Lu, and J Rubinstein. "Nearest-neighbour distribution function for systems on interacting particles". In: *Journal of Physics A: Mathematical and General* 23.3 (Feb. 1990), p. L103. DOI: https://dx.doi.org/10.1088/0305-4470/23/3/005. URL: https://iopscience.iop.org/article/10.1088/0305-4470/23/3/005.

[90] Frédérique Trivaudey et al. "Nonlinear tensile behaviour of elementary hemp fibres. Part II: Modelling using an anisotropic viscoelastic constitutive law in a material rotating frame". In: *Composites Part A: Applied Science and Manufacturing* 68 (2015), pp. 346–355. ISSN: 1359-835X. DOI: https://doi.org/10.1016/j.compositesa.2014.10.020. URL: https://www.sciencedirect.com/science/article/pii/S1359835X14003327.

[91] A. Turon et al. "A damage model for the simulation of delamination in advanced composites under variable-mode loading". In: *Mechanics of Materials* 38.11 (2006), pp. 1072–1089. ISSN: 0167-6636. DOI: https://doi.org/10.1016/j.mechmat.2005.10.003. URL: https://www.sciencedirect.com/science/article/pii/S0167663605002000.

[92] F.P. van der Meer and L.J. Sluys. "Mesh-independent modeling of both distributed and discrete matrix cracking in interaction with delamination in composites". In: *Engineering Fracture Mechanics* 77.4 (2010), pp. 719–735. ISSN: 0013-7944. DOI: https://doi.org/10.1016/j.engfracmech.2009.11.010. URL: https://www.sciencedirect.com/science/article/pii/S0013794409003518.

[93] Swancor Holding Co. Ltd. URL: www.swancor.com/en.

[94] Libo Yan, Nawawi Chouw, and Xiaowen Yuan. "Improving the mechanical properties of natural fibre fabric reinforced epoxy composites by alkali treatment". In: *Journal of Reinforced Plastics and Composites* 31.6 (2012), pp. 425–437. DOI: https://doi.org/10.1177/0731684412439494. URL: https://journals.sagepub.com/doi/10.1177/0731684412439494.

[95] Jan Zeman and Michal Sejnoha. *Micromechanics in practice*. Feb. 2013. ISBN: 978-1-84564-682-0.

[96] T. Zimmermann, E. Pöhler, and T. Geiger. "Cellulose Fibrils for Polymer Reinforcement". In: *Advanced Engineering Materials* 6.9 (2004), pp. 754–761. DOI: https://doi.org/10.1002/adem.200400097. URL: https://onlinelibrary.wiley.com/doi/abs/10.1002/adem.200400097.